Gouy Phase Variation as tuning capability

A thesis submitted to the University of Hyderabad
for the award of the degree of

Doctor of Philosophy

in
Physics

By
SUDHA NIRMALA KALAGATA

School of Physics
University of Hyderabad
P.O. Central University
Hyderabad-500 046
Andhra Pradesh, India.
December 2011

DECLARATION

I here by declare that the work reported in this thesis has been carried out by me independently in the school of physics, University of Hyderabad, under the supervision of Prof. Surya. P. Tewari. I also declare that this is my own work and effort, and it has not been submitted at any other University or Institution for any degree.

K. Sudha Nirmala

Date:

Place:

CERTIFICATE

This is to certify that the work contained in this thesis entitled "**Gouy phase variation as tuning capability**", has been carried out by Miss. **KALAGATA SUDHA NIRMALA**(Reg. No.04PHPH13), under my direct supervision and the same has not been submitted for the award of research degree of any university.

<div align="right">

Prof. Surya. P. Tewari

Thesis Supervisor

School of Physics

University of Hyderabad

</div>

Place: Hyderabad

Date:

The Dean

School of Physics

University of Hyderabad

To The Memory of My Father

Acknowledgements

It is my pleasure to acknowledge my gratitude for all who have directly or indirectly helped me for the successful completion of this thesis.

I would like to express my deep and sincere gratitude to my supervisor, **Prof. Surya. P. Tewari**, who taught me the number of ways to propagate to the depth of the subject and to improve my understanding of **Lasers**. It has been really memorable because he made me to learn through his clear cut discussions which certainly ends with probing questions. I also admire him for cultivating right concepts. It is really a matter of pride to have been associated with him.

I would like to thank the Deans of the school of physics during the period 2004-2011, for making available all the facilities required. I thank my Doctoral committee member Prof. D. Narayana Rao for his helpful comments and suggestions. I thank other faculty members of the optics group who have participated in my Doctoral committee meetings especially Prof. S. Dutta Gupta, Dr. Suneel Singh, Dr. Nirmal Viswanathan and Dr. V. S. Ashoka for their valuable suggestions.

I would like to acknowledge **K. Ram Babu**, Sc F, Dean, ELOIRA and **Dr. M. Sree Ramana**, Scientist, Research Center Imarat(RCI), DRDO, Kanchenbagh, Hyderabad for his discussions and helpful suggestions at various stages of this work. I extend my thanks to him for the keen interest that he took in my work.

I thank all the non teaching staff especially Mr. Abraham and Mr. Srinivas for their support and timely help. I also acknowledge all the faculty, non teaching staff and students of the **ACRHEM** for their support in all the ways.

I owe special respects to my teachers **Moses Garu** in schooling, **Silver**

Anand Garu and **Srinivas Garu** in graduation. It is my pleasure to thank my best and childhood friends **Lalitha**, **Sundari**, **Krishna veni**, Intermediate friends **Devi**, **Bhagat** and **Javvadi**, B. Sc friends **Leela Srinivas**, **Shankar**, **Durga**, **Jyothi**, **Nagamani**, **Timothy** for their affection and encouragement to reach my Goal.

I should also like to thank my M.Sc classmates **Sreekanth**, **Rebecca** for their support.

I greatly acknowledge my HCU friends **Madhavi Latha** and **Harini** who motivated to start my research career. With out their words I would not have done this Ph.D.

I also remember the association with my seniors **Dr. Pamu**, **Dr. Ajith**, **Dr. Sreeranjani**, **Dr. Shiv Chaitanya**, **Dr. Satish**, **Dr. Juby** and colleagues Dr. Jaya Sri, Srinivas, Ramudu. The friendly association of junior colleagues **Arun**, **Sankarayya**, **Deva Raj**, **Anil**, **Rajeswari** and **Yugandhar** is most memorable.

My special thanks to **Bheem** for his timely help at various stages of my ph. D and to my cute sister **Swathi**. I also thank **Leela** for accompanying me at the final stage of my thesis.

I express my enormous thanks to **Rajani**, **Pradeep**, **Miranna**, **Gopal** and **Bharat** for their company who made my stay at UOH most memorable.

A very special thanks to **Dr. Satyavathi** who shared all of my depressions, emotions and joy full moments, especially for her constant encouragement and lovely sisterhood.

I greatly acknowledge **N. Kishore Kumar** for making my stay at UOH most memorable and I thank him for his help at various stages of my work.

I acknowledge my uncles **Nandan Kumar**, **Madhu** and **Srinu** for their constant encouragement. I am very much thankful to **Sanjeev** for his help in latex.

Financial assistance from the **Rajiv Gandhi National Fellowship(RGNF)**

Abstract

The thesis is a study of Gouy phase of electromagnetic field produced by point sources and by lasers -in particular by ring lasers. Gouy observed—— when an electromagnetic radiation field passes through a focus there is sudden change in the phase of the field amplitude, in that it can be observed by a fringe shift in a field pattern obtained by superposition of the two beams- one which went through the focus and the other which carries the phase of the original beam without going through the focus. The thesis investigates the possibility if the Gouy phase seen in laser can be used to tune the frequency of a laser. It is shown by varying either the length of the ring cavity and or the distances between the multiple lens components inside the ring tuning the frequency of laser is possible. A use of such tuning capability is helpful in improving the performance of a ring laser gyro. Using the concept of accumulation of the Gouy phase to an over all $n\pi$- by passing through n - focal region - a study is made to increase the Gouy phase tunability to larger values. The study reveals that with constant focal length lenses, and variable distance between them, one meets with unstable regions of the cavity, and thus one finds that by the Gouy phase method of tunability more than n to $n + \frac{1}{2}$, mode number change can not be achieved. The thesis also elaborates on the intriguing comparison of geometrical focus- a point - with the focal region of a Gaussian mode function. An experiment is proposed in Chapter-3, using which a comparison of the above two images is made. In Chapter-7, the different regions of mode functions are examined with the procedure of geometrical optics. It is concluded there that the Rayleigh range can be interpreted as the expanded region of a geometrical point focus.

Contents

List of Figures

1

Introduction

A cavity resonator is a conducting surface enclosing a space in which an oscillating electromagnetic field can be maintained, the resonant frequency of which is determined by the shape and dimensions of the cavity. It behaves like an ordinary electronic resonant circuit that consists of a coil and a capacitor that are connected either in series or in parallel. Such a closed resonant cavity was considered with highly reflective walls to produce in the microwave region of the electromagnetic spectrum a maser [1].

Schawlow and Townes [2] attempted to extend maser operation to infrared and optical regions of the spectrum i.e., towards very short wavelengths-considerably shorter than one centimeter. They suggested 'open cavity resonators' which consist of two parallel plates of centimeter dimensions sepa-

rated by finite distance. This has also been suggested by Prokorov [3] and also in his patent by Dicke [4]. The experimental realization of open resonators has come through Maiman [5] and Collins et. al [6] using ruby crystal.

The mode configurations of open resonator can be obtained by an iterative procedure using the Kirchhoff-Fresnel diffraction theory [7]. Open resonators have the diffraction losses which are caused due to fraction of energy leaving sides of the cavity. As a result, the number of oscillating modes with low loss reduce in the open resonators. The diffraction losses of an open resonator depend on its Fresnel number and also on the field distribution at the mirror.

Theoretical investigations towards the diffraction losses have been performed by Fox and Li [8], in a Fabry - Perot interferometer which consists of two parallel plane mirrors confining a portion in free space. They have used the scalar formulation of Huygen's principle to compute the electromagnetic field at one of the mirrors in terms of an integral over the surface of the another. Confocal resonators have concave reflective mirrors towards the confined volume in free space. Series, Fox and Li [8] and Lewis [9] have suggested the confocal resonator, Lewis has recognized that it would have lower diffraction losses than the parallel Fabry - Perot and has described the analytic solution. The use of confocal reflectors as an interferometer has been described by Connes [10].

With these suggestions, Boyd and Gordon [11] have realized that the plane - parallel Fabry - Perot is not necessarily ideal as a high frequency multi mode resonator. They have considered a resonator formed by two spherical reflectors of equal curvature separated by their common radius of curvature in detail. They approximated the mode of a resonator by Gaussian Hermite function for the first time.

Later Boyd and Kogelnik [12] generalized the confocal resonator theory to unequal curvature, showed the existence of low-loss regions and high loss regions of the resonator as the reflector spacing is varied in a two dimensional

diagram which is suggested by Fox and Li. Along with these foundations, Fox and Li and many others continued the study of resonator properties and extended to tilted mirrors [13, 14, 15], circular spherical mirrors [16]. An earlier review of the theory of laser beams and resonators is presented extensively by Kogelnik and Li [17], and recently by Siegman [18, 19].

It is very well known that, when a mode of the resonator is approximated by the Hermite-Gaussian function, along the z axis it acquires an additional π phase shift across its beam waist for which Boyd and Gordon [11] gave a convenient expression. The earliest indication of this phase shift was discovered and confirmed experimentally by Gouy [20, 21] in 1890, while working with focused and unfocussed wave fronts in an optical arrangement. He also predicted this phase change for acoustic waves, and realized that it must be a general property of any focused wave. Since then Gouy phase has been discussed extensively in the literature.

A fairly large number of publications deal with the mystery of its origin and others with the imminent Gouy phase in the optical set up of their interest and its concomitant effect in the out put of their concern. Some of the notable attempts to recall are the following.

This phase anomaly was predicted by Debye [22] at the focus and later his treatment has been generalized for the case of an arbitrary diffracting aperture by Rubinowicz [23]. He attempted to show that this sudden jump of π is due to the incident wave and considered this as a geometrical phenomena. Further to obtain a general picture of the phase distribution near focus a sharpened version of Lommels classical analysis is applied [24]. An intuitive explanation of this phase anomaly based on the analysis of Kogelnik and Li [17] is provided by Boyd [25].

This Gouy phase has been interpreted as Berry's phase [26], a geometric phase associated with the underlying Lobachevskian hyperbolic geometry [27], and topological (Berry) phase [28], a geometric quantum effect [29]. It

has been used in controlling the non linear conversion efficiency [30], and also to observe the polarity change of single-cycle tera hertz pulses [31, 32].

Recently, it has been shown that this well-known Gouy phase shift of any focused beam originates from transverse spatial confinement [33]. To understand the connection between the Gaussian beams and tilted waves, an interpretation of the Gouy phase shift is proposed [34]. This tilted wave representation has been extended further to study the Gouy phase shift in the focus region under high numerical aperture illumination [35].

In addition to this, the Gouy phase is extensively studied with highly focused radially polarized beam [36], in the optical lateral trapping of small particles [37], for the application of ultra-short laser pulses [38], to improve the transverse and axial resolution for high resolution imaging [39], in non linear optical imaging for third harmonic generation (THG) [40, 41], in the Sagnac interferometer [42].

It has been discussed that the role of the Gouy phase in the coupling from the fundamental mode to higher order modes [43, 44](with incoherent coupling [43], coherent coupling [44]), not in the context of beam quality. Paschotta [45] gave a resonant mode coupling model, with which he explained the beam quality deterioration with degenerate modes as a resonance phenomena and the mode dependent Gouy phase plays a role in deciding the quality of the laser beam. Kaddour et. al [46] generalized Gouy phase and gave a new approach for the calculation of the resonance condition for the real cavity.

The influence of the Gouy phase anomaly on the axial precision of optical coherence tomography (OCT) measurements [47], to control the photo-induced reactions of a polyatomic molecule [48], in matter waves [49] and in an isotropic left-handed material (LHM) slab [50] has been studied.

Kandpal et. al [51] demonstrated the intensity variation of bright and dark fringes in Young's double slit experiment, showed that a light beam

propagating through the focus of a lens experienced Gouy phase shift with respect to its plane wave counter part. It has also been verified that it provides an imperfection in phase matching for any linearly invariant material [52], observed by Teichman et. al [53].

But what appears to be lacking in this extensive literature is that no one has explored the crucial role of Gouy phase in tuning or controlling actively the frequency of laser.

In this thesis we investigate the possibility of making use of the presence of Gouy phase in an optical set up of interest; particularly to bring out the tuning capability suggested here for the first time in a ring laser out put, without changing the perimeter of the ring either by the use of piezo or by variation of either temperature or by refractive index of a medium placed in it. As it is well known the Gouy phase determines the different resonance frequencies of the laser cavity [54], the attempt here is to present a mechanism by which Gouy phase may be controlled and thus tune the frequency of the ring laser.

After Schawlow and Townes enunciated the principle of laser in 1958, in the following year, Heer [55] proposed the use of a resonant cavity for sensing rotation. The first actual ring laser device was built by Macek and Davis [56].

In such a ring laser, the frequency determining condition for a perimeter L of the cavity, with the Gouy phase term ϕ_G is

$$2n\pi = kL + \phi_G \tag{1.1}$$

where n is the mode number and $k = \dfrac{2\pi}{\lambda}$ is the propagation constant. Along with the condition in Eq. (1.1), the gain and loss for λ determine the continuous or pulse operation of the laser.

It is understood from the Eq. (1.1) that in a ring laser when there is no rotation then the properties of set of modes traveling in the clockwise direction match with the properties of set of modes traveling in the anti-clockwise

direction. But when there is rotation due to the path length variation, there is a frequency difference between the clockwise and anti-clockwise which results in a beat frequency at the detector. Now the questions arise here are when there is a variation ΔL in the path length what happens to the Gouy phase ϕ_G? Whether it can be varied or not? If it can be varied, can we vary it by keeping the total length of the cavity L to be fixed? If it can be done, is it possible to control the frequency of the ring laser using this variable Gouy phase? These exciting questions motivated us to analyze the Gouy phase as a tuning parameter for different configurations in ring laser.

The tunability is a capability of changing wavelength λ of a laser. The frequency ν of the mode of the laser can be tuned in different ways by changing the parameters which constitute the Eq. (1.1). Rewriting Eq. (1.1) as

$$\lambda = \frac{L}{n - (\frac{\phi_G}{2\pi})} \tag{1.2}$$

we club variable parameters on the right hand side.

A possibility of tuning the wave length λ is by keeping n, ϕ_G fixed varying the length of the cavity L. Another possibility is keeping L, ϕ_G fixed, and vary the mode number n . A third possibility is keeping n, L fixed and vary the Gouy phase ϕ_G of the cavity.

The first two methods of tuning have been discussed well [57], we aim at looking for the possibility of tuning the frequency of the ring laser by varying the Gouy phase.

Imaging of the optical modes with intra cavity elements has been discussed by Kogelnik [58] for the first time. Even the presence of a lens or pair of lenses in a ring cavity - used here as well - has been analyzed in [47, 59] with the aim of examining the possible degeneracy of a longitudinal mode with a transverse mode to prevent or tune in the coupling between the degenerate modes in gain medium.

Wagstaff et. al [60], analyzed the stability regions for laser cavities with

two foci with the aim of the frequency doubling of continuous-wave dye lasers, with no off-axis components. In practical cavities of this type Brewster-angled surfaces [61] and other off-axis components are incorporated in order to compensate for the aberrations of astigmatism and coma introduced by focusing through such surfaces. A ring laser cavity with two foci in the presence of off-axis elements has been analyzed and discussed [62]. Stability calculations for a commercial ring dye laser with two foci are derived in [63].

Magni [64] has given a unified formulation for the analysis of linear stable resonators containing a lens of variable focal length which represents the effects of temperature variation of the rod of a solid-state laser. Later this work is extended to Ring lasers [65]. we follow the same analysis given by Magni.

In addition to Magni's work, we present a more detailed analysis, the role of mode dependent Gouy phase is exploited fully in different ring cavity systems, which results in the wanted or unwanted modification of the important characteristics of the laser beam. We vary this accumulated Gouy phase shift which is defined by Fatih Erden and Ozaktas [66] by varying the distance between the lenses in the system.

We show that by placing a single lens-which is made up of three lenses combined together-in a ring cavity and moving them in side, one can modify, one Gaussian mode to two Gaussian modes, two Gaussian modes to three Gaussian modes, thus one can vary phase by π and thus tune the laser within this range, which amounts to one half of the free spectral range of the cavity. Generalizing to insertion of n lenses of suitable focal length one may be able to go from one mode to multiple modes thus creating a capability of introducing two; three; or n modes in the ring cavity by moving the lenses suitably - and hence tunability by n free spectral ranges can be possible by this method.

Very recently it is shown that the origin of the Gouy phase anomaly is

from elementary properties of normal congruences of light rays by the principle of stationary phase [67]. This thesis brings out an important connection between the geometrical approximation and paraxial (Gaussian) approximation which in a sense reveals the connection between stable and unstable resonators.

We have examined the role of Gouy phase in controlling mode hopping; the help this tuning capability renders to ring laser gyro is analyzed.

The thesis is organized as the following.

Contents of the thesis:

2 Mathematical Basis and Linear versus Ring Cavity

3 Single Lens Ring Cavity

4 Two Lens Ring Cavity

5 Three Lens Ring Cavity

6 Four Lens Ring Cavity

7 The structured point and its equivalence to Huygen's point source for secondary wavelets

Appendix A

Appendix B

Chapter-wise discussion:

Chapter 2: In this chapter we reanalyze the elementary concepts of optical resonators, and the mathematical basis to analyze the propagation of the Gaussian mode, which follows the matrix approach, to derive the

properties of the Gaussian beam in the considered systems. It also includes a detailed study of the mode characteristics of the linear cavity and at the end a ring cavity resonator is considered which further is used to understand the complex ring cavity systems.

Next chapter considers Gouy phase of converging diverging wave fronts and comparison of two types of point sources.

Chapter 3: In this chapter a single mode is discussed when the resonator contains only one single lens. In this chapter a single lens in a ring cavity, henceforth given the generic name, SCURC-Single Converging Unit Ring Cavity, is discussed to analyze the concepts of: (1) Huygen's point-source used in his celebrated wave front construction method; (2) the structured point source associated with a Gaussian mode. An experiment is described to compare the two point sources. The experiment reveals the filtering action of the concerned - SCURC and discuses the quick change of Gouy phase across a Huygen's point source compared to the gradual variation of the Gouy phase across the point source associated with the mode. The chapter ends by raising two questions: (a) can variable Gouy phase be used to tune a ring laser cavity output - which is of use in ring laser gyro employed for sensing rotation? (b) Are the Gouy phases across the two point sources considered in this Chapter similar or equivalent? We take the first question in next three chapters.

Chapter 4: We first analyze a two-lens-ring-cavity with focal lengths f_1, f_2 separated by a distance d. This setup is called 2CURC-viz the two converging unit ring cavity. It is demonstrated here that the concept of accumulation of Gouy phases of consecutive Gaussian modes and its variation by the distance between the two converging units leads to π-2π-π; and hence changes the longitudinal mode order from n to

$n + \dfrac{1}{2}$. In this case we give the stability analysis with respect to foci of lenses and distance between the lenses. We get two stable regions which contribute a variable Gouy phase of π. For several cases we study the mode properties, and bring out important features. This chapter establishes how Gouy phase can be used to control the vanishing of the resonant mode at a specific frequency due to the change in the phase over the length of the RC from $2n\pi$ to $2n\pi + \pi$, caused by temperature or pressure variation on the ring length. This is the crucial result of the thesis.

In the next chapter we take up three-lens ring cavity to consider accumulation up to 3π Gouy phase.

Chapter 5: This chapter discusses three-lenses-ring cavity (3CURC) with focal lengths f_1, f_2 and f_3 separated by a distances d_1, d_2 and $L - d_1 - d_2$, L being the perimeter length of the RC. It is noticed that for the chosen cavity parameters, there exist three stable patches in the parameter space, which give a variable Gouy phase by as much as π within each patch. These three stable patches are separated from one another by an unstable region. The variation of Gouy phase is π to 2π, 2π to 3π and 2π to π respectively. The failure to get variation of the accumulation of more than π in a single patch comes as a surprise.

In order to search for the reasons of this failure another study is performed for the 4CURC in the next chapter.

Chapter 6: A four lens ring cavity - the 4CURC - is considered in this chapter. By introducing four lenses in a ring cavity, four Gaussian modes can be created. The three patches in the three lenses can be modified here by the insertion of one more lens in the system. This system is similar to the two reflecting mirrors ring cavity containing He-

Ne discharge region in one arm of the square cavity, with two hundred-percent reflecting plane mirrors making the opposite corners of the four arm cavity, the two lenses suggested here are placed in the other two opposite arms - for example. We discuss the properties of the modes of such a cavity. Here again each patch in the parameter space gives a maximum variation of π amount of Gouy phase situated around π, 2π, 3π and 4π. The reasons for such behaviour are analyzed and discussed in this chapter.

In the next chapter we take the second question which is raised in the Chapter-3.

Chapter 7: This chapter discusses the second question about the two point sources raised in Chapter 3. We discuss two aspects here, one, the Gouy phase like jump in the focal region of Gaussian mode, and, second its connection to a real physical source - like a dipole oscillator. The thesis then records the conclusions.

Appendix A: In this appendix we show the Gouy phase variation for some of the cases of chapter-4.

Appendix B: In this appendix we display the equivalent circle diagrams or Gaussian beam charts for the two considered systems of the thesis.

Bibliography

[1] J. P. Gordon, H. J. Zeiger, AND C. H. Townes, "Molecular Microwave Oscillator and New Hyperfine Structure in the Microwave Spectrum Of NH_3," Phys. Rev. 95, pp. 282-284, 1954.

[2] A. L. Schawlow and C. H. Townes, "Infrared and Optical Masers", Phys. Rev. vol. 112, pp. 1940-1949, Dec 1958.

[3] A. M. Prokhorov, " Molecular amplifier and generator for submillimeter waves," JETP (USSR), vol. 34, pp. 1658-1659, June 1958; Sov. Phys. JETP, vol. 7, pp. 1140-1141, Dec 1958.

[4] R. H. Dicke,"Molecular Amplification and Generation Systems and Methods," U. S. Patent No. 2, 851, 652; September 9, 1958.

[5] T. H. Maiman, "Stimulated Optical Radiation in Ruby," Nature 187, pp. 493-494, Aug 1960.

[6] R. J. Collins, D. F. Collins, A. L. Schawlow, W. Bond, C. G. B. Garrett, and W. Kaiser, "Coherence, Narrowing, Directionality and Relaxation Oscillations in the Light Emission from Ruby," Phys. Rev. Let 5, pp. 303-305, Aug 1960.

[7] M. Born, E. Wolf: Principles of Optics, 7th edn, Cambridge University Press, Cambridge 1996.

[8] A. G. Fox and T. Li, "Resonant modes in an optical maser", Proc. IRE, vol. 48, pp. 1904-1905, Nov 1960; "Resonant modes in a maser interferometer," Bell Sys. Tech. J., vol. 40, pp. 489-508, Mar 1961.

[9] W. D. Lewis, Private commnication.

[10] P. Connes, Revue d'Optique, 35, pp. 37, 1956; J. Phys. Radium, 19, pp. 262, 1958.

[11] G. D. Boyd and J. P. Gordon, "Confocal multimode resonator for millimeter through optical wavelength masers," Bell Sys. Tech. J., vol. 40, pp. 489-508, Mar 1961.

[12] G. D. Boyd and H. Kogelnik, "Generalized Confocal resonator theory," Bell Sys. Tech.J., vol. 41, pp. 1347-1369, July 1962.

[13] A. G. Fox and T. Li, "Modes in a maser interferometer with curved and tilted mirrors," Proc. IEEE, vol. 51, pp. 80-89, Jan 1963.

[14] A. G. Fox and T. Li, "Modes in a maser interferometer with curved mirrors," in Quantum Electronics III, P. Grivet and N. Bloembergen, Eds., Columbia university Press, pp. 1263-1270, New York, 1964.

[15] G. Kotik and M. C. Newstien, "Theory of laser oscillations in Fabry - Perot resonators," J. Appl. Phys., vol. 32, pp. 178-186, Feb 1961.

[16] V. O. Galeta, S. F. Dyubko, V. V. Kamyshan, and R. A. Valitov, "Diffraction losses of an open resonator formed by circular spherical mirrors," Sov. Phys. - Technical Physics, vol. 12, pp. 1633-1634, June 1968.

[17] H. Kogelnik and T. Li, "Laser beams and Resonators," Appl. Opt, vol. 5, pp. 1550-1567, Oct 1966.

[18] A. E. Siegman, "Laser beams and resonators; The 1960s," IEEE J. Select. Topics In Quantum Electron., vol. 6, Issue 6, pp. 1380-1388, 2000.

[19] A. E. Siegman, "Laser beams and resonators; Beyond the 1960s," IEEE J. Select. Topics In Quantum Electron., vol. 6, Issue 6, pp. 1389-1399, 2000.

[20] L. G. Gouy, Sur une propriété nouvelle des ondes lumineuses, C R Hebdomadaires séances Acad. Sci. 110, pp. 1251-1253, 1890.

[21] L. G. Gouy, sur la propagation anomale des ondes, Annales des chimie et de physique 24, pp. 145 6e séries, 1891.

[22] P. Debye, Ann. Phys. 30, pp. 755, 1909.

[23] A. Rubinowicz, "On the anomalous propagation of phase in the focus," Phys. Rev. 54, pp. 931-936, 1938.

[24] E. H. Linfoot and E. Wolf, "Phase Distribution near Focus in a Aberration-free Diffraction Image," Proc. Phys. Soc. London 61, pp. 823-832, 1956.

[25] R. W. Boyd, "Intuitive explanation of the phase anomaly of focused light beams," J. Opt. Soc. Am, vol. 70, No. 7, pp. 877-880, July 1980.

[26] M. V. Berry, "Quantal phase factors accompanying adiabatic changes," Proc. R. Soc. London Ser. A 392, pp. 45-47, 1984.

[27] R. Simon and N. Mukunda, "Bargmann invariant and the geometry of the Gouy effect," Phys. Rev. Lett, vol. 70, Issue 7, pp. 880-883, Feb 1993.

[28] D. Subbarao,"Topological phase in Gaussian beam optics," Optics Letters, vol. 20, Issue 21, pp. 2162-2164, 1995.

[29] P. Hariharan and P. A. Robinson, "The Gouy phase shift as a geometrical quantum effect," J. Mod. Opt. 43, pp. 219, 1996.

[30] A. B. Ruffin, J.V. Rudd, J. F.Whitaker, S. Feng, and H.G. Winful, "Direct Observation of the Gouy Phase Shift with Single-Cycle Terahertz Pulses," Phys. Rev. Lett, vol. 83, Issue 17, pp. 3410 - 3413, Oct 1999.

[31] P. Kuziel, M. A. Khazan, and J. Kroupa, "Spatiotemporal transformations of ultrashort terahertz pulses," J. Opt. Soc. Am. B, vol. 16, Issue 10, pp. 1795-1800, Oct 1999.

[32] R. W. McGowan, R. A. Cheville, and D. Grischkowsky,"Direct observation of the Gouy phase shift in Thz impulse ranging," Appl. Phys. Lett, vol. 76, No. 6, pp. 670-672, Feb 2000.

[33] Simin Feng, Herbert G. Winful, "Physical Origin of the Gouy Phase shift," Opt. Lett. 26, pp. 485-487, Apr 2001.

[34] T. Ackemann, W. Grosse-Nobis and G. L. Lippi, "The Gouy phase shift, the average phase lag of Fourier components of Hermite-Gaussian modes and their application to resonance conditions in optical cavities," Optics Communications 189, pp. 5-14, Mar 2001.

[35] Qiwen Zhan, "Second-order tilted wave interpretation of the Gouy phase shift under high numerical aperture uniform illumination," Optics Communications 242, pp. 351-360, Aug 2004.

[36] Hao Chen, Qiwen Zhan, Yanli Zhang, Yong-Ping Li, "The Gouy phase shift of the highly focused radially polarized beam," Physics Letters A 371, pp. 259-261, May 2007.

[37] J. Arlt, M. J. Padgett, "Generation of a beam with a dark focus surrounded by regions of higher intensity: the optical bottle," Opt. Lett, vol. 25, No. 4, pp. 191-193, Feb 2000.

[38] T. Tritschler, K. D. Hof, M. W. Klein, and M. Wegener, "Variation of the carrier-envelope phase of few-cycle laser pulses owing to the Gouy phase: a solid-state-based measurement," Opt. Lett. 30, pp. 753-755, 2005.

[39] A. I. Whiting, A. F. Abouraddy, B. E. A. Saleh, M. C. Teich, J. T. Fourkas," Polarization-Assisted Transverse and Axial Superresolution," Opt. Express 11, pp. 1714-1723, 2003.

[40] R. W. Boyd, Non linear Optics, Academic, Boston, MA, 1992

[41] J. X. Cheng, X. S. Xie, "Green's function formulation for third-harmonic generation microscopy," J. Opt. Soc. Am. B, vol. 19, Issue 7, pp. 1604-1610, July 2002.

[42] M. Sree Ramana, *Ph.D Thesis*, School of Physics, University of Hyderabad, Hyderabad, INDIA(2002).

[43] A. E. Siegman, "Effects of small-scale phase perturbations on laser oscillator beam quality," IEEE J. Quantum Electron. QE-13, pp. 334-337, May 1977.

[44] T. Klaassen, A. Hoogeboom, M. P. van Exter, and J. P. Woerdman, "Gouy phase of nonparaxial eigenmodes in a folded resonator," J. Opt. Soc. Am. A 21, pp. 1689-1693, Sep 2004.

[45] Rudiger Paschotta,"Beam quality deterioartion of lasers caused by intracavity beam distortions," Opt. Express, vol. 14, No.13, pp. 6069-6074, June 2006.

[46] Z. Derrar Kaddour, A. Taleb, K. Ait-Ameur, G. Martel, "Revisiting the Gouy phase," Optics Communications, vol. 280, Issue 2, pp. 256-263, Dec 2007.

[47] Guy Lamouche, Marc L. Dufour, Bruno Gauthier, Jean-Pierre Monchalin, "Gouy phase anomaly in optical coherence tomography," Optics Communications, vol. 239, pp. 297-301, June 2004.

[48] Vishal J. Barge, Zhan Hu, Joyce Willig, and Robert J. Gordon, "The Role of the Gouy Phase in the Coherent Phase Control of the photoionization and Photodissociation of Vinyl Chloride," Phys. Rev. Lett 97, 263001, 2006.

[49] I G da Paz, M C Nemes and J G Peixoto de Faria,"Gouy phase in matter waves: an experimental proposal," Journal of Physics: Conference Series 84, 012016, 2007.

[50] Hailu Luo, Wei Hu, Zhongzhou Ren, Weixing Shu, Fei Li, "Focusing and phase compensation of paraxial beams by a left-handed material slab," Optics Communications 266, pp. 327-331, Apr 2006.

[51] H. C. Kandpal, Swati Raman, Ranjana Mehrotra, "Observation of Gouy Phase anomaly with an interferometer," Optics and Lasers in Engineering 45, pp. 249-251, July 2007.

[52] Huw E. Major, Corin B. E. Gawith, Peter G. R. Smith, "Gouy phase compensation in quasi-phase matching," Optics Communications, vol. 281, Issue 19, pp 5036-5040, Oct 2008.

[53] Sven Teichmann, Peter Hannaford, and Lap Van D, "Phase-matched emission of few high-harmonic orders from a semi-infinite helium gas cell," Appl. Phys. Lett, vol. 94, Issue 17, 171111, April 2009.

[54] A. E. Siegman, Lasers, University Science Books, Mill Valley, CA, 1986. Note that Gouy's name is misspelled as "'Guoy" in this reference.

[55] C. V. Heer, "Resonant Frequencies of an Electromagnetic Cavity in an Accelerated System of Reference," Phys. Rev, vol. 134, Issue 4A, pp. A779-A804, May 1964.

[56] W. M. Macek and D. T. M. Davis JR, "Rotation-rate sensing with traveling-wave ring lasers," Appl. Phys. Lett. 2, pp. 67-68, 1963.

[57] W. Demtröder, Laser Spectroscopy - Basic Concepts and Instrumentation, Third ed., Springer, Berlin, 2003.

[58] H. Kogelnik, "Imaging of optical mode-Resonators with internal lenses," Bell Sys. Tech. J., vol. 44, pp. 455-494, Mar 1965.

[59] V. I. Kravchenko, Yu. N. Parkhomenko, and V. A. Sokolov, "Selective Properties of Dispersive Ring Cavities," Radio physics and Quantum electronics, vol. 30, No. 12, pp. 1082-1088, Dec 1987.

[60] C. E. Wagstaff, M. H. Dunn, A. I. Ferguson, and S. J. Bastow, "Stability Conditions for Laser Cavities with Two Foci," Optics Communications, vol. 25, No. 23, pp. 379-383, June 1978.

[61] C. E. Wagstaff, and M. H. Dunn, "A second-harmonic, ring dye laser for the generation of continuous-wave, single-frequency UV radiation," J. Phys. D: Appl. Phys, vol. 12, No. 3, pp. 355-368, 1979.

[62] C. E. Dunn, M. H. Dunn, "Stability Conditions for Off-axis Laser Resonators with Two Foci," Journal of Modern Optics, 28, 10, pp. 1413 1423, 1981.

[63] D. M. Kane and M. H. Dunn, "Stability calculations for a commercial Ring Dye Laser Resonator With Two Foci," Optics Communications, vol. 48, No. 5, pp. 295-300, Jan 1984.

[64] V. Magni, "Multielement stable resonators containing a variable lens," J. Opt. Soc. Am. A, vol. 4, No. 10, pp. 1962-1969, Oct 1987.

[65] S. De Silvestri, P. Laporta and V. Magni, "Rod Thermal Lensing Effects in Solid-State Laser Ring Resonators," Optics Communications, vol. 65, No. 5, pp. 373-376, Mar 1988.

[66] M. Fatih Erden and Haldun M. Ozaktas, "Accumulated Gouy phase shift in Gaussian beam propagation through first-order optical systems," J. Opt. Soc. Am. A, vol. 14, No. 9, pp. 2190-2194, Sep 1997.

[67] Max Born and Emil Wolf, "Principles of Optics," Pergamon Press, Sixth ed., 1980.

[68] T. D. Visser, E. Wolf, "The origin of the Gouy phase anomaly and its generalization to astigmatic wave fields," Optics communications 283, Issue 18, pp. 3371-3375, Sep 2010.

2

Mathematical Basis and Linear versus Ring Cavity

The word **LASER** is an acronym for Light Amplification by Stimulated Emission of Radiation. A Laser consists of essentially three components.

(i) The active medium, which can amplify electromagnetic waves;

(ii) The energy pump, which achieves population inversion by selectively pumping energy into the active levels of the medium;

(iii) The optical resonator, which stores part of the spontaneous and induced emission that is to further enhance and concentrate energy within a few resonator modes.

Since the optical resonators provide the optical structure of the laser radiation, a study of the theory of laser resonators is required to analyze the spatial beam characteristics and temporal coherence properties of the light out put of the laser. Therefore, optimization of the design of a laser system requires resonator analysis.

An optical resonator (or resonant optical cavity) is an arrangement of a set of two or more optical components, allows a beam of light to circulate in a closed path. Thus the resonator confines and stores the light at resonance frequencies determined by its configuration.

This **chapter** deals with the theory of passive optical resonators i.e., where no active medium is present within the cavity. In this chapter we discuss the following.

1 Basic types of Resonators

2 Matrix Formalism

2.1 Basic types of Resonators

There are two basic types of resonators. (1) Linear resonator (2) Ring resonator.

2.1.1 Linear (or Standing-wave) Resonator

Linear (or standing-wave) resonators are the ones, where light bounces back and forth between two end mirrors. Fig. (2.1) shows a linear cavity resonator with two spherical mirrors having radii of curvature R_1, R_2, separated by a distance L.

This linear cavity consists of a double pass of the distance between the mirrors. Since the beam must replicate itself for successive passes over the cavity length, there will be nodes at the two mirrors and the two oppositely
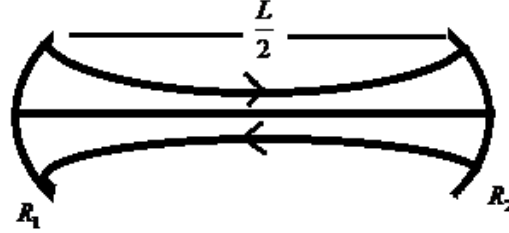
Figure 2.1: **Representation of Linear Cavity Resonator**

directed beams with equal amplitudes and frequencies comprise a standing wave.

2.1.2 Ring (or Traveling-wave) Resonator

Ring (or Traveling-wave) cavities are the ones where the light can do round trips in both the clock-wise and counter clock-wise directions.
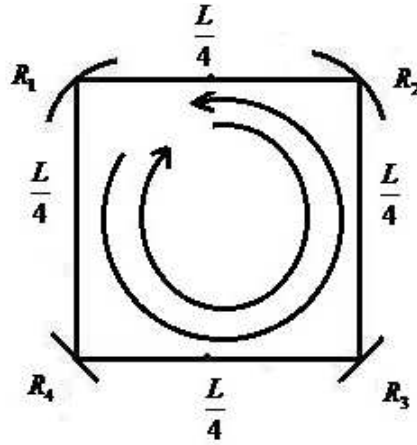
Figure 2.2: **Representation of Ring Cavity Resonator**

Fig. (2.2) shows a schematic representation of a square ring configuration,

with two spherical mirrors of radii R_1 and R_2 and two plane mirrors with radii R_3 and R_4. The two oppositely directed beams are traveling waves, and the node constraint at the mirrors no longer exists, thus they can be independent of each other and each can oscillate at a different frequency and different amplitude. In the absence of rotation, the set of modes traveling in the clockwise direction has a corresponding mode of the same frequency traveling in the counter clockwise direction, and then these matching modes are said to be degenerate. The oscillation frequency of each is determined by the optical path length. Thus any physical mechanism that causes the optical paths to be different for the two beams, results in the oscillation frequencies being different.

Therefore, the basic requirement for maintaining the steady state laser oscillation in either of the configurations is the round trip constancy of the amplitude and phase of the field in the cavity. The former is achieved by equilibrium of gain and loss while the later is a closure condition, which requires that the round trip phase shift must be a half integer $\frac{n}{2}$ multiple of 2π for linear cavity where as for ring cavity it must be an integer n multiple of 2π. This phase condition determines the frequency ν at which the laser can oscillate. The integer n is called the axial mode order. For visible region n is very high number.

The resonance frequencies are separated by a gap called free spectral range $FSR = \delta\nu = \dfrac{c}{2L}$ is for linear cavity, where L is the distance between the mirrors, $FSR = \delta\nu = \dfrac{c}{L}$ is for ring cavity, where L is the perimeter of the ring cavity with c being the speed of the light in vacuum.

Even though an understanding of resonator requires the knowledge of Fresnel diffraction theory [1-3], we use the simple form of bilinear transformation known as the 'ABCD law' which is proposed by Kogelnik [4, 5] to understand the propagation of optical rays through the optical elements contained in the resonator. The basic matrix formalism of the optical resonators

is presented in the following section.

2.2 Matrix Formalism

An optical resonator system is characterized by the 2×2 ray-transfer matrix relating the position and inclination of the transmitted ray to the incident ray in the paraxial ray-optics approximation. Let r_{in} and $r\prime_{in}$ be the position and inclination of an optical input ray. For a given r_{in} and $r\prime_{in}$, we determine r_{out} and $r\prime_{out}$ of the output ray by tracing the ray through the system. For paraxial rays, which are rays that make small angles with the optic axis z, the relation between $(r_{out}, r\prime_{out})$ and $(r_{in}, r\prime_{in})$ is linear and can be written in matrix form as

$$\begin{pmatrix} r_{out} \\ r\prime_{out} \end{pmatrix} = \begin{pmatrix} A & B \\ C & D \end{pmatrix} \begin{pmatrix} r_{in} \\ r\prime_{in} \end{pmatrix} \tag{2.1}$$

This analysis is restricted to the fundamental mode described by the Gaussian intensity profile.

In general, the solution of Maxwell equations for the scalar electric field $E(x, y, z)$ of the fundamental Gaussian beam can be written as

$$\begin{aligned} E(x, y, z) &= E_0 \frac{\omega_0}{\omega(z)} \\ &\times exp\left[-i\left[kz - \phi_G(z)\right]\right] \\ &\times exp\left[-r^2\left[\frac{1}{\omega^2(z)} + \frac{ik}{2R(z)}\right]\right] \end{aligned} \tag{2.2}$$

The expression Eq. (2.2) describes the behavior of the laser beam amplitude and phase as a function of the transverse coordinates x, y and the axial coordinate z. Here $q(z)$ is the complex beam parameter related to the radius of curvature $R(z)$ and spot size $\omega(z)$ of the beam at any plane z by

$$\frac{1}{q(z)} = \frac{1}{R(z)} - i\frac{\lambda}{\pi\omega^2(z)} \tag{2.3}$$

and $\phi_G(z)$ is the Gouy phase shift which deserves a special attention through out the thesis. The change or transformation of the q parameter as the beam traverses through optical systems can also be obtained using the $ABCD$ matrices as in the case of ray optics as given below.

$$q_{out} = \frac{Aq_{in} + B}{Cq_{in} + D} \tag{2.4}$$

where $\begin{pmatrix} A & B \\ C & D \end{pmatrix}$ is the product matrix of the individual matrices of lens like components occupying the space between the 'output' plane and the 'input' plane.

Now consider the self consistent treatment i.e., the beam should reproduce itself in shape, amplitude, and phase, after each round trip. This requires that the condition $q_{out} = q_{in} = q$ to be satisfied.

Solving Eq. (2.4) for q gives

$$q = \frac{(A - D) \pm \sqrt{(D - A)^2 + 4BC}}{2C} \tag{2.5}$$

The ray matrix is uni modular, that is using $AD - BC = 1$, Eq. (2.5) can be written as

$$q^{(\pm)} = \frac{A - D}{2C} \pm \frac{\sqrt{(A + D)^2 - 4}}{2C} \tag{2.6}$$

For the mode to stable, $\sqrt{(A + D)^2 - 4}$ should be imaginary. Simplifying the above Eq. (2.7)

$$q^{(\pm)} = \frac{A - D}{2C} \pm i \frac{\sqrt{1 - (\frac{A+D}{2})^2}}{C} \tag{2.7}$$

It is known that in free space the complex beam parameter q obeys the propagation law

$$q = z + iz_0 \tag{2.8}$$

where z_0 is the half Rayleigh range. We find by comparing the Eqs. (2.7), (2.8), the position of the spot size and the Rayleigh range in terms of the round trip matrix elements as

$$z = \frac{A - D}{2C} \tag{2.9}$$

$$z_0 = \frac{\sqrt{1 - (\frac{A+D}{2})^2}}{C} \tag{2.10}$$

From Eq. (2.10), the condition for a confined Gaussian beam is satisfied by either $q^{(+)}$ or $q^{(-)}$ provided

$$\left| \frac{A + D}{2} \right| \leq 1 \tag{2.11}$$

The condition in Eq. (2.11) is a generalized confinement condition to any arbitrary resonator. The spot size ω_0 at the reference plane is then given in terms of z_0, λ as

$$\omega_0 = \sqrt{\frac{\lambda z_0}{\pi}} \tag{2.12}$$

All the properties of the Gaussian beam are related to the beam waist radius ω_0 and the ratio $\dfrac{z}{z_0}$ as

$$\omega^2(z) = \omega_0^2 \left[1 + \left(\frac{z}{z_0} \right)^2 \right] \tag{2.13}$$

$$R(z) = z \left[1 + \left(\frac{\pi \omega_0^2}{\lambda z} \right)^2 \right] \tag{2.14}$$

$$\phi_G = \arctan \left(\frac{z}{z_o} \right) \tag{2.15}$$

By using the conditions which are given in Eqs. (2.12), (2.13), (2.14) and (2.15) one can check the stability criteria required for an optical cavity resonator and the corresponding Gaussian beam properties of the cavity. We study these conditions in detail for the considered resonators in the remaining chapters of the thesis.

Bibliography

[1] A. G. Fox and T. Li, "Resonant modes in an optical maser", Proc. IRE, vol. 48, pp.1904-1905, Nov 1960; "Resonant modes in a maser interferometer," Bell Sys. Tech. J., vol.40, pp. 489-508, Mar 1961.

[2] G. D. Boyd and J. P. Gordon, "Confocal multimode resonator for millimeter through optical wavelength masers," Bell Sys. Tech. J., vol. 40, pp. 489-508, Mar 1961.

[3] G. D. Boyd and H. Kogelnik, "Generalized Confocal resonator theory," Bell Sys. Tech. J., vol. 41, pp. 1347-1369, July 1962.

[4] H. Kogelnik, "Imaging of optical mode-Resonators with internal lenses," Bell Sys. Tech. J., vol. 44, pp. 455-494, Mar 1965.

[5] A. E. Siegman, Lasers, University Science Books, Mill Valley, CA, 1986.

3

Single Lens Ring Cavity

In this chapter a single-converging-unit ring cavity with acronym SCURC is considered. It consists of a lens L_1 of focal length F placed as shown in the Fig. (3.1) in a ring cavity of length L. This system can have under suitable condition Gaussian modes in it. Let fundamental Gaussian mode with half Rayleigh range z_{01} exist in it. The properties of the existing mode are analyzed in the following section.

3.1   Single Converging Unit Ring Cavity(SCURC)

As shown in the schematic Fig. (3.1), the considered SCURC configuration consists of four 100% plane mirrors M_1, M_2, M_3, M_4 in addition to the

lens L_1.

In order to analyze the modes inside the SCURC, round trip matrix has to be evaluated. To obtain the round trip matrix, assume that the starting point of the Gaussian mode is just before the mirror M_1. The beam gets reflected from mirror M_1, travels a distance of x before it strikes the thin lens L_1. It refracts through the lens, travels the remaining distance $(L - x)$, encountering the mirrors M_2, M_3, M_4 in the order, completes the round trip just before the mirror M_1 where it started its journey in the ring. This defines the coordinate x_p in the clockwise sense in the ring with M_1 at $x_p = 0$ and lens at $x_p = x$. For the Gaussian mode with half Rayleigh range z_{01}, the point x_0 $(x_p = x_0)$ determines the position of the beam waist ω_0. The thin
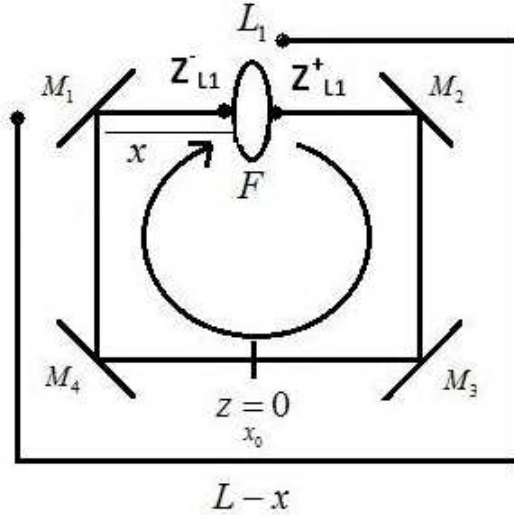
Figure 3.1: **A Single-Converging-Unit Ring Cavity (SCURC)**

lens L_1 is at $Z_{L1}^+ = x_0 - x$. Z_{L1}^+ is positive in anticlockwise direction of the ring, with $z > 0$ in the same direction with $z = 0$ at the beam waist. In the Gaussian mode (frame of reference) the thin lens L_1 is also placed at $Z_{L1}^- = -\left(L - (Z_{L1}^+)\right)$. Minus sign implies clockwise direction from $z = 0$, in

the frame of reference of the Gaussian mode.

The round trip $ABCD$-matrix at M_1, when lens is at a point x in the ring, is represented by

$$\begin{pmatrix} A & B \\ C & D \end{pmatrix} = \begin{pmatrix} 1 & L - x \\ 0 & 1 \end{pmatrix} \begin{pmatrix} 1 & 0 \\ -\frac{1}{F} & 1 \end{pmatrix} \begin{pmatrix} 1 & x \\ 0 & 1 \end{pmatrix} \tag{3.1}$$

$$\begin{pmatrix} A & B \\ C & D \end{pmatrix} = \begin{pmatrix} 1 - \dfrac{L - x}{F} & x + (L - x)\left(1 - \dfrac{x}{F}\right) \\ -\dfrac{1}{F} & 1 - \dfrac{x}{F} \end{pmatrix} \tag{3.2}$$

As discussed in the chapter-2 the self consistency requires

$$(A + D)^2 - 4 \leq 0 \tag{3.3}$$

Therefore, for the considered SCURC the marginal stability condition given by the equality sign in Eq. (3.3) gives

$$(A + D)^2 - 4 = \frac{L\,(L - 4F)}{F^2} = 0 \tag{3.4}$$

Solving for the stable L for a given F, one gets

$$L = 0 \tag{3.5}$$

or

$$L = 4F \tag{3.6}$$

Recall that in terms of the matrix elements the complex parameter $q_{M_1}[1]$ is given by

$$q_{M_1} = \frac{L}{2} - x \pm i\frac{\sqrt{L(4F - L)}}{2} \tag{3.7}$$

Equation (3.7) implies that the beam waist is at the position of the mirror M_1 if lens is placed at $x = \dfrac{L}{2}$ from it. For an arbitrary position x of the lens with respect to the mirror M_1 the beam waist is at x_0. The beam waist is $\dfrac{L}{2}$ away from the lens on each direction. It is also realized from the $ABCD$

matrix analysis, that to have a confined Gaussian mode $L \leq 4F$. Then only the half Rayleigh range z_{01} will be real and the stable mode can exist inside the ring.

The beam waist is obtained as

$$\omega_0 = \sqrt{\frac{\lambda}{2\pi}} \, [L(4F - L)]^{(1/4)} \qquad (3.8)$$

The beam aperture at any value of z can be estimated by using

$$\omega^2(z) = \omega_0^2 \left[1 + \left(\frac{z}{z_{01}} \right)^2 \right] \qquad (3.9)$$

The Gouy phase is $\phi_G(z) = \arctan\left(\dfrac{z}{z_{01}}\right)$ at a point z (z is the distance from the beam waist position i.e., $z = 0$).

Accumulated Gouy phase $\phi_G(RT)$ for one round trip in the cavity is

$$\phi_G(RT) = \phi_G\left(\frac{z + L}{z_{01}}\right) - \phi_G\left(\frac{z}{z_{01}}\right) = 2\arctan\left(\frac{L}{2z_{01}}\right) \qquad (3.10)$$

for all values of z in the cavity. The round trip Gouy phase $\phi_G(RT)$ is a variable using (3.10) and (3.11) below.

There can be two methods of varying z_{01} based on L and F. The first method chosen here is to keep F constant and vary L. In the plot which is shown in Fig. (3.2) L is varied from 0 to $4F$, for a fixed F=100cm. For this range of L, the parameters z_{01}, x_0 and $\phi_G(RT)$ are plotted in Fig. (3.2).

Eq. (3.7) of the half Rayleigh range z_{01} can be written as

$$z_{01}^2 + \left(\frac{L}{2} - F\right)^2 = F^2 \qquad (3.11)$$

which represents a circle$(x, y, a) = (L, 2z_{01}, F)$, with center at $(2F, 0)$ and radius $a = 2F$. Note that the position of the beam waist lies always at $x_p = \dfrac{L}{2}$, for all values of L. The half Rayleigh range z_{01} however varies from 0 to F as L is varied from 0 to $2F$; and reverts back from F to 0 as L goes
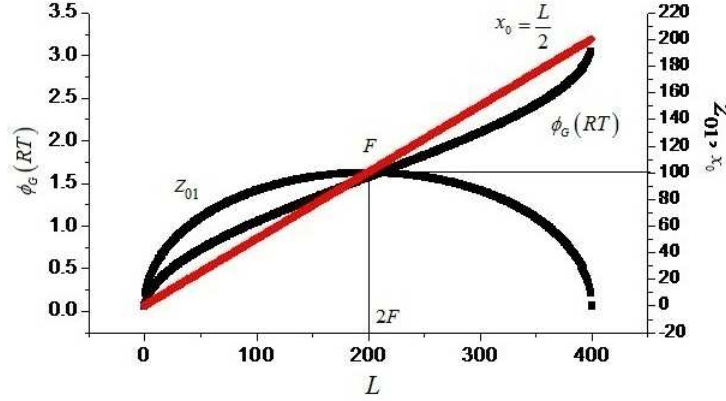
Figure 3.2: **Variation of x_0, z_{01}, $\phi_G(RT)$ as a function of length L for an example of F=100cm**

from $2F$ to $4F$. $\phi_G(RT)$ varies from 0 to π as L varies from 0 to $4F$. In the next section we use these data to design an experiment to characterize what may be called a structured point source.

3.2 A Consideration of two point Sources (i) A structured Point Source (ii) The Huygens' Point Source

It is proposed to consider here onwards the Gaussian mode - focal region - lying in between $-z_0$ to $+z_0$ with the beam waist ω_0 at $z = 0$ - as a structured point - of longitudinal dimension $2z_0$ and transverse dimension of $2\omega_0$. The solution of the wave equation inside the structured point is that of a fundamental Gaussian mode inside these dimensions. Interestingly size of the so-defined structured point is variable as depicted in Fig. (3.2). In order to compare the structured point with a real point source and also with

35

a Huygens point source (i.e., the point with secondary wavelets on a wave front) we presume that the mirror M_3 is partially transmitting such that a fraction of light that is enclosed inside the ring created with the help of a gain medium placed suitably in the ring, leaks out of the ring and interacts with another lens L_2 having the focal length and aperture exactly same as that of the lens L_1. The lens L_2 is supposed to be always at $\dfrac{L}{2}$ away from the centre of the structured point source. The just described improvisation is depicted in Fig. (3.3). The $ABCD$ transformation for the mode inside the cavity will be repeated by the lens L_2(for the transmitted portion as well) to recreate the Gaussian mode outside the ring. For exactly the distances depicted in the Fig. (3.3), the arrangement matches the plane of the beam waist after the lens L_2 with the plane of the waist of the beam inside the ring due to lens L_1 as shown. Thus for the improvised system we have - two structured points for the ring of length $L < 4F$, one inside the ring and the other outside the ring - created by exactly the same $ABCD$ matrix.

On the other hand if at the beam waist inside the cavity we place a real point source(a self luminous object of size less than $2\omega_0$), then, by the laws of geometrical optics, its image position v, for the object position of $u = \dfrac{L}{2}$, with respect to the lens L_2 is given by $v = \dfrac{LF}{L-2F} > (2F)$, which is way beyond the matching plane of the two beam waists, if $L < 4F$. On varying L in the Fig. (3.3) - for the ring and for the lens L_2 simultaneously; for $L < 2F$, one has the image on the same side as the object with respect to the lens L_2 - the image being virtual; and for $L > 2F$, the image is real and farther than $\dfrac{L}{2}$ on the other side of the lens L_2(See Fig. (3.4)). At $L = 4F$ the beam waist becomes zero and the structured point becomes a zero point-thus- there is creation of a real zero-size point source inside the ring and the image of this point then coincides with the point image created by the lens L_2, at $u = v = 2F = \dfrac{L}{2}$, exactly at the matching plane of the zero-beam-waist - inside and outside the ring in Fig. (3.3). Since, the beam
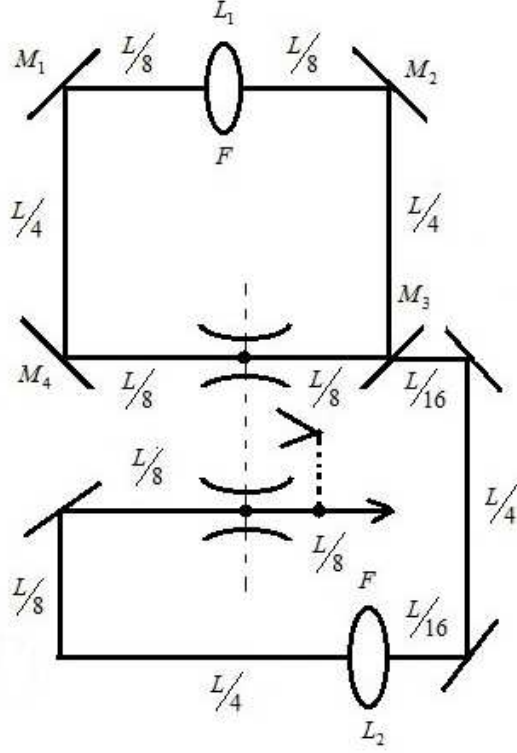
Figure 3.3: **An experiment set up to analyse the distinction between Huygens point source and a structured point source of a Gaussian beam. The black dot inside the ring can be a self illuminated point source while outside dots depict images of the inside dot**

waist has also been reduced from a surface (radius ω_0) to a point ($\omega_0 = 0$) it may be assumed that it can be compared with the supposed point source of Huygens. The $\omega_0 = 0$ point now has the entire intensity of the wave front picked up from the gain medium, it is concentrated on the point of the wave front. This point now represents the entire wave front- this is not like a point source created by a variable aperture placed ahead of the wave front as a diffracting point gate. In that case the intensity on the gate is reduced

37
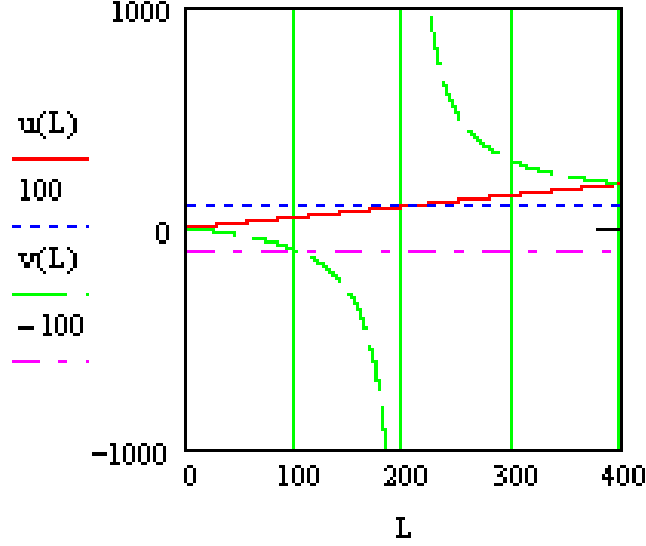
Figure 3.4: **The positions $u(-)$ of the object and $v(--)$ of the image with respect to lens L_2 are plotted as a function of length L of the ring**

in proportion, by the fraction given by the ratio of the area of the aperture to the area of the wave front on which the entire intensity is spread.

It is interesting to compare the point source obtained at $L = 4F$, and the properties of the structured point behaviour as $(4F - L) \rightarrow +0$, with the Huygens point source. This is due to a lively debate in the literature on three counts. Firstly, the Huygens point source itself[2]; secondly the mysterious phase it must have[3], and thirdly the Gouy phase being poorly understood[4].

We come back to this comparison later in the thesis- here we digress and note (a) that the wave front at $z = 0$ is a perfect plane wave, (b) that at $z = \infty$ it has the same behaviour of the amplitude as that of an out going spherical wave at large distance from point source i.e., similar to a plane wave

but reduced in intensity by the inverse square law rule(check $\lim z \gg z_0$ on Eq. 2.2), and (c) that the field at ∞ $(z \gg z_0)$ is ahead in phase compared to that field that one has at $z = 0$, by $\left(exp^{\frac{i\pi}{2}} \right)$. These properties arise due to Fresnel-Stokes-Kirchhoff integral representation of the solution of the scalar wave equation. Just as it does in the Fresnel zone plate analysis presented on pages 371-375 in the book by Born and Wolf. Note further that this difference in phase occurs naturally as a limit of Gouy phase. We note that the Gouy phase of the round trip in SCURC can be varied and that this is a consequence of the diffraction theory by Huygens[5]-Fresnel[6]-Stokes[7]-Kirchhoff[8].

While all that is noted above, besides the improvised experimental arrangement shown in Fig. (3.3), is well known in literature, it is important to attempt in this thesis, with respect to the optics inside and outside the ring, to have a relook at the assumption of Huygens and the analysis that followed due to Fresnel, Stokes, Kirchhoff, and the modern analysis in terms of Gaussian beams - strongly driven - initially on the basis of numerical analysis (Fox-Li[9], Goubau-Schwering[10], Boyd-Gordon[11], Boyd-Kogelnik[12]) and later analytically too (Kogelnik[13], Yariv[1])- based on the formalism due to the Huygens-Fresnel-Stokes-Kirchhoff-Fraunhoffer. The analysis of the experiment inspired by the formalism of images of optical modes presented by Kogelnik[14] is also discussed in chapter VII.

We discuss next an alternative way of varying Gouy phase in a ring cavity. The second method of creating the variable Gouy phase is to keep L constant vary F. From the stability condition of the cavity, it is learned that $L \leq 4F$. Therefore for a fixed L, the focal length has to be $F \geq \dfrac{L}{4}$. The parameters z_{01}, x_0 and $\phi_G \left(RT \right)$ are plotted as shown in the Fig. (3.5) for a fixed L=400cm, varying F.

The half Rayleigh range z_{01} increases with F and increases linearly for large values of F. This method also shows that the position of the beam
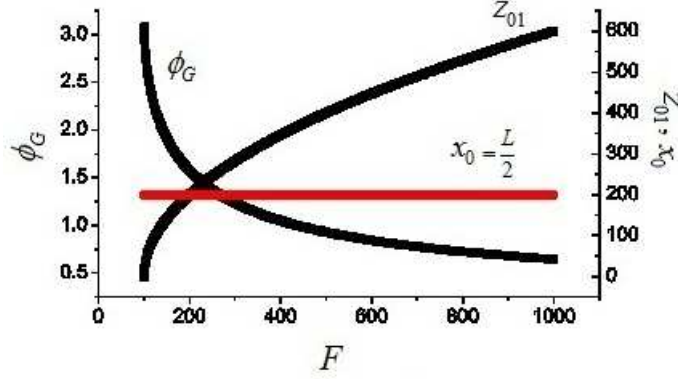
Figure 3.5: **Variation of x_0, z_{01}, $\phi_G\,(RT)$ as a function of focal length F for an example of L=400cm**

waist lies at $x_p = \dfrac{L}{2}$, for all values of F. As F varies from $\dfrac{L}{4}$ to $10\dfrac{L}{4}$, the accumulated Gouy phase is varying from π to 0.645.

On noting the existence and variability of Gouy phase the questions that emerge are

- (a) Can variable Gouy phase be used to tune a ring laser cavity output? And what may the uses of it be, if possible?

- (b) Are the phases, (i) the mysterious phase of Huygens point source and (ii) the variable Gouy phase of the structured point source-similar or equivalent?

We take up the questions in (a) on variability and its uses in the chapters 4, 5, and 6. We discuss some important conclusions which are drawn from the above improvisation in the 7th chapter of the thesis, to discuss the answers to the questions in (b).

In the next chapter we consider two converging unit ring cavity - in an attempt to vary the effective focal length inside the ring by keeping two lenses

separated by a variable distance between the two.

Bibliography

[1] A. Yariv, ***Quantum Electronics***, Third Edition, John Wiley& Sons Inc, 1988.

[2] Bevan B Baker and E. T. Copson, ***The Mathematical Theory of Huygens' Principle***, Oxford University Press, 1939.

[3] Max Born and Emil Wolf, ***Principles of Optics***, Sixth (Corrected) Edition, Pergamon Press, 1984.

[4] T. D. Visser, E. Wolf, "The origin of the Gouy phase anomaly and its generalization to astigmatic wave fields," Optics communications 283, Issue 18, pp. 3371-3375, Sep 2010.

[5] Chr. Huygens, Traite de la Lumiere (completed in 1678, published in Leyden in 1690).

[6] A. Fresnel, Ann Chim et Phys, (2), 1 (1816), Oeuvres, Vol.1, 89, 129

[7] Stokes, "Dinamical Theory of Diffraction," Trans. Camb. Phil. Soc. 9(1849), 1; Math. and Phys. Papers, 2, 243.

[8] G. Kirchoff, Berl. Ber (1882), 641; Ann d Physik (2), 18(1883), 663.

[9] A. G. Fox and T. Li, "Resonant modes in an optical maser", Proc. IRE, vol. 48, pp. 1904-1905, Nov 1960; "Resonant modes in a maser interferometer," Bell Sys. Tech. J., vol. 40, pp. 489-508, Mar 1961.

[10] G. Goubau, F. Schwering, "On the guided propagation of electromagnetic wave beams," IRE Trans. Antennas Propag. Ap-9, pp. 248-256, 1961.

[11] G. D. Boyd and J. P. Gordon, "Confocal multimode resonator for millimeter through optical wavelength masers," Bell Sys. Tech. J., vol. 40, pp. 489-508, Mar 1961.

[12] G. D. Boyd and H. Kogelnik, "Generalized Confocal resonator theory," Bell Sys. Tech.J., vol. 41, pp. 1347-1369, July 1962.

[13] H. Kogelnik and T. Li, "Laser beams and Resonators," Appl. Opt, vol. 5, pp. 1550-1567, Oct 1966.

[14] H. Kogelnik, "Imaging of optical mode-Resonators with internal lenses," Bell Sys. Tech. J., vol. 44, pp. 455-494, Mar 1965.

4

Two Lens Ring Cavity

It is understood from the analysis of a single converging unit ring cavity (SCURC) that, the Gouy phase of the single Gaussian mode which exists inside the cavity can be varied by using two methods. The first method is to keep the focal length F constant and vary the length of the ring L. The second method is to keep the length L constant and vary the focal length F. It is possible to vary the focal length F in the cavity for a SCURC, by using the variation in the refractive index of the lens electro optically, which is too small to vary focal length in a range of interest in this chapter. In the present chapter we consider a two converging unit ring cavity with acronym 2CURC. It consist of two lenses L_1 and L_2 as shown in Fig. (4.1), which can accommodate two Gaussian modes in the cavity, when the lenses

are separated by a finite distance. If the separation distance is zero, i.e., when the two lenses are joined together, this 2CURC behaves like a SCURC with an effective focal length $F_{eff} = \dfrac{f_1 f_2}{f_1 + f_2}$, under the stability condition $L < L_{eff} = 4 F_{eff}$. One could imagine the variation of focal length of the two lenses in the manner considered in Fig. (3.1) of the last chapter, for a given length L. However we choose to vary the effective focal length inside the ring by varying the separation distance between the two lenses. In this case variation of accumulated Gouy phase per round trip $\phi_G (RT)$ becomes possible in a new way without changing the length of cavity. However before we discuss the $\phi_G (RT)$ behavior we need to study the different cases of the stable mode that can exist for 2CURC. The stability and properties of such 2CURC are discussed in the sections 4.1 to 4.4. We return to the discussion of $\phi_G (RT)$ in 4.5.

4.1   2 Converging Unit Ring Cavity (2CURC)

A schematic of the two converging unit ring cavity (2CURC) of the length L, consisting of two lenses L_1 and L_2 of focal lengths f_1 and f_2, which are separated by a distance d_1, is shown in Fig. (4.1). Here the mirrors M_1, M_2, M_3 and M_4 are 100% plane mirrors. There exist two Gaussian modes, one in the arm of length d_1 in between the lenses L_1 and L_2 and the second mode in the arm of length $L - d_1$ on the other side in between the lenses L_2 and L_1. The Gaussian beams in the respective sections constitute a part of stable configuration of radiation-travel in the ring, with half Rayleigh ranges z_{0s} in d_1 arm and z_{0b} in the $L - d_1$ arm; with waist locations x_{0s}, x_{0b} respectively. Each Gaussian mode contributes its Gouy phase to the round trip Gouy phase in the ring. To vary $\phi_G (RT)$ the sum of the Gouy phases of the two parts of the 2CURC by varying the effective focal length, we vary the distance d_1 between the two lenses L_1 and L_2.
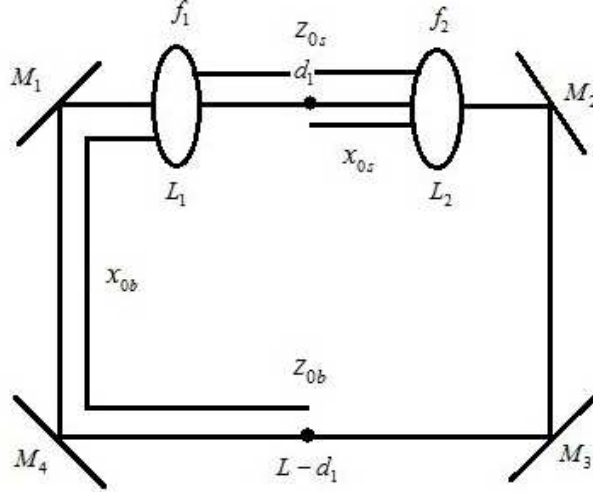
Figure 4.1: **2 Converging Unit Ring Cavity(2CURC)**

For consideration of stability of this configuration let the radiation just enter before the lens L_1 of focal length f_1 and refract through the lens L_1 in the clockwise direction, travel through a distance d_1 from the lens L_1, as it strikes another lens L_2 of the focal length f_2, refract through the lens L_2, reflecting off the mirrors M_2, M_3, M_4, M_1 in that order, travel through the distance $(L - d_1)$ to complete the round trip just before the lens L_1 where it started its journey in the ring.

We define here the coordinate x_p in the clockwise sense in the ring with L_1 at $x_p = 0$ and lens L_2 at $x_p = d_1$. For the two Gaussian modes with half Rayleigh ranges z_{0s}, z_{0b}, the points x_{0s} $(x_p = d_1 - x_{0s})$ and x_{0b} $(x_p = L - d_1 - x_{0b})$ determine the positions of the beam waists ω_{0s} and ω_{0b}.

The round trip $ABCD$-matrix at the entrance to the lens L_1 in the ring for this case is represented by

$$\begin{pmatrix} A & B \\ C & D \end{pmatrix} = \begin{pmatrix} 1 & L - d_1 \\ 0 & 1 \end{pmatrix} \begin{pmatrix} 1 & 0 \\ -\frac{1}{f_2} & 1 \end{pmatrix} \begin{pmatrix} 1 & d_1 \\ 0 & 1 \end{pmatrix} \begin{pmatrix} 1 & 0 \\ -\frac{1}{f_1} & 1 \end{pmatrix} \tag{4.1}$$

after simplification

$$\begin{pmatrix} A & B \\ C & D \end{pmatrix} = \begin{pmatrix} 1 - \frac{d_1}{f_1} + (L - d_1)\left\{-\frac{1}{f_2} + \frac{d_1}{f_1 f_2} - \frac{1}{f_1}\right\} & d_1 + (L - d_1)\left\{-\frac{d_1}{f_2} + 1\right\} \\ -\frac{1}{f_2} + \frac{d_1}{f_1 f_2} - \frac{1}{f_1} & 1 - \frac{d_1}{f_2} \end{pmatrix}$$

(4.2)

The self consistency requires that

$$(A + D)^2 - 4 \leq 0$$

(4.3)

Taking the marginal stability case of Eq. (4.3), we have two alternatives

$$(A + D) + 2 = 0$$

(4.4)

$$(A + D) - 2 = 0$$

(4.5)

For the considered system the first marginal stability function (4.4) in terms of the system parameters d_1, L, f_1 and f_2 is obtained as

$$-\frac{d_1^2 - 4 f_1 f_2 - d_1 L + f_1 L + f_2 L}{f_1 f_2} = 0$$

(4.6)

which can be written as

$$-\frac{1}{f_1 f_2}\left[\left(d_1 - \frac{L}{2}\right)^2 - \left(\frac{p}{2}\right)^2\right] = 0$$

(4.7)

where $p^2 = (L - 4 f_1)(L - 4 f_2)$.

The second marginal stability condition (4.5) becomes

$$-\frac{d_1^2 - d_1 L + (f_1 + f_2)L}{f_1 f_2} = 0$$

(4.8)

and it can be written as

$$-\frac{1}{f_1 f_2}\left[\left(d_1 - \frac{L}{2}\right)^2 - \left(\frac{m}{2}\right)^2\right] = 0$$

(4.9)

where $m^2 = L(L - 4f_1 - 4f_2)$. The Eqs. (4.6) and (4.8) are parabolic in nature with respect to d_1. With respect to the common axis of symmetry $d_1 = \dfrac{L}{2}$, the two parabolas are

$$\left(d_1 - \frac{L}{2}\right)^2 = \left(\frac{L}{2}\right)^2 + 4f_1 f_2 - (f_1 + f_2)L \tag{4.10}$$

$$\left(d_1 - \frac{L}{2}\right)^2 = \left(\frac{L}{2}\right)^2 - (f_1 + f_2)L \tag{4.11}$$

We use (4.10) and (4.11) to analyse the stability condition (4.3) which simplifies to

$$(A + D)^2 - 4 = \frac{(d_1^2 - d_1 L + (f_1 + f_2)L)\,(d_1^2 - d_1 L + f_2 L + f_1(-4f_2 + L))}{f_1^2 f_2^2} \tag{4.12}$$

Consider the case when $d_1 = 0$. Then the stability function (4.10) becomes

$$(A + D)^2 - 4 = -4 + \left(1 + \frac{f_1\,(f_2 - L) - f_2 L}{f_1 f_2}\right)^2 \tag{4.13}$$

Solving for marginal stability case one gets solutions of L as

$$L = 0 \tag{4.14}$$

or

$$L = \frac{4f_1 f_2}{f_1 + f_2} = L_{eff} \tag{4.15}$$

The stable L given by (4.14) and (4.15) for the case of $d_1 = 0$ of 2CURC exactly match with the stable L of SCURC which are given by (3.5) and (3.6), with $L_{eff} = \dfrac{4f_1 f_2}{f_1 + f_2}$, which has been already shown in the Fig. (3.2). For $f_1 = 50$cm, $f_2 = 100$cm, for the cases of $L = 0$cm and $L = L_{eff} = 133.3333$cm, the function (4.12) is plotted in the Fig. (4.2). It is noted that there is a common solution of d_1 i.e., $d_1 = 0$cm, for (4.14) as well as (4.15), for which the considered 2CURC behaves as a SCURC. However, for $L = L_{eff}$
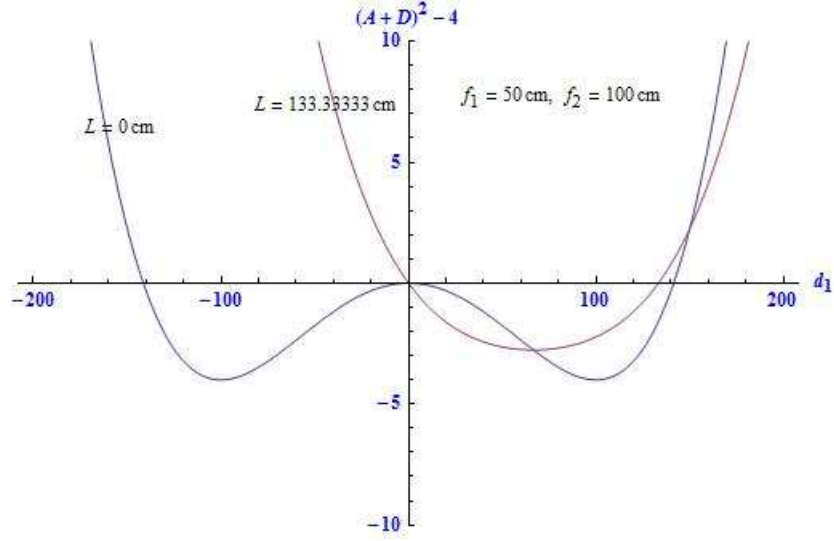
Figure 4.2: **For $f_1 = 50$cm, $f_2 = 100$cm, the stability function $(A + D)^2 - 4$(4.12) is plotted with** d_1 for $L = 0$cm, and $L = 133.3333$cm.

there is a range of d_1 available $0 < d_1 < L_{eff}$. This raises several questions. What happens when the two lenses are separated by a finite distance d_1? What are the conditions on L, to get the real values of d_1, for which the considered 2CURC is to be stable? For finite d_1, can we have L to be larger than L_{eff}? To answer these questions we analyze the condition (4.12) for finite d_1, in the following way.

4.1.1   Stable solutions for a range of d_1 for a given L, f_1 and f_2

For a given cavity length L, and for fixed f_1 and f_2 we look for the solutions of d_1 satisfying the stability function (4.12). It is noted that the stability function is quartic polynomial in d_1. If we look for the marginal stability of (4.12) with respect to d_1, then we get four solutions of d_1, two of

which are from (4.4) and the other two are from (4.5). From (4.4) one has

$$d_{1_+}^{(1,2)} = \frac{L}{2} \pm \frac{p}{2} \tag{4.16}$$

For $d_{1_+}^{(1,2)}$ to be real one requires (i) $L \leq 4f_1$ and (ii) $L \leq 4f_2$. Similarly from (4.5) one has

$$d_{1_-}^{(1,2)} = \frac{L}{2} \pm \frac{m}{2} \tag{4.17}$$

Here $L \geq 4f_1 + 4f_2$, for $d_{1_-}^{(1,2)}$ to be real. From the above it is clear that, for 2CURC to become stable for real $d_1 > 0$, one can have (unlike SCURC) L to be greater than L_{eff}. Specifically for an illustration, for $f_1 = 50$cm, $f_2 = 100$cm, $L = 700$cm, the stability function (4.12), and the two parabolas (4.10), (4.11) with respect to $d_1 = \frac{L}{2}$ are plotted in the Fig. (4.3). The stability function i.e., the product of $(A + D + 2)$ and $(A + D - 2)$ is an inverted parabola, inverted with respect to individual parabolas of $A + D \pm 2$. It changes sign with the signs of these two parabolas as shown. The above four solutions $d_{1_+}^{(1)}, d_{1_+}^{(2)}, d_{1_-}^{(1)}, d_{1_-}^{(2)}$ are identified in the Fig. (4.3). To know the behaviour of the function (4.12) further, we determine its extremum points by taking the partial derivative with respect to d_1,

$$\begin{aligned} \frac{\partial}{\partial d_1} \left[(A + D)^2 - 4 \right] &= \frac{2\left(d_1 - \frac{L}{2}\right)}{f_1^2 f_2^2} \\ &\quad \left\{ 2\left(d_1 - \frac{L}{2}\right)^2 - \left(\frac{m}{2}\right)^2 - \left(\frac{p}{2}\right)^2 \right\} \\ &= 0 \end{aligned} \tag{4.18}$$

The solutions of d_1 obtained from (4.18) are

$$d_1 = \frac{L}{2} \tag{4.19}$$

$$d_1 = \frac{L}{2} \pm \frac{1}{2}\sqrt{\frac{m^2 + p^2}{2}} \tag{4.20}$$
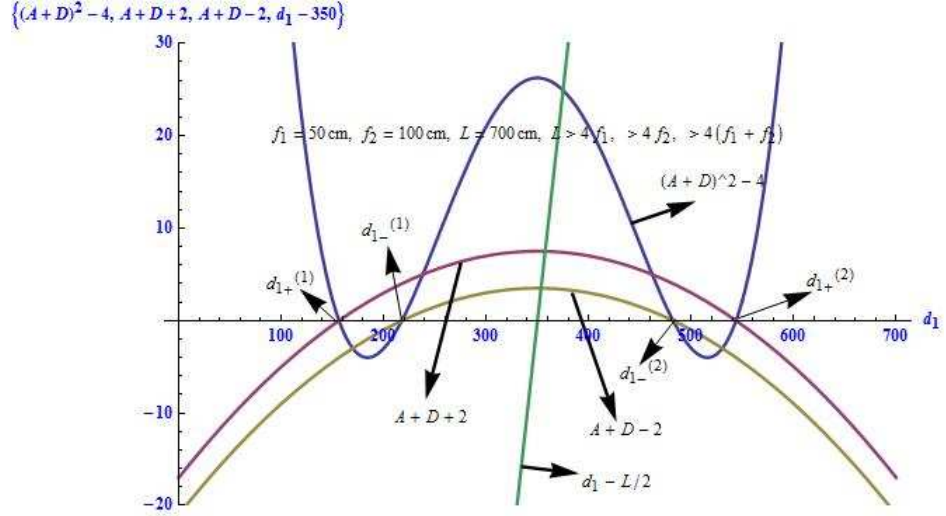
Figure 4.3: **For $f_1 = 50$cm, $f_2 = 100$cm, $L = 700$cm, the stability functions $(A + D)^2 - 4$(4.12), $A + D + 2$(4.8), $A + D - 2$(4.9) with respect to $d_1 = \dfrac{L}{2}$.**

The three extremas of (4.12) are displayed in Figs. (4.4), (4.6), (4.9) for different cases to be considered below. To analyse further systematically we note that the value of (4.12) at $d_1 = \dfrac{L}{2}$ determines the height H_1 from axis d_1 of the central extremum. We have

$$H_1 = \frac{p^2 m^2}{16 f_1^2 f_2^2} \tag{4.21}$$

which in terms of the positions of the extremas can be written as

$$H_1 = \frac{L(L - L_M)(L - L_{M1})(L - L_{M_2})}{16 f_1^2 f_2^2} \tag{4.22}$$

where $L_{M1} = 4f_1$, $L_{M2} = 4f_2$ and $L_M = (L_{M1} + L_{M2})$. One can look also for the values of L, at which the three extremas (4.19& 4.20) become one, which happens at $p^2 + m^2 = 0$, which occurs at $L = L_{H_{min1}}$; $L_{H_{min2}}$ where,

$$L_{H_{min1,2}} = \frac{(L_M) \mp \sqrt{L_{M1}^2 + L_{M1}^2}}{2} \tag{4.23}$$

At these values of L, H_1 is minimum, ($H_1 = -4$). These lengths are useful in distinguishing between two behaviours of the curve (4.12) as a function of d_1 discussed below. Carrying the analysis further with the help of H_1 one observes that $H_1 \gtrless 0$. We classify cases using H_1.
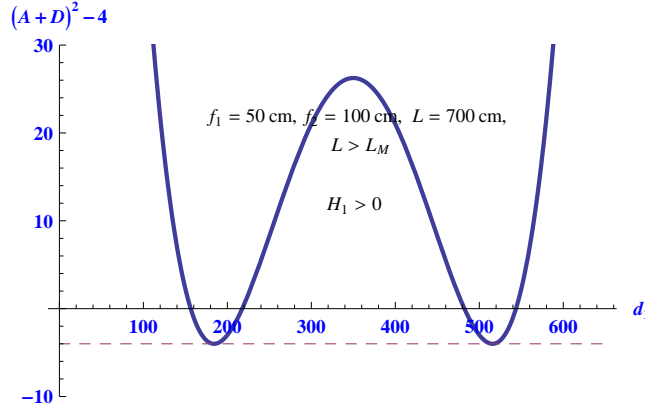
Figure 4.4: **For $f_1 = 50$cm, $f_2 = 100$cm, $L > L_M = 700$cm, the stability function $(A + D)^2 - 4$(4.12) is plotted which $H_1 > 0$.**

1. H_1 can be positive for two cases.

    1(a). The first case [1] is for $L > L_M$, for which there are two unconnected stable regions as shown in the Fig. (4.4). In this case there exist four solutions of d_1.

    1(b). The second case is for $L_{M1} < L < L_{M2}$. Interestingly, there is no stable region of d_1 at all in this region(as no portion of the curve lies below the d_1- axis.) and of no use to us because it does not contribute any Gouy phase to $\phi_G(RT)$. It is plotted in the Fig. (4.5) and marked as forbidden zone in Fig. (4.16).

---

[1]Specific cases appear in the summary of different cases prepared and presented in Fig. (4.16).
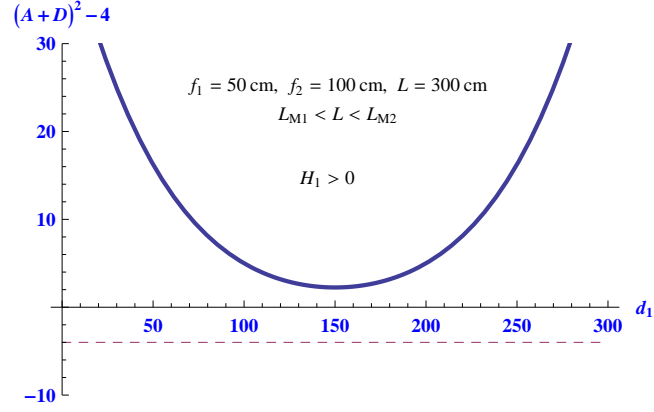
Figure 4.5: **For $f_1 = 50$cm, $f_2 = 100$cm, $L = 300$ $(L_{M1} < L < L_{M2})$cm, the stability function $(A + D)^2 - 4$(4.12) is plotted for which $H_1 > 0$.**
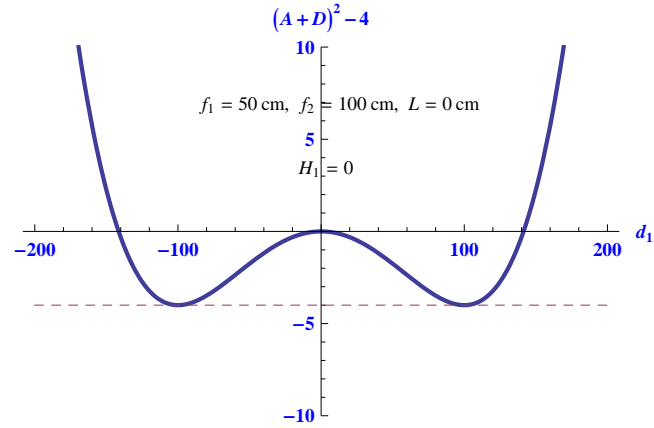
Figure 4.6: **For $f_1 = 50$cm, $f_2 = 100$cm, $L = 0$cm, the stability function $(A + D)^2 - 4$(4.12) is plotted for which $H_1 = 0$.**

2. H_1 can be zero for the cases when $L = 0$ or $L = L_{M1}$ or $L = L_{M2}$ or $L = L_M$.

2(a). As it is not possible to have a cavity of zero length, we do not consider the case $L = 0$cm but for demonstration we show in Fig.
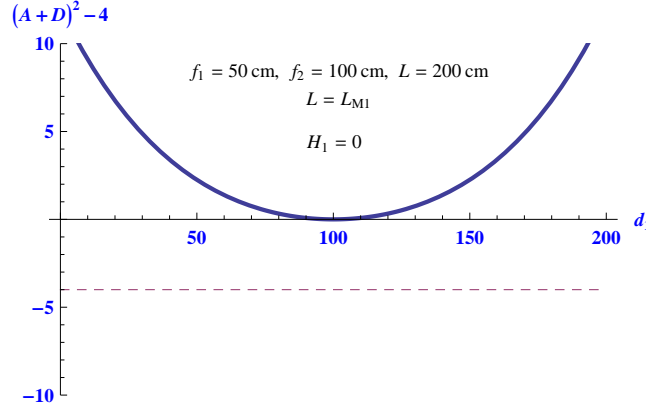
Figure 4.7: **For $f_1 = 50$cm, $f_2 = 100$cm, $L = L_{M1} = 200$cm, the stability function $(A + D)^2 - 4$(4.12) is plotted for which $H_1 = 0$.**
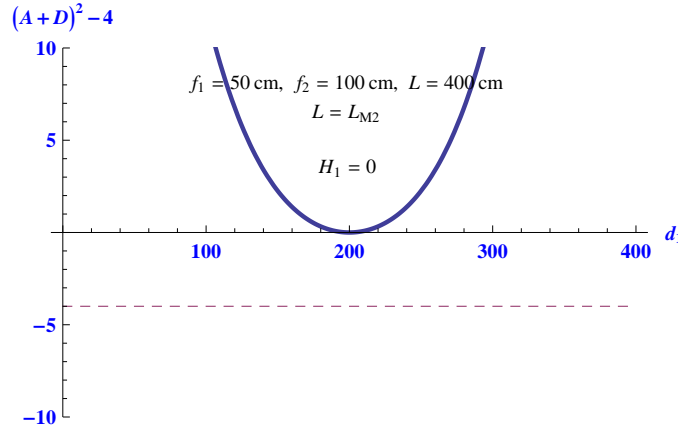
Figure 4.8: **For $f_1 = 50$cm, $f_2 = 100$cm, $L = L_{M2} = 400$cm, the stability function $(A + D)^2 - 4$(4.12) is plotted for which $H_1 = 0$.**

(4.6). Only positive values of d_1 make sensible solution. However these solutions are not of any practical use since $L = 0$.

2(b). For both the cases $L = L_{M1}$ and $L = L_{M2}$, there exists only one real solution of d_1 i.e., $d_{1+}^{(1)} = d_{1+}^{(2)} = \dfrac{L}{2}$ and the other two solutions

$d_{1-}^{(1)} = d_{1-}^{(2)}$ are complex as shown in the Figs. (4.7), (4.8). These solutions are of no use to us being positive unstable regions.

2(c). For $L = L_M$ there exit three solutions of d_1, and are given by

$$d_{1+}^{(1,2)} = \frac{L_M}{2} \pm \frac{\sqrt{L_{M1} L_{M2}}}{2} \qquad (4.24)$$

$$d_{1-}^{(1,2)} = \frac{L_M}{2} \qquad (4.25)$$

These three solutions are shown in the Fig. (4.9). Entire $d_{1+}^{(1)} < d_1 < d_{1+}^{(2)}$ is of relevance and realizable in practice.
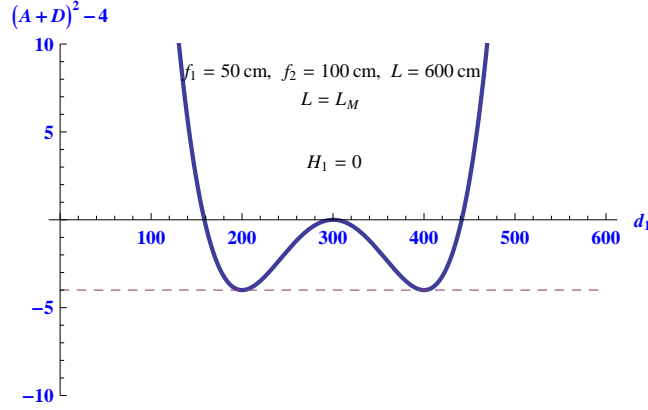
Figure 4.9: **For $f_1 = 50$cm, $f_2 = 100$cm, $L = L_M = 600$cm, the stability function $(A + D)^2 - 4$(4.12) is plotted for which $H_1 = 0$.**

3. H_1 can be negative for the following six cases, shown in respective figures indicated below.

3(a). $L_{H_{min2}} < L < L_M$ (see Fig. (4.10)).

3(b). $0 < L < L_{eff}$ (see Fig. (4.11)).

3(c). $L = L_{eff}$ (see Fig. (4.12)).

3(d). $L_{Hmin1} < L < L_{eff}$ (see Fig. (4.13)).
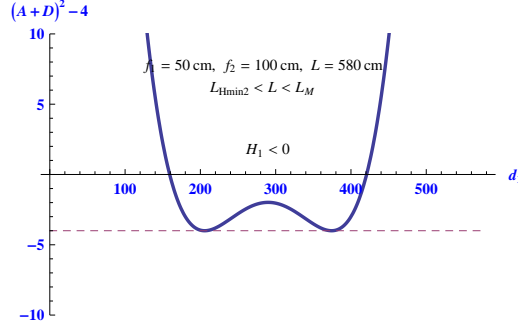
Figure 4.10: **For $f_1 = 50$cm, $f_2 = 100$cm, $L = 580$cm, where $L_{H_{Min2}} < L < L_M$, the stability function $(A+D)^2 - 4$(4.12) is plotted for which $H_1 < 0$.**
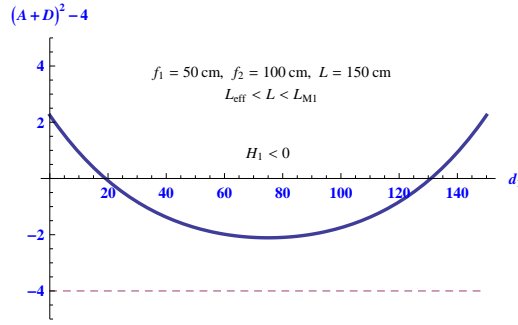
Figure 4.11: **For $f_1 = 50$cm, $f_2 = 100$cm, $L = 150$cm, where $L_{eff} < L < L_{M1}$, the stability function $(A + D)^2 - 4$(4.12) is plotted for which $H_1 < 0$.**

3(e). $L = L_{H_{min1}}$ (see Fig. (4.14)).

3(f). $L = L_{H_{min2}}$ (See Fig. (4.15)).

For the above six cases there exist a stable region $d_{1+}^{(1)} < d_1 < d_{1+}^{(2)}$ of d_1, for which a continuous variation of round trip Gouy phase $\phi_G\left(RT\right)$ is possible and for the last two of them one can have nearly linear variation of round trip Gouy phase $\phi_G\left(RT\right)$.
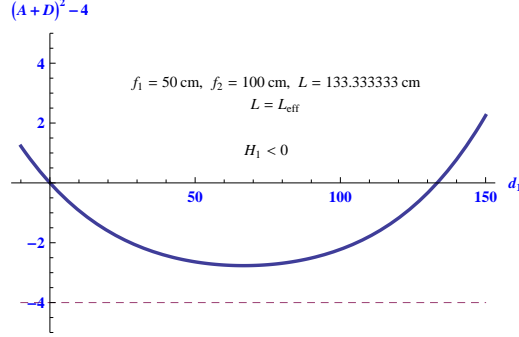
Figure 4.12: **For $f_1 = 50$cm, $f_2 = 100$cm, $L = 133.33333\,(L_{eff})$cm, the stability function $(A+D)^2 - 4$(4.12) is plotted for which $H_1 < 0$.**
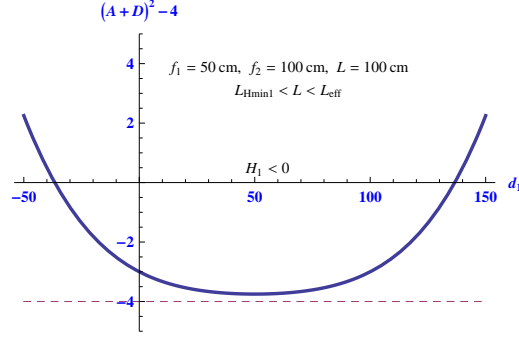
Figure 4.13: **For $f_1 = 50$cm, $f_2 = 100$cm, $L = 100(L_{Hmin1} < L < L_{eff})$cm, the stability function $(A+D)^2 - 4$(4.12) is plotted for which $H_1 < 0$.**

The value of the stability function (4.12) at $d_1 = \dfrac{L}{2} \pm \dfrac{1}{2}\sqrt{\dfrac{m^2 + p^2}{2}}$, (4.20) gives the height from the axis of d_1 to the local minimum of the function. It is estimated as $H_1 = -4$ at both the values of d_1(4.20) and it is fixed only for the cases satisfying $L > 4f_1$ and $L > 4f_2$ of chart in the Fig. (4.16) (see Figs. (4.4), (4.6), (4.9), (4.10)).

In summary the cases Fig. (4.4)-(4.15) are consolidated in Fig. (4.16), with appropriate specifications. For the first three cases of L from the top $L <$
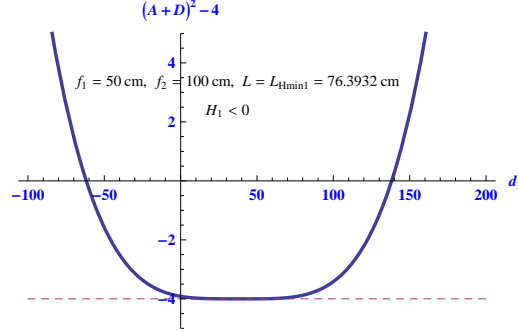
Figure 4.14: **For $f_1 = 50$cm, $f_2 = 100$cm, $L = L_{Hmin1} = 76.3932$cm, the stability function $(A + D)^2 - 4$(4.12) is plotted, for which $H_1 < 0$.**
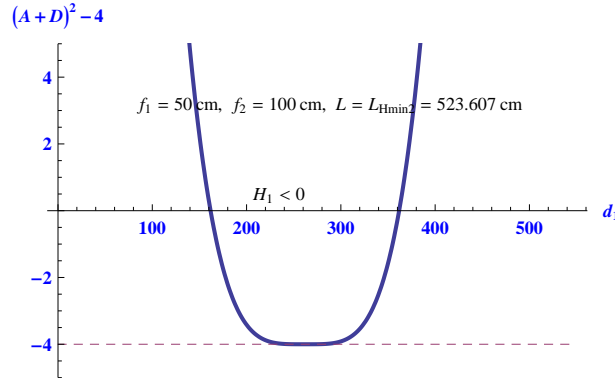
Figure 4.15: **For $f_1 = 50$cm, $f_2 = 100$cm, $L = L_{Hmin2} = 523.607$cm, the stability function $(A + D)^2 - 4$(4.12) is plotted, for which $H_1 < 0$.**

L_{eff} for which 2CURC behaves as a SCURC, and for the remaining cases $L \geq L_{eff}$. This is the new result of 2CURC. It is also noted that the region of L, i.e., $L_{M1} < L < L_{M2}$ is a forbidden zone where one can not have any stable range of d_1, for $f_1 < f_2$.

Before we discuss the Gouy phase behavior in each of these cases we first consider symmetric case i.e., $f_1 = f_2 = f$ case below and analyse its stability and modes in the d_1 and $L - d_1$ arms.

Figure 4.16: **The possible cases of L with respect to f_1 and f_2 for the case $f_1 < f_2$.**

4.1.2 Symmetric case of focal lengths $f_1 = f_2 = f$

For the symmetric case $f_1=f_2=f$, the four solutions of d_1 (4.16-4.17) become

$$d_{1+}^{(1)} = 2f \tag{4.26}$$

$$d_{1+}^{(2)} = L - 2f \tag{4.27}$$

$$d_{1-}^{(1)} = \frac{1}{2}\left(L - \sqrt{L^2 - 8fL}\right) \tag{4.28}$$

$$d_{1-}^{(2)} = \frac{1}{2}\left(L + \sqrt{L^2 - 8fL}\right) \tag{4.29}$$

Therefore for the reality of the roots the conditions on L for this symmetric case are $L \geq 2f$ and $L \geq 8f$. For a given f, one has to look for the stable domain of d_1 and L. We construct the three dimensional stability diagram in Fig. (4.17), where $[(A + D)^2 - 4]$(4.12) is along z axis, while d_1 and L are respectively along x and y axes, for a fixed $f = 30$cm. It is observed from the

(a) **Side view of the plot**   (b) **Top view of the plot(a)**
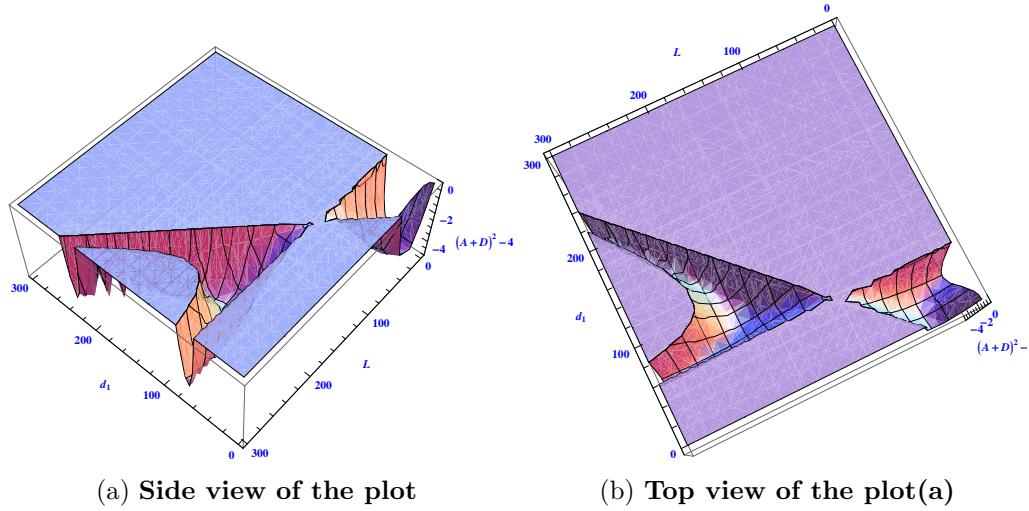
Figure 4.17: **Stability diagram -ve region of (4.12) as a function of d_1 and L for a fixed $f = 30$cm in the side view and top view. See text for description.**

Fig. (4.17a) that initially for small values of L, there is a very small stable region of $d_1 > 0$; as L increases there exist one continuous stable region of d_1. At $L = 120$cm, i.e., at $4f$ there exists only one solution of d_1. Again from $L = 121$cm onwards there is one stable continuous region of d_1 and at $L = 240$cm, it gives three stable solutions of d_1. As L increases beyond this, there will be two unconnected stable regions. The Fig. (4.17a) is rotated in the Fig. (4.17b) for additional clarity. These diagrams are indicative of the type of stability surface one encounters in the analysis of such cases.

4.1.3   Stable solutions of f_1 and f_2 for a given L and d_1

The stable solutions of the focal lengths f_1 and f_2 for a given L and d_1 are discussed as the following. Solving (4.4) for f_2 in terms of d_1, L and f_1

$$f_2^{(+)} = \frac{d_1^2 - d_1 L + f_1 L}{4f_1 - L} \tag{4.30}$$

Solving (4.5) for f_2

$$f_2^{(-)} = \frac{-d_1^2 + d_1 L - f_1 L}{L} \tag{4.31}$$

In terms of radius of curvatures R_1, R_2 i.e., $f_1 = \dfrac{R_1}{2}$, and $f_2 = \dfrac{R_2}{2}$

$$R_2^{(+)} = \frac{-2d_1^2 + 2d_1 L - LR_1}{L - 2R_1} \tag{4.32}$$

$$R_2^{(-)} = \frac{-2d_1^2 + 2d_1 L - LR_1}{L} \tag{4.33}$$

For the symmetric f, the solutions of f are obtained as

$$f^{(+)} = \frac{d_1}{2}, \frac{L - d_1}{2} \tag{4.34}$$

$$f^{(-)} = \frac{d_1(L - d_1)}{2L} \tag{4.35}$$

In terms of radius of curvature R

$$R^{(+)} = d_1, L - d_1 \tag{4.36}$$

$$R^{(-)} = \frac{d_1(L - d_1)}{L} \qquad (4.37)$$

Therefore, for a given L and d_1 one can choose the range of the focal lengths or radius of curvature of mirrors to get a stable cavity configuration. It is also important to look at the stable domain of f and d_1 for a given L. Here we construct a 3D plot where (4.12) i.e., $(A + D)^2 - 4$ is along z axis, while d_1 and f are respectively along x and y axes, for a fixed $L = 240$cm. It is noted
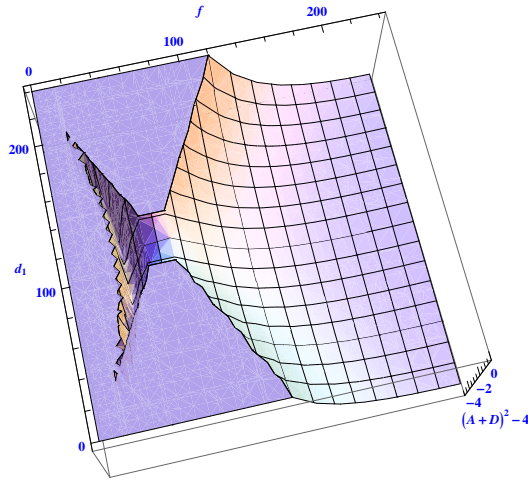
Figure 4.18: **A graph between f and d_1 for a fixed cavity of length $L = 240$cm.**

that initially for small values of f there is a long continuous range of d_1, for the range of $f = 20$cm to $f = 40$cm, there are two unconnected stable regions of d_1, and as f increases again one stable region of d_1 exists and the allowed stable range of f is up to $\dfrac{L}{2}$ as shown in Fig. (4.18). This is important to note here that for the symmetric f, one can convert the forbidden zone of L i.e., $4f_1 < L < 4f_2$ in the chart of Fig. (4.16) to a stable zone as shown in Fig. (4.18).

Therefore the stability of the 2CURC is analyzed for a given f, in terms of L and d_1 and for a given L, in terms of f and d_1. Next we keep the length

of the cavity L constant, and for a given f, we study the behaviour of the mode structures and the corresponding round trip Gouy phase.

In order to know the mode structures and other properties of the two portions of existing modes in the cavity, we consider the round trip propagation of the corresponding stable configuration of the Gaussian beam in the arm d_1 and as well as in the arm $L - d_1$ separately. By making use of the corresponding ray matrices one can calculate the half Rayleigh range and the position of the beam waist using the following conditions.

$$z_{0i} = \pm \frac{1}{C} \sqrt{1 - \left(\frac{A + D}{2} \right)^2} \tag{4.38}$$

$$x_{0i} = \frac{A - D}{2C} \tag{4.39}$$

Here the index $i = s$ corresponds to the arm d_1 and $i = b$ corresponds to the arm $L - d_1$ of the cavity. We take up these calculations in the following sections.

4.2   Calculations in the arm d_1

To calculate the spot size and the position of the beam waist in the arm d_1, let the radiation start at a distance x_{0s} from the lens L_2, strike and refract through the lens L_2 of the focal length f_2, reflecting off the plane mirrors in the order M_2, M_3, M_4, M_1, travel through a distance $(L - d_1)$, hit the lens L_1 and travel through a distance of $(d_1 - x_{0s})$ to reach the starting point to cover one full round trip.

The round trip $ABCD$-matrix at x_{0s} in the ring for this case is represented by

$$\begin{pmatrix} A & B \\ C & D \end{pmatrix} = \begin{pmatrix} 1 & d_1 - x_{0s} \\ 0 & 1 \end{pmatrix} \begin{pmatrix} 1 & 0 \\ -\frac{1}{f_1} & 1 \end{pmatrix} \begin{pmatrix} 1 & L - d_1 \\ 0 & 1 \end{pmatrix} \begin{pmatrix} 1 & 0 \\ -\frac{1}{f_2} & 1 \end{pmatrix} \begin{pmatrix} 1 & x_{0s} \\ 0 & 1 \end{pmatrix}$$
$$\tag{4.40}$$

The final matrix elements turn out to be

$$A = 1 - \frac{L - d_1}{f_2} + (d_1 - x_{0s}) \left\{ -\frac{1}{f_1} + \frac{(L - d_1)}{f_1 f_2} - \frac{1}{f_2} \right\} \tag{4.41}$$

$$B = x_{0s} + (L - d_1) \left\{ -\frac{x_{0s}}{f_2} + 1 \right\} + (d_1 - x_{0s}) \left\{ -\frac{x_{0s}}{f_1} - \frac{(L - d_1)}{f_1} \left\{ -\frac{x_{0s}}{f_2} + 1 \right\} - \frac{x_{0s}}{f_2} + 1 \right\} \tag{4.42}$$

$$C = -\frac{1}{f_1} + \frac{(L - d_1)}{f_1 f_2} - \frac{1}{f_2} \tag{4.43}$$

$$D = -\frac{x_{0s}}{f_1} - \frac{(L - d_1)}{f_1} \left\{ -\frac{x_{0s}}{f_2} + 1 \right\} - \frac{x_{0s}}{f_2} + 1 \tag{4.44}$$

The half Rayleigh range and the position of the beam waist in the arm d_1 can be obtained directly by the substitution of the $ABCD$ matrix elements in Eqs. (4.38) and (4.39), one gets

$$z_{0s} = \pm \frac{f_1 f_2}{(-f_2 - f_1 + (L - d_1))} \sqrt{1 - \frac{1}{4} \left[2 - \frac{L}{f_1 f_2}(f_1 + f_2) + \frac{d_1(L - d_1)}{f_1 f_2} \right]^2} \tag{4.45}$$

$$x_{0s} = \frac{d_1}{2} + \frac{(L - d_1)(f_1 - f_2)}{2(f_2 + f_1 - (L - d_1))} \tag{4.46}$$

For the case of symmetric resonator i.e., $f_1 = f_2 = f$,

$$z_{0s} = \pm \frac{f^2}{(-2f + L - d_1)} \sqrt{1 - \frac{1}{4} \left[2 - \frac{2L}{f} + \frac{d_1(L - d_1)}{f^2} \right]^2} \tag{4.47}$$

$$x_{0s} = \frac{d_1}{2} \tag{4.48}$$

The beam waist ω_{0s} can be obtained by using

$$\omega_{0s} = \sqrt{\frac{\lambda z_{os}}{\pi n_{ref}}} \tag{4.49}$$

The beam aperture $\omega_{1x_{0s}}$ on the lens L_2 can be estimated using

$$\omega_1^2(x_{0s}) = \omega_{0s}^2 \left[1 + \left(\frac{x_{0s}}{z_{0s}} \right)^2 \right] \tag{4.50}$$

The beam aperture $\omega_{2x_{0s}}$ on the lens L_1 can be estimated using

$$\omega_2^2(x_{0s}) = \omega_{0s}^2 \left[1 + \left(\frac{d_1 - x_{0s}}{z_{0s}} \right)^2 \right] \tag{4.51}$$

Using (4.46) and (4.49) one can calculate the position of the beam waist and the size of beam waist in the arm d_1 of the cavity. The contribution to the round trip Gouy phase $\phi_G(RT)$ from the arm d_1 is given by

$$\phi_{G1}(RT) = \arctan\left(\frac{x_{0s}}{z_{0s}} \right) - \arctan\left(\frac{-d_1 + x_{0s}}{z_{0s}} \right) \tag{4.52}$$

In section 4.4 above equation (4.50) is discuussed in detail. In sections 4.3, 4.3.1 we consider the arm $L - d_1$ and the special case where the ring at $d_1 = L - d_1$, leads one to a linear cavity.

4.3 Calculations in the arm $L - d_1$

To perform the same calculations in the arm $L - d_1$ of the cavity, let the radiation start at a distance x_{0b} from the lens L_1, strike and refract through the lens L_1 of the focal length f_1, travel through a distance d_1, hit the lens L_2, reflecting off the plane mirrors in the order M_2, M_3, M_4, M_1, travel through a distance $(L - d_1 - x_{0b})$ to reach the starting point to cover one full round trip. The round trip $ABCD$-matrix at x_{0s} in the ring for this case is represented by

$$\begin{pmatrix} A & B \\ C & D \end{pmatrix} = \begin{pmatrix} 1 & L - d_1 - x_{0b} \\ 0 & 1 \end{pmatrix} \begin{pmatrix} 1 & 0 \\ -\frac{1}{f_2} & 1 \end{pmatrix} \begin{pmatrix} 1 & d_1 \\ 0 & 1 \end{pmatrix} \begin{pmatrix} 1 & 0 \\ -\frac{1}{f_1} & 1 \end{pmatrix} \begin{pmatrix} 1 & x_{0b} \\ 0 & 1 \end{pmatrix} \tag{4.53}$$

After simplification, the matrix elements turn out to be

$$A = 1 - \frac{d_1}{f_1} + (L - d_1 - x_{0b}) \left\{ -\frac{1}{f_2} + \frac{d_1}{f_1 f_2} - \frac{1}{f_1} \right\} \tag{4.54}$$

$$B = x_{0b} + d_1\left\{-\frac{x_{0b}}{f_1}+1\right\} + (L - d_1 - x_{0b})\left\{-\frac{x_{0b}}{f_2} - \frac{d_1}{f_2}\left\{-\frac{x_{0b}}{f_1}+1\right\} - \frac{x_{0b}}{f_1}+1\right\}$$
$$(4.55)$$

$$C = -\frac{1}{f_2} + \frac{d_1}{f_1 f_2} - \frac{1}{f_1} \tag{4.56}$$

$$D = -\frac{x_{0b}}{f_2} - \frac{d_1}{f_2}\left\{-\frac{x_{0b}}{f_1}+1\right\} - \frac{x_{0b}}{f_1} + 1 \tag{4.57}$$

Using the $ABCD$ matrix elements the half Rayleigh range z_{0b} and the position of the beam waist x_{0b} can be obtained as

$$z_{0b} = \pm\frac{f_1 f_2}{(-f_2 - f_1 + d_1)}\sqrt{1 - \frac{1}{4}\left[2 - \frac{L}{f_1 f_2}(f_1 + f_2) + \frac{d_1(L - d_1)}{f_1 f_2}\right]^2} \tag{4.58}$$

$$x_{0b} = \frac{(L - d_1)}{2} + \frac{d_1(f_2 - f_1)}{2(f_2 + f_1 - d_1)} \tag{4.59}$$

For the case of symmetric resonator i.e., $f_1 = f_2 = f$, these quantities become

$$z_{0b} = \pm\frac{f^2}{(-2f + d_1)}\sqrt{1 - \frac{1}{4}\left[2 - \frac{2L}{f} + \frac{d_1(L - d_1)}{f^2}\right]^2} \tag{4.60}$$

$$x_{0b} = \frac{L - d_1}{2} \tag{4.61}$$

It is realized that from the equations of x_{0s} and x_{0b} that for a 2CURC consisting the two lenses of symmetric focal lengths the beam waists of the two arms lie always at the center. The beam waist ω_{0b} can be obtained by using

$$\omega_{0b} = \sqrt{\frac{\lambda z_{ob}}{\pi n_{ref}}} \tag{4.62}$$

The beam aperture $\omega_{1x_{0b}}$ on the lens L_1 can be estimated using

$$\omega_1^2(x_{0b}) = \omega_{0s}^2\left[1 + \left(\frac{x_{0b}}{z_{0b}}\right)^2\right] \tag{4.63}$$

The beam aperture $\omega_{2x_{0b}}$ on the lens L_2 can be estimated using

$$\omega_2^2(x_{0b}) = \omega_{0b}^2\left[1 + \left(\frac{L - d_1 - x_{0b}}{z_{0b}}\right)^2\right] \tag{4.64}$$

Using (4.59) and (4.62) one can calculate the position of the beam waist and the size of beam waist in the arm of length $(L - d_1)$. The contribution to the round trip Gouy phase $\phi_G(RT)$ from the arm $L - d_1$ is given by

$$\phi_{G2}(RT) = \arctan\left(\frac{x_{0b}}{z_{0b}}\right) - \arctan\left(\frac{-L + d_1 + x_{0b}}{z_{0b}}\right) \tag{4.65}$$

The accumulated round trip Gouy phase $\phi_G(RT)$ for the considered system can be written as the sum of $\phi_{G1}(RT)$ and $\phi_{G2}(RT)$ and is given by

$$
\begin{aligned}
\phi_G(RT) &= \arctan\left(\frac{x_{0s}}{z_{0s}}\right) - \arctan\left(\frac{-d_1 + x_{0s}}{z_{0s}}\right) \\
&\quad + \arctan\left(\frac{x_{0b}}{z_{0b}}\right) - \arctan\left(\frac{-L + d_1 + x_{0b}}{z_{0b}}\right)
\end{aligned}
\tag{4.66}
$$

Study of equation (4.66) for variety of cases for which $H_1 < 0$ is presented in the appendix A. A few results shown with simple cases are considered in the sections 4.4 and 4.5 below;

4.4 A Special case of 2CURC

It is known that by adjusting the length of the arm d_1 to be $d_1 = \dfrac{L}{2}$, then the 2CURC because of physical overlapping of arms for two mirror situation behaves as a linear (standing) cavity. For this case the solutions of focal length become as

$$f^{(+)} = \frac{L}{4}, \frac{L}{4} \tag{4.67}$$

$$f^{(-)} = \frac{L}{8} \tag{4.68}$$

$L = 4f$ case, i.e., $L = 120$cm, the solutions of f are $f^{(+)} = 30, 30$cm and $f^{(-)} = 15$cm which coincide with the solutions of the linear cavity. Having equipped ourselves with the detailed knowledge about various stable regions of the 2CURC, we proceed below to study the Gouy phase in these cases and record the conclusion in section 4.6.

4.5 The variable Gouy phase of 2CURC

In the case of SCURC we have seen that the Gouy phase variation $0 - \pi$ for fixed a F and varying L, $\pi - 0$ for a fixed L and varying F. Even though the total Gouy phase amounts to π, the existing mode structure of SCURC corresponding to these two cases are different.

The considered 2CURC behaves as SCURC for $L < L_{eff}$, in this case one can have the Gouy phase variation $0 - \pi$ and $\pi - 0$. In addition to this, one can have variety of cases of L, for $L > L_{eff}$ which can give different variable Gouy phases as will be presented in the Appendix A. Here we discuss a special case of L i.e, $L = L_M$, where one gets the Gouy phase variation of $\pi - 2\pi - \pi$.

For the given $f = 30$cm, $L = 240$cm the marginal stable solutions of d_1 are $d_1 = 60$cm, 120cm, 120cm, 180cm. Therefore the region of d_1 from 60cm to 180cm is a continuous stable region. For this range of parameters the half Rayleigh ranges z_{0s} and z_{0b} are plotted in the Fig. (4.19)(see 4.47 and 4.60). At $d_1 = 60$cm, z_{0s} is 0, and it increases further as d_1 increases. z_{0s} is large and the mode is almost parallel at $d_1 = 180$cm. However, the half Rayleigh range z_{0b} in the arm $L - d_1$, just behaves reverse to the beam in the arm d_1, i.e., initially z_{0b} is large at $d_1 = 60$cm, which means that the mode is almost parallel and it decreases further as d_1 increases, and it becomes zero at $d_1 = 180$cm. In the Fig. (4.20) the positions of the beam waists x_{0s} and x_{0b} varying d_1 are plotted. These beam waists always lie at the middle of corresponding arms of the cavity as d_1 increases. The beam apertures on the lenses are plotted in the Fig. (4.21) varying d_1. The aperture $\omega_{1x_{0s}}$ before the lens L_2 matches with the aperture $\omega_{2x_{0b}}$ after the lens L_2. Similarly $\omega_{1x_{0b}}$ matches with $\omega_{2x_{0s}}$ which are the apertures before and after the lens L_1 for the stable range of d_1 of the considered case.

Fig. (4.22) shows the variation of the round trip Gouy phases $\phi_{G1}(RT)$
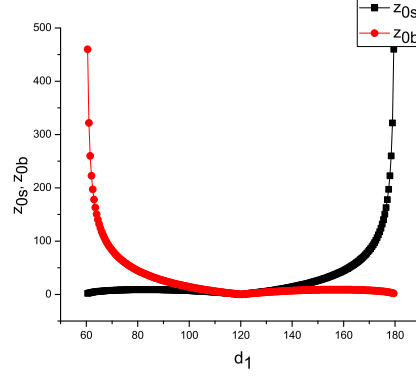
Figure 4.19: **Half Rayleigh ranges z_{0s}, z_{0b} with varying d_1**
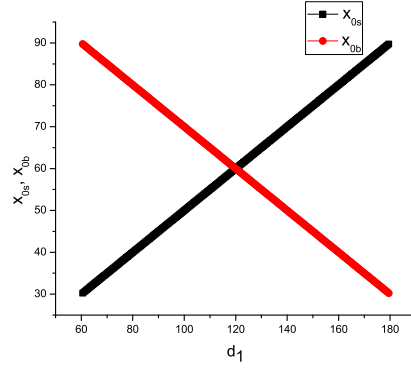
Figure 4.20: **The positions of beam spot sizes x_{0s}, x_{0b} varying d_1**

and $\phi_{G2}(RT)$ in the arm d_1 and in the arm $L - d_1$, also the accumulated Gouy phase $\phi_G(RT)$ of the cavity. It is observed that as d_1 increases the sum of Gouy phases $\phi_G(RT)$ shows the variation as $\pi - 2\pi - \pi$, and hence changes the longitudinal mode order from $n - \left(n + \dfrac{1}{2}\right) - n$. Therefore one has to check whether this Gouy phase variation is useful for RLG applications or not? In the next chapter we take up the above question.

70
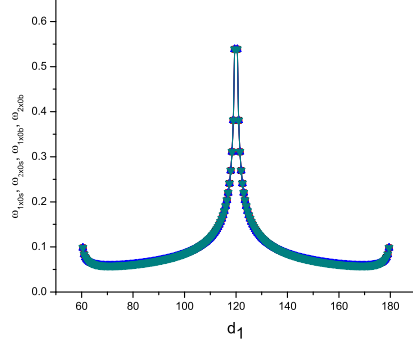
Figure 4.21: **The spot sizes on the mirrors $\omega_{1x_{0s}} = \omega_{2x_{0b}}$, $\omega_{1x_{0b}} = \omega_{2x_{0s}}$, varying d_1**
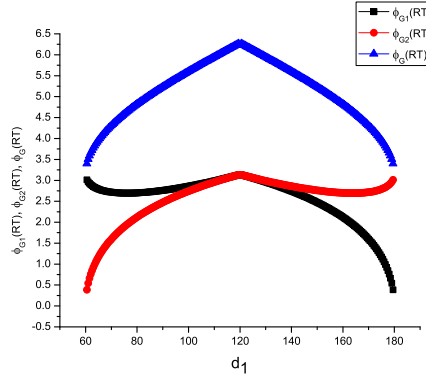
Figure 4.22: **The Gouy phases $\phi_{G1}(RT)$, $\phi_{G2}(RT)$ and the accumulated Gouy phase $\phi_G(RT)$ varying d_1**

4.6 Conclusion

The important variant of controlling the $\phi_G(RT)$ by varying only the distance d_1 for varying the mode structures inside the ring cavity has been analyzed above. This is an important variant from the application point of

view, wherein changing the position of lens in a ring cavity leads to variation of mode structure and the $\phi_G\left(RT\right)$ without changing the focal lengths of each lens and/or the total length of the ring cavity. In the next chapter we consider the application of the control of Gouy phase by displacing a lens in a ring cavity to tune the frequency of the ring laser and there by that of a ring laser gyro.

5

Three Lens Ring cavity

The important conclusions drawn from the analysis of the two converging unit ring cavity(2CURC) are (i) It behaves as a SCURC if the distance between the lenses $d_1 = 0$, with $0 < L < L_{eff}$(see the discussion of Eq. (4.13)); (ii) This 2CURC can accommodate two Gaussian modes in it if d_1 is finite, and in such a case the stability zone exceeds beyond L_{eff}, where $L_{eff} < L_M < L$ is possible as shown in the Fig. (4.16)); (iii) We have seen that for $L = L_M$, there is a Gouy phase variation of $\pi - 2\pi - \pi$(see Fig. (4.22)), where as $\pi - \left(\pi + \frac{1}{2}\right) - \pi$ for $L_{eff} < L < L_M$ (see Appendix of 2CURC).

These phase variations are for different values of cavity length L. But, our aim is to keep the length L of the cavity constant and yet create a mechanism

for controlling the Gouy phase so that one can tune the frequency of the ring laser.

Therefore, the questions emerge out of the analysis of 2CURC are (i) Is it possible to get the same stability behaviour of 2CURC for a fixed L, i.e., without changing the length (L) of the cavity? (ii) Can we tune or change the mode order of the oscillating mode of the ring laser using this Gouy phase? To answer, in this chapter, we analyze the three converging unit ring cavity (3CURC) consisting of three lenses L_1, L_2 and L_3 with the separation distances d_1, d_2 and $L - d_1 - d_2$ as shown in Fig. (5.1). Specifically, for
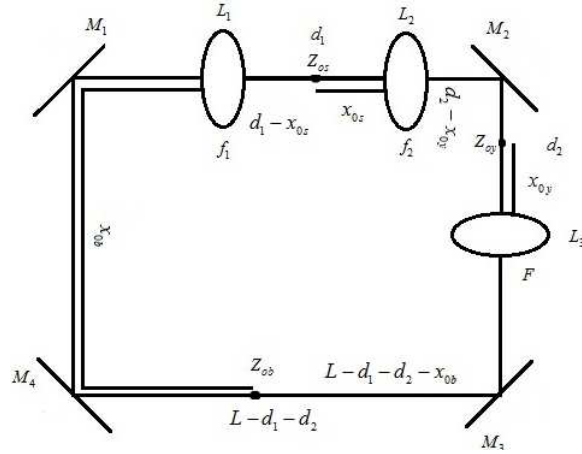
Figure 5.1: **3 Converging Unit Ring Cavity (3CURC)**

the purpose of ring laser gyro(RLG), we consider 3CURC with a particular configuration shown in Fig. (5.2) i.e., with two spherical mirrors of focal lengths f_1, f_2 and a lens of focal length F. This type of configurations are useful for RLG applications because it is necessary to have a ring cavity with minimum three mirrors for RLGs. We move further with this configuration and the details are given in the following.

5.1   3 Converging Unit Ring Cavity (3CURC)

A schematic of the 3CURC of the length L, consisting of two spherical mirrors M_1 and M_2 of focal lengths f_1 and f_2, and a lens L_1 of focal length F is shown in Fig. (5.2). The two spherical mirrors M_1 and M_2 are separated by a distance l_s, where as the lens L_1 is kept at a distance y_1 from the spherical mirror M_2. Here the mirrors M_3 and M_4 are plane mirrors. All mirrors are 100% reflecting. In general for this configuration there exist three modes,
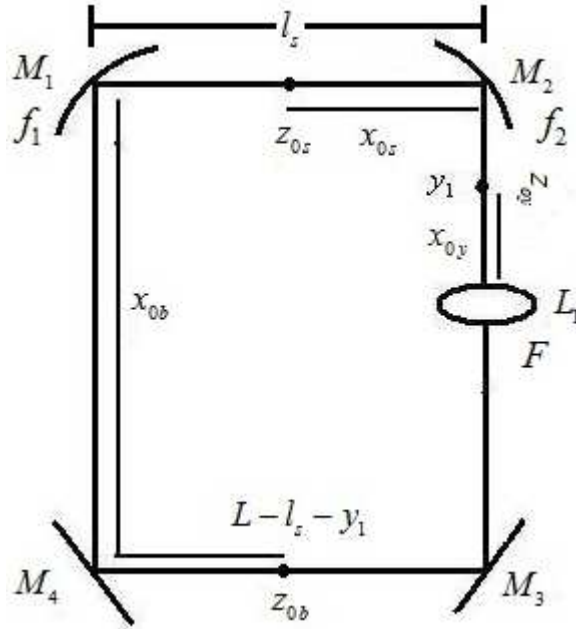
Figure 5.2: **3 Converging Unit Ring Cavity (3CURC)**

one in the arm of l_s in between the two spherical mirrors M_1 and M_2, the second mode in the arm of length y_1, in between the mirror M_2 and lens L_1 and the third mode in the arm of length $L-l_s-y_1$ in between the lens L_1 and the mirror M_1. The Gaussian beams in the respective sections constitute a part of stable configuration of radiation-travel in the ring, with half Rayleigh

ranges z_{0s} in the l_s arm, z_{0y} in the y_1 arm, and z_{0b} in the $L - l_s - y_1$ arm; with waist locations x_{0s}, x_{0y}, and x_{0b} respectively. Here also each Gaussian mode contributes its Gouy phase to the round trip Gouy phase in the ring. One can fix any one of the parameters l_s or y_1 and vary the distances y_1 or l_s, to vary the effective focal length of the combination M_2 and L_1 or M_1 and M_2, to vary $\phi_G(RT)$ which is the sum of the Gouy phases of the three parts of the 3CURC.

We define here the coordinate x_p in the clockwise sense in the ring with M_1 at $x_p = 0$, M_2 at $x_p = l_s$ and L_1 at $x_p = l_s + y_1$. For the three Gaussian modes with half Rayleigh ranges z_{0s}, z_{0y} and z_{0b}, the points $x_{0s}\,(x_p = l_s - x_{0s})$, $x_{0y}\,(x_p = y_1 - x_{0y})$ and $x_{0b}\,(x_p = L - l_s - y_1 - x_{0b})$ determine the positions of the beam waists ω_{0s}, ω_{0y} and ω_{0b} respectively. We study and analyze the stability of the 3CURC in the section 5.2.

5.2   Stability Analysis

For consideration of the stability let the radiation just enter before the mirror M_1 of focal length f_1 and reflects off it, in the clockwise direction travel through a distance l_s from the mirror M_1, as it hits another mirror M_2 of focal length f_2, it reflects off it, and strike the lens L_1 of focal length F, reflecting off the mirrors M_3 and M_4, travel through the distance $(L - l_s - y_1)$ complete the round trip just before the mirror M_1 where it starts its journey. The round trip $ABCD$-matrix at M_1 in the ring for this case is

$$
\begin{pmatrix} A & B \\ C & D \end{pmatrix} = \begin{pmatrix} 1 & L - l_s - y_1 \\ 0 & 1 \end{pmatrix} \begin{pmatrix} 1 & 0 \\ -\frac{1}{F} & 1 \end{pmatrix} \begin{pmatrix} 1 & y_1 \\ 0 & 1 \end{pmatrix} \begin{pmatrix} 1 & 0 \\ -\frac{1}{f_2} & 1 \end{pmatrix} \begin{pmatrix} 1 & l_s \\ 0 & 1 \end{pmatrix} \begin{pmatrix} 1 & 0 \\ -\frac{1}{f_1} & 1 \end{pmatrix}
$$
$$(5.1)$$

After simplification, the matrix elements A, B, C and D can be obtained as

$$A = \frac{1}{Ff_1f_2} \left\{ \begin{array}{c} F\left(-f_2L + Ll_s - l_s^2 + f_1\left(f_2 - L + l_s\right)\right) \\ -\left(L - l_s - y_1\right)\left(f_1\left(f_2 - y_1\right) + l_sy_1 - f_2\left(l_s + y_1\right)\right) \end{array} \right\} \tag{5.2}$$

$$B = \frac{1}{Ff_2} \left\{ \begin{array}{c} F\left(f_2L + l_s\left(-L + l_s\right)\right) \\ +\left(L - l_s - y_1\right)\left(l_sy_1 - f_2\left(l_s + y_1\right)\right) \end{array} \right\} \tag{5.3}$$

$$C = \frac{1}{Ff_1f_2} \left\{-F(f_1 + f_2 - l_s) + f_2l_s + f_2y_1 - l_sy_1 + f_1(-f_2 + y_1)\right\} \tag{5.4}$$

$$D = \frac{1}{Ff_2} \left\{F(f_2 - l_s) + l_sy_1 - f_2(l_s + y_1)\right\} \tag{5.5}$$

The self consistency requires that

$$(A + D)^2 - 4 \leq 0 \tag{5.6}$$

For this case

$$A + D = \frac{1}{Ff_1f_2} \left\{ \begin{array}{c} F\left(2f_1f_2 - f_1L - f_2L + Ll_s - l_s^2\right) \\ -f_1\left(f_2L + y_1\left(-L + y_1\right)\right) \\ +\left(L - l_s - y_1\right)\left(-l_sy_1 + f_2\left(l_s + y_1\right)\right) \end{array} \right\} \tag{5.7}$$

The two alternatives for the marginal stability case of (5.6)

$$A + D + 2 = \frac{1}{Ff_1f_2} \left\{ \begin{array}{c} F\left(4f_1f_2 - f_1L - f_2L + Ll_s - l_s^2\right) \\ -f_1\left(f_2L + y_1\left(-L + y_1\right)\right) \\ +\left(L - l_s - y_1\right)\left(-l_sy_1 + f_2\left(l_s + y_1\right)\right) \end{array} \right\} \tag{5.8}$$

$$A + D - 2 = \frac{1}{Ff_1f_2} \left\{ \begin{array}{c} F\left(-f_1L - f_2L + Ll_s - l_s^2\right) \\ -f_1\left(f_2L + y_1\left(-L + y_1\right)\right) \\ +\left(L - l_s - y_1\right)\left(-l_sy_1 + f_2\left(l_s + y_1\right)\right) \end{array} \right\} \tag{5.9}$$

For this case the marginal stability of the condition (5.6) becomes

$$\begin{aligned}
(A + D)^2 - 4 &= -4 + \frac{1}{F^2f_1^2f_2^2}[(-2Ff_1f_2 + l_s^2(-y_1 + F + f_2) + y_1^2(f_1 + f_2) \\
&\quad + Ff_1L + Ff_2L + f_1f_2L - y_1L\left(f_1 + f_2\right) \\
&\quad - l_s\left(y_1^2 + (F + f_2)L - y_1(2f_2 + L)\right))^2]
\end{aligned} \tag{5.10}$$

This stability function (5.10) is same for both the configurations shown in Fig. (5.1) and Fig. (5.2), with the change in the system parameters $d_1 \to l_s$ and $d_2 \to y_1$. For the configuration of Fig. (5.1), 3CURC can get converted to 2CURC and as well as a SCURC. These cases may not be possible with the configuration in Fig. (5.2) since it is not possible to combine the chosen mirrors. In the following we discuss these cases in detail.

5.2.1   Conversion from 3CURC to 2CURC

The three possible configurations where one can convert 3CURC to 2CURC are shown in the Fig. (5.3).

1(a). Consider the case when $d_1 = 0$, then (5.10) becomes (4.12), with the effective focal length $\left(\dfrac{f_1 f_2}{f_1 + f_2} \right)_{3CURC}$ of the combination of lenses L_1 and L_2 now behaves as a lens L_1 of 2CURC as shown in the first configuration of the Fig. (5.3). For this case of 2CURC the value of $L_{M_{(1,2),3}}$ is given by

$$L_{M_{(1,2),3}} = 4 \left(\frac{f_1 f_2}{f_1 + f_2} \right) + 4F \qquad (5.11)$$

1(b). Consider the case when $d_2 = 0$, then (5.10) becomes (4.12), with the effective focal length $\left(\dfrac{f_2 F}{f_2 + F} \right)_{3CURC}$ of the combination of lenses L_2 and L_3 now behaves as a lens L_2 of 2CURC as shown in the second configuration of the Fig. (5.3). Here the value of $L_{M_{1,(2,3)}}$ is given by

$$L_{M_{1,(2,3)}} = 4f_1 + 4 \left(\frac{f_2 F}{f_2 + F} \right) \qquad (5.12)$$

1(c). For the case of $L = d_1 + d_2$ also (5.10) becomes (4.12), with the effective focal length $\left(\dfrac{F f_1}{F + f_1} \right)_{3CURC}$ of the combination of lenses L_3 and L_1
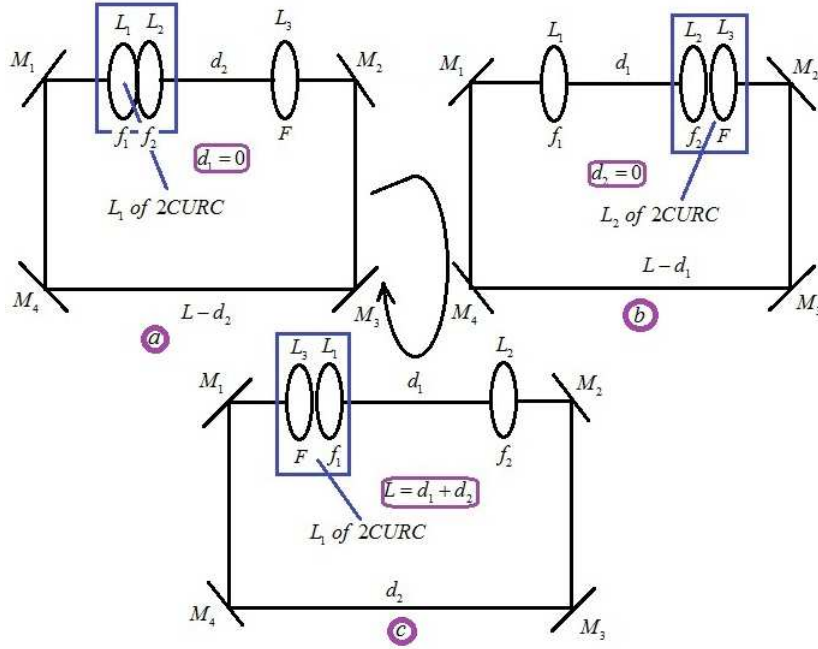
Figure 5.3: **Conversion of 3CURC to different forms of 2CURC**

now behaves as a lens L_1 of 2CURC as shown in the third configuration of the Fig. (5.3). In this case the value of $L_{M_{(3,1),2}}$ is given by

$$L_{M_{(3,1),2}} = 4 \left(\frac{F f_1}{F + f_1} \right) + 4 f_2 \qquad (5.13)$$

For the case of $f_1 < f_2 < F$, the value of $L_{M_{(1,2),3}}$(5.11) is greater than the remaining two which are given by (5.12) and (5.13). In the following we look for the possibility of converting 3CURC to SCURC.

5.2.2   Conversion from 3CURC to SCURC

The one and only possibility where the 3CURC can behave as a SCURC is shown in the Fig. (5.4), that is when all the lenses L_1, L_2 and L_3 are joined
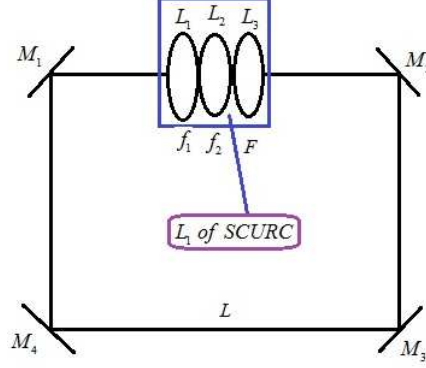
Figure 5.4: **Conversion of 3CURC to SCURC**

together with $d_1 = 0$ and $d_2 = 0$. In this case $L_{eff_{123}}$ is given by

$$L_{eff_{123}} = 4 \frac{f_1 f_2 F}{f_1 f_2 + f_2 F + F f_1} \tag{5.14}$$

It is understood from the above analysis that in 3CURC one can create one mode (Fig. (5.4)), two modes (Fig. (5.3)) and three modes (Fig. (5.1)). We have seen that the Gouy phase variation in the case of SCURC is $0 - \pi$ or $\pi - 0$ and in 2CURC is $\pi - 2\pi - \pi$ or $\pi - 2\pi$ or $2\pi - \pi$. Therefore, what happens when all the three modes of 3CURC are present? Whether these regions of different phases merge or not? To go into the details, we study the stability of 3CURC in the following section.

5.2.3 Stability of 3CURC

The stability function (5.10) of the considered 3CURC is quartic in y_1 and l_s. First, we study (5.10) with respect to l_s, keeping the rest of the system parameters fixed as the following.

5.2.4 Stable solutions of l_s for a given L, f_1, f_2, F and y_1

We look for the stable solutions of l_s for fixed L, f_1, f_2, F and y_1.

The marginal stability of (5.8) gives

$$
\begin{aligned}
l_{s_+}^{(1,2)} &= \frac{1}{2(-F-f_2+y_1)}[\left(-FL-f_2L+2f_2y_1+Ly_1-y_1^2\right) \\
&\pm\sqrt{-4Ff_2+FL+f_2L-Ly_1+y_1^2} \\
&\sqrt{-4Ff_1-4f_1f_2+FL+f_2L+4f_1y_1-Ly_1+y_1^2}\,]
\end{aligned} \quad (5.15)
$$

which can be written as

$$
\begin{aligned}
l_{s_+}^{(1,2)} &= \frac{1}{2(-F-f_2+y_1)}\left\{\left(y_1-\left(\frac{L+2f_2}{2}\right)\right)^2\pm\frac{n_1^2}{4}\right\} \\
&\pm\frac{1}{2(-F-f_2+y_1)}\sqrt{\left\{\left(y_1-\left(\frac{L}{2}\right)\right)^2\pm\frac{p_1^2}{4}\right\}\left\{\left(y_1-\left(\frac{L-4f_1}{2}\right)\right)^2\pm\frac{r_1^2}{4}\right\}}
\end{aligned}
$$
$$(5.16)$$

where

$$n_1^2 = L(L-4F)-4f_2^2 \qquad (5.17)$$

$$p_1^2 = (L-4F)(L-4f_2) \qquad (5.18)$$

$$r_1^2 = (4f_1-L)(4F+4f_1+4f_2-L) \qquad (5.19)$$

For $l_{s_+}^{(1,2)}$ to be real, there are four conditions on y_1 for the marginal stability of the discriminant of (5.16), which are given by

$$y_1 = \frac{L}{2}\mp\frac{p_1}{2} \qquad (5.20)$$

$$y_1 = \frac{L-4f_1}{2}\mp\frac{r_1}{2} \qquad (5.21)$$

Similarly from (5.9)

$$
\begin{aligned}
l_{s_-}^{(1,2)} &= \frac{1}{2(-F - f_2 + y_1)}[\left(-FL - f_2 L + 2f_2 y_1 + Ly_1 - y_1^2\right) \\
&\pm \sqrt{\left(-4f_1 f_2 + f_2 L + F(-4f_1 - 4f_2 + L) + 4f_1 y_1 - Ly_1 + y_1^2\right)} \\
&\sqrt{\left(FL + f_2 L + y_1(-L + y_1)\right)}]
\end{aligned}
\tag{5.22}
$$

and can be written as

$$
\begin{aligned}
l_{s_-}^{(1,2)} &= \frac{1}{2(-F - f_2 + y_1)}\left\{\left(y_1 - \left(\frac{L + 2f_2}{2}\right)\right)^2 \pm \frac{n_1^2}{4}\right\} \\
&\pm \frac{1}{2(-F - f_2 + y_1)}\sqrt{\left\{\left(y_1 - \left(\frac{L}{2}\right)\right)^2 \pm \frac{s_1^2}{4}\right\}\left\{\left(y_1 - \left(\frac{L - 4f_1}{2}\right)\right)^2 \pm \frac{m_1^2}{4}\right\}}
\end{aligned}
\tag{5.23}
$$

Here for $l_{s_-}^{(1,2)}$ to be real, there are four conditions on y_1 for marginal stability of the discriminant of (5.23) and are given by

$$
y_1 = \frac{L - 4f_1}{2} \mp \frac{s_1}{2}
\tag{5.24}
$$

and

$$
y_1 = \frac{L}{2} \mp \frac{m_1}{2}
\tag{5.25}
$$

where

$$
s_1^2 = (4F + 4f_1 - L)(4f_1 + 4f_2 - L)
\tag{5.26}
$$

$$
m_1^2 = L(L - 4F - 4f_2)
\tag{5.27}
$$

It is clear from the solutions of l_s, (5.15) and (5.22) that there will be no real solution of l_s exist at $y_1 = F + f_2$. From the coefficients p_1, r_1(5.18-5.19) and s_1, m_1(5.26-5.27), it is noticed that there are some new lengths have generated and the maximum limit of L i.e., L_M of 3CURC exceeds beyond the stable zone of 2CURC. Therefore one has to check the stability of l_s and y_1 at these new lengths too.

Before going to that, for $f_1 = 50$cm, $f_2 = 75$cm, $F = 100$cm, $L = 700$cm, $y_1 = 50$cm, we demonstrate the stability function (5.10), and the two parabolas (5.8), (5.9) with respect to $l_s = \dfrac{L}{2}$ and are shown in the Fig. (5.5). The stability function i.e., the product of $(A+D+2)$ and $(A+D-2)$ is an inverted parabola as in the case of 2CURC, inverted with respect to individual parabolas of $A + D \pm 2$, but for a given y_1. The above four solutions $l_{s+}^{(1,2)}$, $l_{s-}^{(1,2)}$ are identified in the Fig. (5.5). To know the behaviour
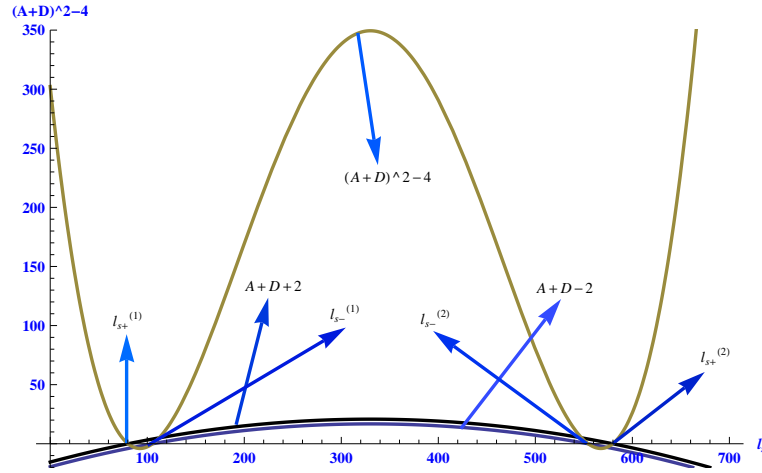
Figure 5.5: **For $f_1 = 50$cm, $f_2 = 75$cm, $F = 100$cm, $L = 700$cm, $y_1 = 50$cm, the stability functions $(A + D)^2 - 4$(5.10), $A + D + 2$(5.8), $A + D - 2$(5.9) with respect to $l_s = \dfrac{(L - y_1)}{2}$**

of the function (5.10) further, we determine its extremum points by taking

the partial derivative with respect to l_s,

$$\frac{\partial}{\partial l_s}\left[(A+D)^2 - 4\right] = -\frac{1}{F^2 f_1^2 f_2^2}\left\{\begin{array}{c} 2\left((F+f_2)(L-2l_s) - (2f_2 + L - 2l_s)y_1 + y_1^2\right) \\ \left(\begin{array}{c} F\left(f_2 L + f_1(-2f_2 + L) - Ll_s + l_s^2\right) \\ +f_1(f_2 L + y_1(-L + y_1)) \\ +(L - l_s - y_1)(l_s y_1 - f_2(l_s + y_1)) \end{array}\right) \end{array}\right\} = 0$$

(5.28)

The solutions of l_s obtained from (5.28)

$$l_s = \frac{FL + f_2 L - 2f_2 y_1 - Ly_1 + y_1^2}{2(F + f_2 - y_1)}$$

(5.29)

$$l_{s_-}^{(1,2)} = \frac{1}{2(-F - f_2 + y_1)}\left\{\begin{array}{c}(-FL - f_2 L + 2f_2 y_1 + Ly_1 - y_1^2) \\ \pm\sqrt{\begin{array}{c}(FL + f_2 L + y_1(-L + y_1))^2 - 4(-F - f_2 + y_1) \\ \left(-Ff_1 L - Ff_2 L - f_1 f_2 L + f_1 Ly_1 + f_2 Ly_1 - f_1 y_1^2 - f_2 y_1^2\right)\end{array}}\end{array}\right\}$$

(5.30)

To analyse further systematically we note that the value of (5.10) at l_s given by (5.29) determines the height H_1 from axis l_s of the central extremum.

We have

$$H_1 = \frac{\left[\left(y_1 - \frac{L}{2}\right)^2 - \frac{p_1^2}{4}\right]\left[\left(y_1 - \frac{L-4f_1}{2}\right)^2 - \frac{r_1^2}{4}\right]\left[\left(y_1 - \frac{L-4f_1}{2}\right)^2 - \frac{s_1^2}{4}\right]\left[\left(y_1 - \frac{L}{2}\right)^2 - \frac{m_1^2}{4}\right]}{16F^2 f_1^2 f_2^2 \left(F + f_2 - y_1\right)^2}$$

(5.31)

$H_1 \gtreqless 0$ depending on the values of y_1 for a given L, f_1, f_2 and F, also decide the stable zones of l_s. $H_1 > 0$ when the considered system is unstable i.e., $(A + D)^2 - 4 > 0$, $H_1 = 0$ when the stability function (5.10) is zero, the regions of which are shown in the Fig. (5.6), for stable zones of l_s and y_1 for a given $f_1 = 50$cm, $f_2 = 75$cm, $F = 100$cm, $L > L_M = 1000$cm. For the same set of parameters, the regions of $H_1 < 0$ i.e., when the system lies in the stable domain for which $(A + D)^2 - 4 < 0$, and are shown in the Fig. (5.7).
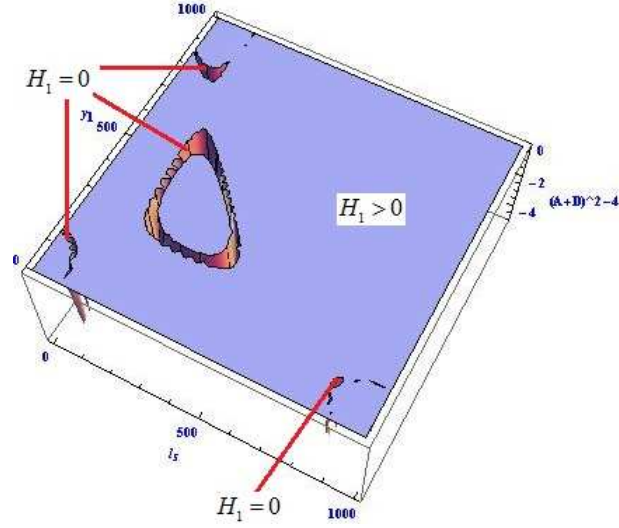
Figure 5.6: **The regions of** $H_1 \geq 0$**, for stable range of** l_s **and** y_1 **for a given** $f_1 = 50$**cm,** $f_2 = 75$**cm,** $F = 100$**cm,** $L > L_M$**=1000cm**
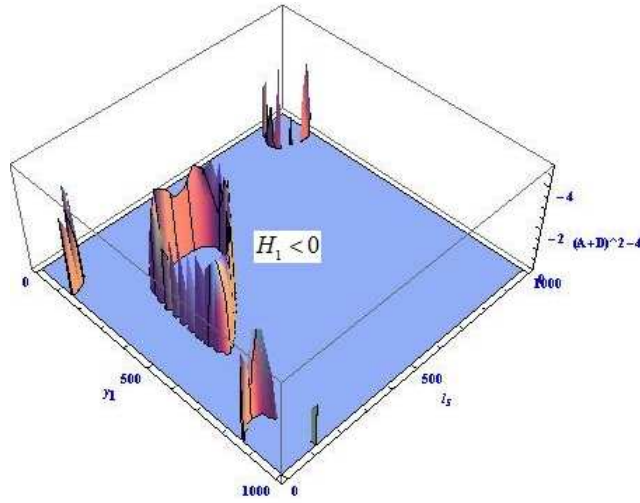
Figure 5.7: **The regions of** $H_1 < 0$**, for stable range of** l_s **and** y_1 **for a given** $f_1 = 50$**cm,** $f_2 = 75$**cm,** $F = 100$**cm,** $L > L_M$**=1000cm**

One can look for the values of L, at which the three extremum (5.29& 5.30) become one, which happens only when

$$(FL+f_2L+y_1(-L+y_1))^2 = 4(-F-f_2+y_1)\left((f_1+f_2)(Ly_1-FL-y_1^2)-f_1f_2L\right)$$
(5.32)

i.e., at $L=L_{H_{min1}}$; $L_{H_{min2}}$ given by

$$L_{Hmin1,2} \;=\; \frac{1}{2\,(y_1-F-f_2)}\left\{\begin{array}{c}[(y_1+f_1)^2-(2Ff_1+f_1^2+2Ff_2+2f_1f_2)]\\ \pm 4\sqrt{[F^2\,(f_1^2+f_2^2)+2Ff_1^2\,(f_2-y_1)+f_1^2\,(f_2-y_1)^2]}\end{array}\right\}$$
(5.33)

At these values of L, H_1 is minimum, $(H_1=-4)$. One has to know under what conditions of p_1, r_1, s_1 and m_1 and for what L one can have a wider and continuous stable region of l_s or y_1 for a fixed y_1 or l_s. For this, Next we study the stability condition (5.10) for different cases of p_1, r_1, s_1 and m_1 corresponding to different L which are consolidated in the Fig. (5.8).

5.2.5   The Length-Chart of 3CURC

For the case of $f_1<f_2<F$, the length chart of 3CURC which covers L from $L>L_M$ to $L=0$(from bottom to top) is shown in the Fig. (5.8).

We construct 3D plots for different cases of L of 3CURC, when all three modes present, where $(A+D)^2-4$(5.10) is along z axis, while l_s and y_1 are respectively along x and y axes as noted in Fig. (5.8). But for the cases of L, where 3CURC can get converted to 2CURC and SCURC, we construct 2D plots to show the behaviour of stability function with the corresponding variation of the length of the arms which also noted in Fig. (5.8).

Note that the considered L for the length chart of the 3CURC are the marginal L of the coefficients p_1, r_1, s_1 and m_1. It is also interesting to note that a few new marginal L have generated for 3CURC compare to 2CURC.

$$L_{eff_{123}} = \frac{4f_1f_2f_3}{f_2f_3 + f_3f_1 + f_1f_2}$$

$$L_{eff_{12}} = \frac{4f_1f_2}{f_1+f_2}; \quad L_{eff_{13}} = \frac{4f_1f_3}{f_1+f_3}; \quad L_{eff_{23}} = \frac{4f_2f_3}{f_2+f_3}$$

$$L_{M1} = 4f_1; \quad L_{M2} = 4f_2; \quad L_{M3} = 4F;$$

$$L_M = L_{M1} + L_{M2} + L_{M3}$$

$$p_1^2 = (L - L_{M3})(L - L_{M2})$$
$$s_1^2 = (L_{M1} - L)(L_M - L)$$
$$r_1^2 = (L_{M1} + L_{M3} - L)(L_{M1} + L_{M2} - L)$$
$$m_1^2 = L(L - L_{M3} - L_{M2})$$

$$f_1 < f_2 < F$$

$L = 0$;	$p_1^2 > 0, r_1^2 > 0, s_1^2 > 0, m_1^2 = 0$	See 3D plot in Fig: 5.21
$L = L_{eff_{123}}$;	$p_1^2 > 0, r_1^2 > 0, s_1^2 > 0, m_1^2 < 0$	See 2D plot in Fig: 5.20
$L = L_{M1}$;	$p_1^2 > 0, r_1^2 = 0, s_1^2 > 0, m_1^2 < 0$	See 3D plot in Fig: 5.19
$L = L_{M2}$;	$p_1^2 = 0, r_1^2 < 0, s_1^2 > 0, m_1^2 < 0$	See 3D plot in Fig: 5.18
$L = L_{M_{1/23}}$;	$p_1^2 < 0, r_1^2 < 0, s_1^2 > 0, m_1^2 < 0$	See 2D plot in Fig: 5.17
$L = L_{M3}$;	$p_1^2 = 0, r_1^2 < 0, s_1^2 > 0, m_1^2 < 0$	See 3D plot in Fig: 5.16
$L = L_{M_{(3,1)12}}$;	$p_1^2 > 0, r_1^2 < 0, s_1^2 > 0, m_1^2 < 0$	See 2D plot in Fig: 5.15
$L = L_{M1} + L_{M2}$;	$p_1^2 > 0, r_1^2 < 0, s_1^2 = 0, m_1^2 < 0$	See 3D plot in Fig: 5.14
$L = L_{M_{(1,2)3}}$;	$p_1^2 > 0, r_1^2 < 0, s_1^2 < 0, m_1^2 < 0$	See 2D plot in Fig: 5.13
$L = L_{M1} + L_{M3}$;	$p_1^2 > 0, r_1^2 < 0, s_1^2 = 0, m_1^2 < 0$	See 3D plot in Fig: 5.12
$L = L_{M2} + L_{M3}$;	$p_1^2 > 0, r_1^2 < 0, s_1^2 > 0, m_1^2 = 0$	See 3D plot in Fig: 5.11
$L = L_M$;	$p_1^2 > 0, r_1^2 = 0, s_1^2 > 0, m_1^2 > 0$	See 3D plot in Fig: 5.10
$L > L_M$;	$p_1^2 > 0, r_1^2 > 0, s_1^2 > 0, m_1^2 > 0$	See 3D plot in Fig: 5.9

Figure 5.8: **Length chart for 3CURC for the case of** $f_1 < f_2 < F$

Now the question is, is this 3CURC stable for the entire range of l_s and y_1,

at all the possible new lengths?

Let us consider $f_1 = 50$cm, $f_2 = 75$cm, and $F = 100$cm satisfying $f_1 < f_2 < F$.

(a). $L > L_M$. For a given $L > L_M = 1000$cm, the stable zones of l_s and
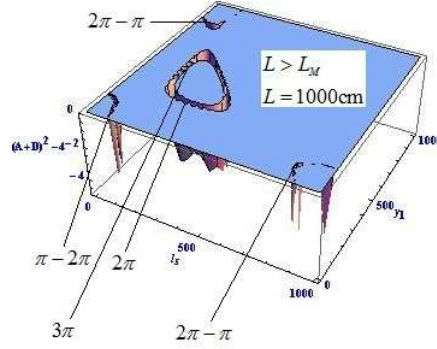
Figure 5.9: **Stability diagram as a function of l_s and y_1 for $f_1 = 50$cm, $f_2 = 75$cm, $F = 100$cm, $L > L_M = 1000$cm**

y_1, which satisfies (5.10) are shown in the Fig. (5.9). There exist four disconnected stable contours which are surrounded completely in side and out side by an unstable region. Out of these four, there are three contours showing the Gouy phase variation of $\pi - 2\pi$, $2\pi - \pi$ are identified and marked in the Fig. (5.9), which have already been existed for the case of 2CURC. In addition there exist one new central contour, the inner contour of which corresponds to 3π phase region where as the outer contour corresponds to 2π phase region.

(b). $L = L_M$. For the considered $L_M = 900$cm, the stable zones of l_s and y_1 are shown in the Fig. (5.10). For this case also there exist four disconnected stable contours but the middle stable contour has become stable inside. The expanded version of the central contour has a central peak which corresponds to the phase 3π and the outer

88
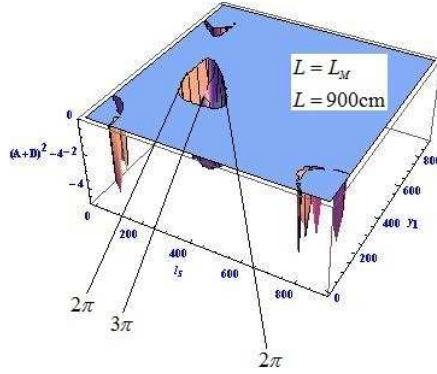
Figure 5.10: **Stability diagram as a function of l_s and y_1 for $f_1 = 50$cm, $f_2 = 75$cm, $F = 100$cm, $L = L_M = 900$cm**

contour corresponds to the Gouy phase variation of 2π as shown in the Fig. (5.11).
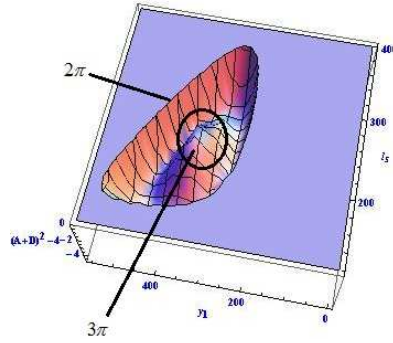
Figure 5.11:   **The expanded central contour of the case $L = L_M = 900$cm**

(c). $L = L_{M2} + L_{M3}$. Surprisingly, the middle stable contour disappears at $L = 700$cm as shown in the Fig. (5.12). Only the three stable contours exist, which are of $\pi - 2\pi$ and $2\pi - \pi$.
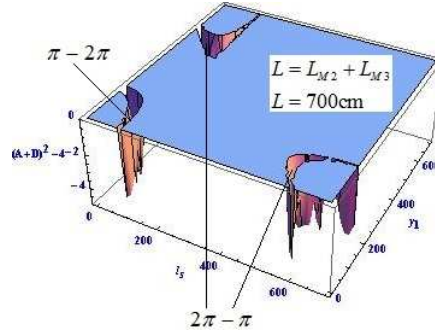
Figure 5.12: **Stability diagram as a function of l_s and y_1 for $f_1 = 50$cm, $f_2 = 75$cm, $F = 100$cm, $L = L_{M2} + L_{M3} = 700$cm**

(d). $L = L_{M1} + L_{M3}$. As shown in the Fig. (5.13), for the case of $L = 600$cm,
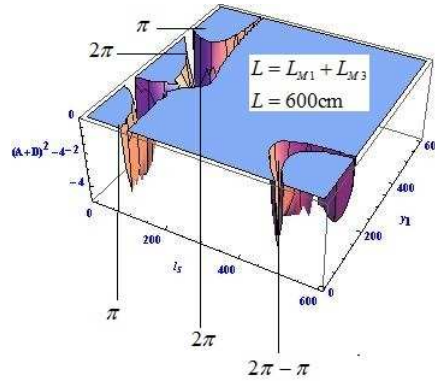
Figure 5.13: **Stability diagram as a function of l_s and y_1 for $f_1 = 50$cm, $f_2 = 75$cm, $F = 100$cm, $L = L_{M1} + L_{M3} = 600$cm**

two of the stable contours of y_1 are now connected for the range of l_s around 100cm, even though there exist two unconnected stable contours of y_1 for smaller values of l_s i.e., for $l_s < 100$cm. The corresponding phase regions are identified in the Fig. (5.13).

It is excited us to check for the other cases of L, to see the possibilities

where all of the stable contours can get connected. Here onwards the region of L where 3CURC can behave as 2CURC will come into the picture and the corresponding 2D plots are shown in the following.

(e). $L = L_{M_{(1,2),3}}$. For this case of $L_{M_{(1,2),3}} = 520$cm, there exist three
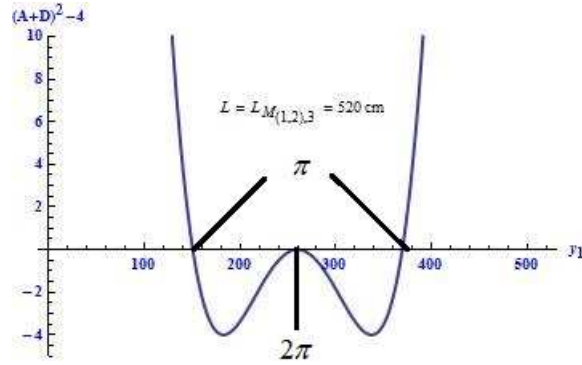
Figure 5.14: **Stability diagram as a function of y_1 for $f_1 = 50$cm, $f_2 = 75$cm, $F = 100$cm, $l_s = 0$, $L = L_{M_{(1,2),3}} = 520$cm**

marginal stable solutions of y_1 as shown the Fig. (5.14). The region of y_1, i.e., $y_{1_+}^{(1)} < y_1 < y_{1_-}^{(2)}$ is a stable region, $y_{1_+}^{(1)} - y_1$ corresponds to the Gouy phase region of $\pi - 2\pi$, where as the region $y_1 - y_{1_-}^{(2)}$ corresponds to $2\pi - \pi$ region.

This is the highest value of L_M of 2CURC for which 3CURC can become 2CURC.

(f). $L = L_{M1} + L_{M2}$. For the case of $L = 500$cm now there exist two stable contours only as shown in the Fig. (5.15). This is unlike the case when $L = L_{M1} + L_{M3}$, because the unstable zone for smaller values of l_s has been removed and a stable zone of y_1 for a range of l_s from 0 to 210cm is possible. The second stable contour of y_1 starts when l_s is around 250cm and continues up to $l_s = 500$cm.
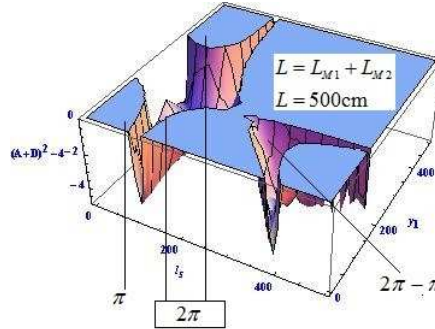
Figure 5.15: **Stability diagram as a function of l_s and y_1 for $f_1 = 50$cm, $f_2 = 75$cm, $F = 100$cm, $L = L_{M1} + L_{M2} = 500$cm**

(g). $L = L_{M_{(3,1),2}}$. For $L_{M_{(3,1),2}} = 433.333$cm, there is stable region of y_1,
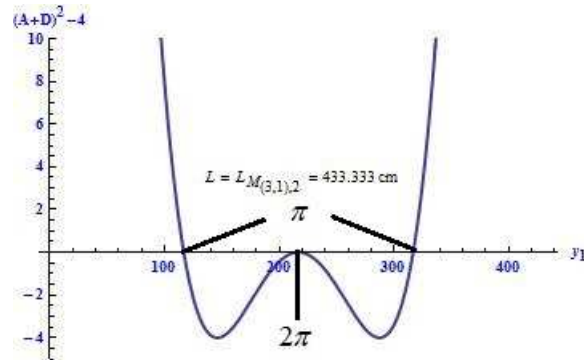
Figure 5.16: **Stability diagram as a function of y_1 for $f_1 = 50$cm, $f_2 = 75$cm, $F = 100$cm, $L = L_{M_{(3,1),2}} = 433.333$cm**

i.e., $y_{1_+}^{(1)} < y_1 < y_{1_-}^{(2)}$ exists, which shows a phase variation of $\pi - 2\pi - \pi$ as shown in the Fig. (5.16),

(h). $L = L_{M3}$. For $L = 400$cm, we found that there exists an interesting and continuous stable contour which has not been seen for the earlier cases of L as shown in the Fig. (5.17). For this case of L all the stable

92
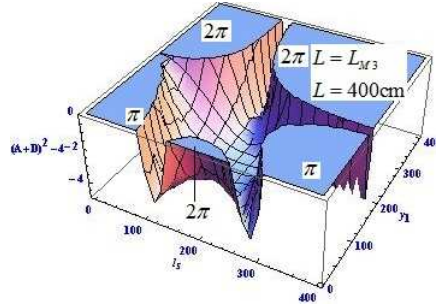
Figure 5.17: **Stability diagram as a function of l_s and y_1 for $f_1 = 50$cm, $f_2 = 75$cm, $F = 100$cm, $L = L_{M3} = 400$cm**

contours are merged and finally a single stable contour is achieved.

(i). $L = L_{M_{1,(2,3)}}$. This value of L is lowest value of L_M of the cases of
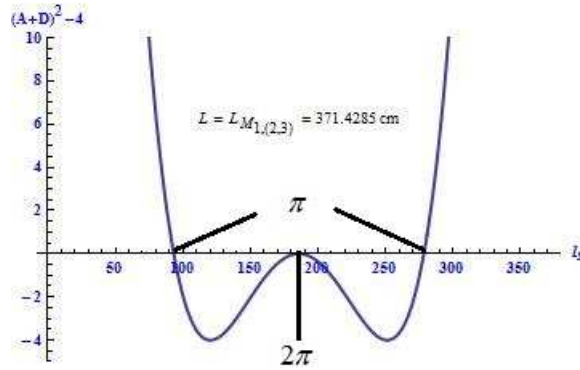
Figure 5.18: **Stability diagram as a function of l_s for $f_1 = 50$cm, $f_2 = 75$cm, $F = 100$cm, y_1=0cm, $L = L_{M_{1,(2,3)}} = 371.4285$cm**

2CURC. For this case of $L_{M_{1,(2,3)}} = 371.4285$cm also there is a stable region of y_1, i.e., $y_{1+}^{(1)} < y_1 < y_{1-}^{(2)}$ exists as shown in the Fig. (5.18).

(j). $L = L_{M2}$. For $L = 300$cm, from $l_s = 0$ to 100cm, there is no stable
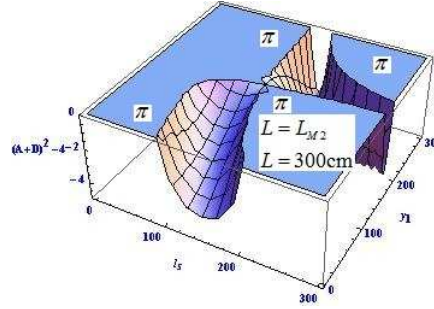
Figure 5.19: **Stability diagram as a function of l_s and y_1 for $f_1 = 50$cm, $f_2 = 75$cm, $F = 100$cm, $L = L_{M2} = 300$cm**

region of y_1 exists. However, for $l_s = 100$ to 300cm there exists a continuous stable range of y_1 as shown in Fig. (5.19).

(k). $L = L_{M1}$. For $L = 200$cm, there is a very small stable region of y_1
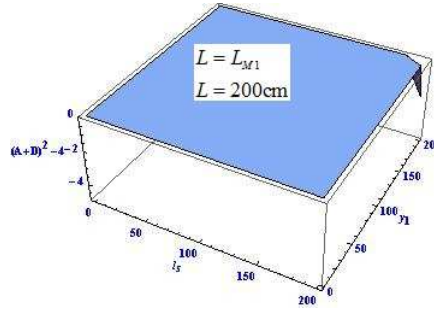
Figure 5.20: **Stability diagram as a function of l_s and y_1 for $f_1 = 50$cm, $f_2 = 75$cm, $F = 100$cm, $L = L_{M1} = 200$cm**

when l_s approaches L i.e., from $l_s = 185$cm onwards as shown in the Fig. (5.20).

(l). $L = L_{eff_{123}}$. For this value of L, the stable range of L is $0 < L < L_{eff_{123}}$ exists which corresponds to the Gouy phase variation of $0 - \pi$

94

as shown in the Fig. (5.21). For the considered f_1, f_2 and F, $L_{eff_{123}} = 92.3077$cm.
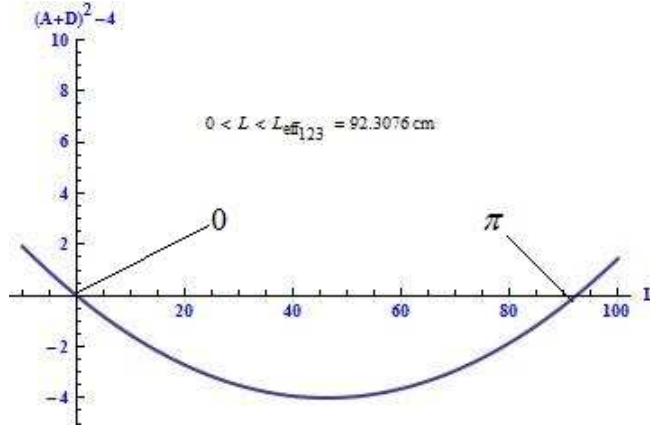
Figure 5.21: **Stability diagram as a function of L for $f_1 = 50$cm, $f_2 = 75$cm, $F = 100$cm**

(m). $L = 0$. As $L = 0$ is of no use to us, but for the demonstration we show the 3D plot for this case and is shown in the Fig. (5.22).

To summarize, the stability analysis for distinct focal lengths f_1, f_2 and F suggested that, the new lengths which are generated, are creating the new forbidden regions. This occurs as a result of the coefficients p_1, r_1, s_1 and m_1 which are forcing the length L to satisfy certain conditions simultaneously which is really impossible. Therefore we are forced to do the same analysis for symmetric f, as we are hoping that these forbidden zones can be eliminated if we choose symmetric f. We discuss the stability for the symmetric case of focal lengths in the following section.
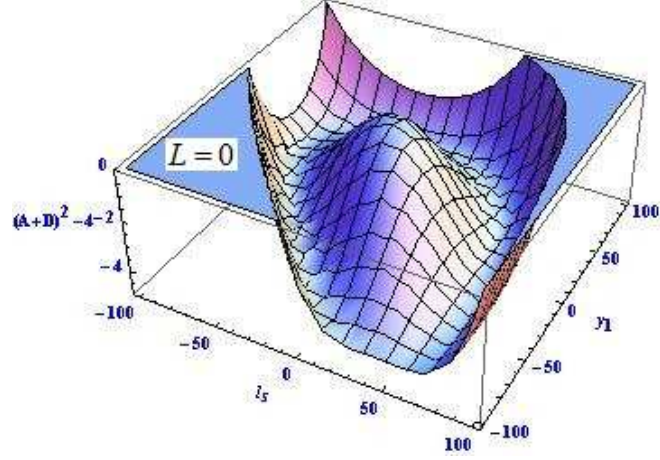
Figure 5.22: **Stability diagram as a function of l_s and y_1 for $f_1 = 50$cm, $f_2 = 75$cm, $F = 100$cm, $L = 0$cm**

5.2.6   For the case of symmetric focal lengths $f_1 = f_2 = F = f$

We look for the stable solutions of l_s for a given L, y_1 for a symmetric f where $f_1 = f_2 = F = f$.

For marginal stability (5.8) gives

$$l_{s_+}^{(1,2)} = \frac{L - y_1}{2} \pm \frac{\sqrt{(2f - y_1)(2f - L + y_1)\left(8f^2 + (L - y_1)y_1 - 2f(L + 2y_1)\right)}}{4f - 2y_1}$$

(5.34)

For marginal stability (5.9) gives

$$l_{s_-}^{(1,2)} = \frac{L - y_1}{2} \pm \frac{\sqrt{(-2f + y_1)(6f - L + y_1)(2fL + y_1(-L + y_1))}}{-4f + 2y_1} \quad (5.35)$$

For this case we will not present the discussion of the length chart of 3CURC, but we discuss two important cases of L, for which all stable zones are merged. For the case of $L = 5f$, for a given $f = 100$cm, a 3D plot is constructed as shown in the Fig. (5.23). There exists a single and continuous

stable contour but there are the regions at the corners where the instability lies even for symmetric f. Similar unstable regions can be seen in the Fig. (5.24) for the case of $L = 6f$. The Gouy phase regions are identified in each of these plots. So far we have analyzed the stability function with respect
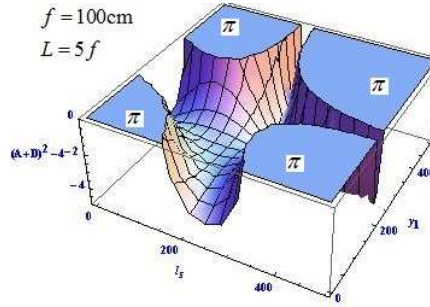
Figure 5.23: **Stability diagram as a function of l_s and y_1 for $f_1 = f_2 = F = f = 100$cm, $L = 5f$cm**
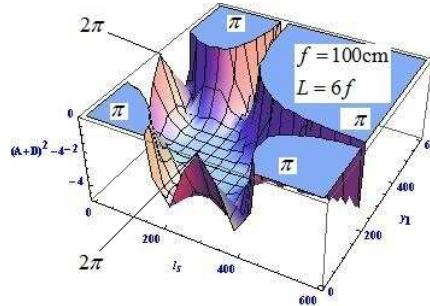
Figure 5.24: **Stability diagram as a function of l_s and y_1 for $f_1 = f_2 = F = f = 100$cm, $L = 6f$cm**

to l_s, for distinct f_1, f_2, F and for the symmetric f for a fixed y_1. It is understood that it is impossible to get rid off the forbidden zones for the case of 3CURC. One of the reasons could be the creation of the odd number

of modes. There are other options like where one can fix the focal length F of the lens inserted, for a given L, f_1, f_2, l_s and y_1.

We discuss the stable solutions of F for a given L, f_1, f_2, l_s and y_1 in the following.

5.2.7 Stable solutions of F for a given L, f_1, f_2, l_s and y_1

Here we look for the marginal stability with respect to the focal length of the lens F for a given L, f_1, f_2, l_s and y_1.

Solving (5.8) for marginal stability for F gives

$$
\begin{aligned}
F^{(+)} &= \frac{1}{(l_s^2 - 4f_1f_2 - l_sL + f_1L + f_2L)}[l_s^2 y_1 + l_s y_1^2 - y_1^2 f_1 - l_s^2 f_2 \\
&\quad - 2l_s y_1 f_2 - y_1^2 f_2 - l_s y_1 L + y_1 f_1 L + l_s f_2 L + y_1 f_2 L - f_1 f_2 L]
\end{aligned}
$$
(5.36)

Similarly (5.9) for marginal stability for F gives

$$
\begin{aligned}
F^{(-)} &= \frac{1}{(l_s^2 - l_sL + f_1L + f_2L)}[l_s^2 y_1 + l_s y_1^2 - y_1^2 f_1 - l_s^2 f_2 \\
&\quad - 2l_s y_1 f_2 - y_1^2 f_2 - l_s y_1 L + y_1 f_1 L + l_s f_2 L + y_1 f_2 L - f_1 f_2 L]
\end{aligned}
$$
(5.37)

For a symmetric resonator $f_1 = f_2 = f$, the above solutions turn out to be

$$
F^{(+)} = \frac{l_s^2 y_1 + l_s y_1^2 - l_s^2 f - 2l_s y_1 f - 2y_1^2 f - l_s y_1 L + l_s f L + 2y_1 f L - f^2 L}{(l_s - 2f)(l_s + 2f - L)}
$$
(5.38)

$$
F^{(-)} = \frac{l_s^2 y_1 + l_s y_1^2 - l_s^2 f - 2l_s y_1 f - 2y_1^2 f - l_s y_1 L + l_s f L + 2y_1 f L - f^2 L}{l_s^2 - l_sL + 2fL}
$$
(5.39)

Instead of choosing the focal length of the lens F randomly, one can choose any stable F, from the range $F^{(+)} < F < F^{(-)}$.

In the following sections we consider the round trip propagation of the corresponding stable configuration of the Gaussian beam in each of the arms l_s , y_1 and $L - l_s - y_1$ separately to calculate the beam waist and the other mode properties. By making use of the corresponding ray matrices we calculate the half Rayleigh ranges and the positions of the beam waists in each of these arms using

$$z_{0i} = \pm \frac{1}{C} \sqrt{1 - \left(\frac{A + D}{2} \right)^2} \qquad (5.40)$$

$$x_{0i} = \frac{A - D}{2C} \qquad (5.41)$$

Here the index $i = s$ corresponds to the arm l_s, $i = y$ corresponds to the arm y_1 and $i = b$ corresponds to the arm $L - l_s - y_1$ of the cavity. First we take up the calculations in the arm l_s of the cavity.

5.3   Calculations in the arm l_s

To calculate the spot size and the position of the beam waist in the arm l_s, let the radiation start at a distance x_{0s} from the mirror M_2, strike and reflects off from the mirror M_2 of the focal length f_2, travel through the arm of length y_1, hit the lens L_1 of focal length F, refract through it, reflecting off the plane mirrors M_3, M_4 while traveling through a distance $(L - l_s - y_1)$, strike the mirror M_1 of focal length f_1, reflects off it and finally travel through a distance of $(l_s - x_{0s})$ to reach the starting point to cover one full round trip. One can express its round trip propagation in terms of the $ABCD$ matrices

as

$$\begin{pmatrix} A & B \\ C & D \end{pmatrix} = \begin{pmatrix} 1 & l_s - x_{0s} \\ 0 & 1 \end{pmatrix} \begin{pmatrix} 1 & 0 \\ -\frac{1}{f_1} & 1 \end{pmatrix} \begin{pmatrix} 1 & L - l_s - y_1 \\ 0 & 1 \end{pmatrix} \begin{pmatrix} 1 & 0 \\ -\frac{1}{F} & 1 \end{pmatrix}$$
$$\begin{pmatrix} 1 & y_1 \\ 0 & 1 \end{pmatrix} \begin{pmatrix} 1 & 0 \\ -\frac{1}{f_2} & 1 \end{pmatrix} \begin{pmatrix} 1 & x_{0s} \\ 0 & 1 \end{pmatrix}$$

$$(5.42)$$

On simplification the round trip matrix elements can be obtained as

$$
\begin{aligned}
A &= \frac{1}{F f_1 f_2} \{ (l_s - x_{0s}) \left(FL - Ly_1 + y_1^2 + l_s (-F + y_1) - f_2 (F - L + l_s + y_1) \right) \\
&\quad + f_1 \left(-FL + x_{0s} (F - y_1) + Ly_1 - y_1^2 + f_2 (F - L + x_{0s} + y_1) \right) \}
\end{aligned}
$$
$$(5.43)$$

$$
\begin{aligned}
B &= \frac{1}{F f_1 f_2} \{ F \left(f_1 (f_2 L + x_{0s}(-L + x_{0s})) - (l_s - x_{0s})((-L + l_s)x_{0s} + f_2(L - l_s + x_{0s})) \right) \\
&\quad + (-x_{0s} y_1 + f_2 (x_{0s} + y_1))(-(l_s - x_{0s})(-L + l_s + y_1) + f_1(-L + x_{0s} + y_1)) \}
\end{aligned}
$$
$$(5.44)$$

$$C = -\frac{F(f_1 + f_2 - L + l_s) + (f_2 - y_1)(f_1 - L + l_s + y_1)}{F f_1 f_2} \qquad (5.45)$$

$$D = \frac{F f_2(f_1 - L + l_s) - F(f_1 + f_2 - L + l_s)x_{0s} - (f_1 - L + l_s + y_1)(-x_{0s}y_1 + f_2(x_{0s} + y_1))}{F f_1 f_2}$$

$$(5.46)$$

The half Rayleigh range z_{0s} using (5.40) is obtained as

$$z_{0s} = \mp \frac{\sqrt{-4F^2 f_1^2 f_2^2 + \left(\begin{array}{c} F \left(2f_1 f_2 - f_1 L - f_2 L + Ll_s - l_s^2 \right) - f_1(f_2 L + y_1(-L + y_1)) \\ + (L - l_s - y_1)(-l_s y_1 + f_2(l_s + y_1)) \end{array} \right)^2}}{2(F(f_1 + f_2 - L + l_s) + (f_2 - y_1)(f_1 - L + l_s + y_1))}$$
$$(5.47)$$

The position of the beam waist x_{0s} using (5.41)

$$x_{0s} = \frac{\begin{array}{c} F f_1 L - F f_2 L + f_1 f_2 L + 2F f_2 l_s - FL l_s - f_2 L l_s + F l_s^2 + f_2 l_s^2 - 2f_1 f_2 y_1 - f_1 L y_1 \\ + f_2 L y_1 + Ll_s y_1 - l_s^2 y_1 + f_1 y_1^2 - f_2 y_1^2 - l_s y_1^2 \end{array}}{2 \left(F f_1 + F f_2 + f_1 f_2 - FL - f_2 L + F l_s + f_2 l_s - f_1 y_1 + f_2 y_1 + L y_1 - l_s y_1 - y_1^2 \right)}$$
$$(5.48)$$

100

The beam waist ω_{0s} can be obtained using

$$\omega_{0s} = \sqrt{\frac{\lambda z_{0s}}{\pi n_{ref}}} \tag{5.49}$$

The beam aperture $\omega_{1x_{0s}}$ on the mirror M_2 can be estimated using

$$\omega_1^2(x_{0s}) = \omega_{0s}^2 \left[1 + \left(\frac{x_{0s}}{z_{0s}} \right)^2 \right] \tag{5.50}$$

The beam aperture $\omega_{2x_{0s}}$ on the mirror M_1 can be estimated using

$$\omega_2^2(x_{0s}) = \omega_{0s}^2 \left[1 + \left(\frac{l_s - x_{0s}}{z_{0s}} \right)^2 \right] \tag{5.51}$$

The contribution of the Gouy phase from the arm l_s is given by

$$\phi_{G1}(RT) = \arctan \left(\frac{x_{0s}}{z_{0s}} \right) - \arctan \left(\frac{-l_s + x_{0s}}{z_{0s}} \right) \tag{5.52}$$

We go through the calculations of other arms y_1 and $(L - l_s - y_1)$ before we study the Gouy phase variation in each of the arms.

5.4   Calculations in the arm y_1

To perform the same calculations, here in the arm y_1 of the cavity, let the radiation start at a distance x_{0y} from the lens L_1, strike and refract through the lens L_1 of the focal length F, reflecting off the plane mirrors M_3, M_4 while traveling through a distance $(L - l_s - y_1)$, strike the mirror M_1 of focal length f_1, reflects off it, travel through the arm of length l_s, hit the mirror M_2 of focal length f_2, reflect off it and finally travel through a distance of $(y_1 - x_{0y})$ to reach the starting point to cover one full round trip. One can

express its round trip propagation in terms of the $ABCD$ matrices as

$$\begin{pmatrix} A & B \\ C & D \end{pmatrix} = \begin{pmatrix} 1 & y_1 - x_{0y} \\ 0 & 1 \end{pmatrix} \begin{pmatrix} 1 & 0 \\ -\frac{1}{f_2} & 1 \end{pmatrix} \begin{pmatrix} 1 & l_s \\ 0 & 1 \end{pmatrix} \begin{pmatrix} 1 & 0 \\ -\frac{1}{f_1} & 1 \end{pmatrix}$$
$$\begin{pmatrix} 1 & L - l_s - y_1 \\ 0 & 1 \end{pmatrix} \begin{pmatrix} 1 & 0 \\ -\frac{1}{F} & 1 \end{pmatrix} \begin{pmatrix} 1 & x_{0y} \\ 0 & 1 \end{pmatrix}$$

$$(5.53)$$

On simplification the matrix elements can be written as

$$A = \frac{\begin{array}{c} f_1(f_2(-L + x_{0y}) + (L - y_1)(-x_{0y} + y_1)) + F(f_1(f_2 + x_{0y} - y_1) + l_s(-x_{0y} + y_1)) \\ -Ff_2(l_s - x_{0y} + y_1) + (L - l_s - y_1)(l_s(x_{0y} - y_1) + f_2(l_s - x_{0y} + y_1)) \end{array}}{Ff_1f_2}$$

$$B = \frac{\begin{array}{c} x_{0y}\left(f_1\left(f_2\left(-L + x_{0y}\right) + (L - y_1)\left(-x_{0y} + y_1\right)\right)\right) \\ +x_{0y}\left((L - l_s - y_1)\left(l_s\left(x_{0y} - y_1\right) + f_2\left(l_s - x_{0y} + y_1\right)\right)\right) \\ +F\left(f_1\left(f_2 L + \left(x_{0y} - y_1\right)\left(L + x_{0y} - y_1\right)\right)\right) \\ -F\left(L - l_s + x_{0y} - y_1\right)\left(l_s\left(x_{0y} - y_1\right) + f_2\left(l_s - x_{0y} + y_1\right)\right) \end{array}}{Ff_1f_2}$$

$$(5.54)$$

$$C = \frac{1}{Ff_1f_2}(l_s^2 - Ff_1 - Ff_2 - f_1f_2 - y_1(f_1 + f_2) + l_s(y_1 + F - f_2 - L) + f_1 L + f_2 L)$$

$$(5.55)$$

$$D = \frac{1}{Ff_1f_2}\begin{pmatrix} Ff_1f_2 - Ff_1 L - Ff_2 L + y_1(f_1 + f_2)(F - x_{0y}) - Ff_1 x_{0y} \\ -Ff_2 x_{0y} - f_1f_2 x_{0y} + f_1 L x_{0y} + f_2 L x_{0y} + l_s^2(-F + x_{0y}) \\ +l_s(-(f_2 + L)x_{0y} + y_1(-F + x_{0y}) + F(f_2 + L + x_{0y})) \end{pmatrix}$$

$$(5.56)$$

We determine the half Rayleigh range z_{0y} as

$$z_{0y} = \mp \frac{\sqrt{-4F^2 f_1^2 f_2^2 + \begin{pmatrix} -2Ff_1f_2 + l_s^2(y_1 + F + f_2) + y_1^2(f_1 + f_2) \\ +Ff_1 L + Ff_2 L + f_1f_2 L - y_1(f_1 + f_2)L \\ -l_s(y_1^2 + (F + f_2)L - y_1(2f_2 + L)) \end{pmatrix}^2}}{2\begin{pmatrix} -l_s^2 + Ff_1 + Ff_2 + f_1f_2 + y_1(f_1 + f_2) \\ -(f_1 + f_2)L + l_s(-y_1 - F + f_2 + L) \end{pmatrix}}$$

$$(5.57)$$

The position of the beam waist x_{0y} is obtained as

$$x_{0y} = \frac{\begin{array}{c} -l_s^2 y_1 - l_s y_1^2 - l_s^2 F - 2l_s y_1 F + y_1^2 f_1 + 2y_1 F f_1 \\ +l_s^2 f_2 + 2l_s y_1 f_2 + y_1^2 f_2 + 2l_s F f_2 + 2y_1 F f_2 + l_s y_1 L \\ +l_s F L + y_1 f_1 L - F f_1 L - l_s f_2 L - y_1 f_2 L - F f_2 L + f_1 f_2 L \end{array}}{2 \left(\begin{array}{c} l_s^2 + l_s y_1 + l_s F - y_1 f_1 - F f_1 - l_s f_2 \\ -y_1 f_2 - F f_2 - f_1 f_2 - l_s L + f_1 L + f_2 L \end{array} \right)} \quad (5.58)$$

The beam waist ω_{0y} can be obtained using

$$\omega_{0y} = \sqrt{\frac{\lambda z_{0y}}{\pi n_{ref}}} \quad (5.59)$$

The beam aperture $\omega_{1 x_{0y}}$ on the lens L_1 can be estimated using

$$\omega_1^2(x_{0y}) = \omega_{0y}^2 \left[1 + \left(\frac{x_{0y}}{z_{0y}} \right)^2 \right] \quad (5.60)$$

The beam aperture $\omega_{2 x_{0y}}$ on the mirror M_2 can be estimated using

$$\omega_2^2(x_{0y}) = \omega_{0y}^2 \left[1 + \left(\frac{y_1 - x_{0y}}{z_{0y}} \right)^2 \right] \quad (5.61)$$

The contribution of the Gouy phase from this section is given by

$$\phi_{G2}(RT) = \arctan \left(\frac{x_{0y}}{z_{0y}} \right) - \arctan \left(\frac{-y_1 + x_{0y}}{z_{0y}} \right) \quad (5.62)$$

Next we consider the beam propagation in the arm $(L - l_s - y_1)$ of the cavity.

5.5 Calculations in the arm $(L - l_s - y_1)$

We perform once again the same calculations in the arm $(L - l_s - y_1)$ of the cavity. To do this, let the radiation start at a distance x_{0b} from the mirror M_1, strike and reflect off the mirror M_1 of the focal length f_1, travel through the arm of length l_s, strike the mirror M_2 of focal length f_2, reflect

off it, travel through the arm of length y_1, hit the lens L_1 of focal length F and refract through it, reflecting off the plane mirrors M_3, M_4 while traveling through a distance $(L - l_s - y_1 - x_{0b})$ to reach the starting point to cover one full round trip. One can express its round trip propagation in terms of the $ABCD$ matrices as

$$\begin{pmatrix} A & B \\ C & D \end{pmatrix} = \begin{pmatrix} 1 & L - l_s - y_1 - x_{0b} \\ 0 & 1 \end{pmatrix} \begin{pmatrix} 1 & 0 \\ -\frac{1}{F} & 1 \end{pmatrix} \begin{pmatrix} 1 & y_1 \\ 0 & 1 \end{pmatrix} \begin{pmatrix} 1 & 0 \\ -\frac{1}{f_2} & 1 \end{pmatrix}$$
$$\begin{pmatrix} 1 & l_s \\ 0 & 1 \end{pmatrix} \begin{pmatrix} 1 & 0 \\ -\frac{1}{f_1} & 1 \end{pmatrix} \begin{pmatrix} 1 & x_{0b} \\ 0 & 1 \end{pmatrix}$$

(5.63)

On simplification the matrix elements can be written as

$$A = \frac{\begin{pmatrix} l_s^2(y_1 - F - f_2) + Ff_1f_2 - y_1^2(f_1 + f_2) - Ff_1L - Ff_2L - f_1f_2L \\ +y_1(f_2(L - x_{0b}) + f_1(f_2 + L - x_{0b})) \\ +l_s\left(y_1^2 + (F + f_2)(f_1 + L - x_{0b}) - d_2(f_1 + 2f_2 + L - x_{0b})\right) \\ +Ff_1x_{0b} + Ff_2x_{0b} + f_1f_2x_{0b} \end{pmatrix}}{Ff_1f_2}$$

(5.64)

$$B = \frac{1}{Ff_1f_2} \left\{ \begin{array}{c} Ff_1f_2L - l_s^2(y_1 - F - f_2)(f_1 - x_{0b}) \\ -Ff_1Lx_{0b} - Ff_2Lx_{0b} - f_1f_2Lx_{0b} + Ff_1x_{0b}^2 + y_1^2(f_1(f_2 - x_{0b}) - f_2x_{0b}) \\ +y_1(f_2(L - x_{0b})x_{0b} - f_1(f_2L - 2f_2x_{0b} - Lx_{0b} + x_{0b}^2)) \\ +Ff_2x_{0b}^2 + f_1f_2x_{0b}^2 + d_1(y_1^2(-f_1 + x_{0b}) - (F + f_2)(f_1(L - 2x_{0b}) \\ +x_{0b}(-L + x_{0b}) + y_1(f_1(2f_2 + L - 2x_{0b}) + x_{0b}(-2f_2 - L + x_{0b})))) \end{array} \right\}$$

(5.65)

$$C = \frac{1}{Ff_1f_2}\left(-Ff_1 - Ff_2 - f_1f_2 + l_s(-y_1 + F + f_2) + y_1(f_1 + f_2)\right) \quad (5.66)$$

$$D = \frac{1}{Ff_1f_2}\begin{pmatrix} Ff_1f_2 + l_s(y_1 - F - f_2)(f_1 - x_{0b}) - Ff_1x_{0b} \\ -Ff_2x_{0b} - f_1f_2x_{0b} + y_1(-f_1f_2 + f_1x_{0b} + f_2x_{0b}) \end{pmatrix}$$

(5.67)

We determine the half Rayleigh range z_{0b} as

$$z_{0b} = \mp \frac{\sqrt{-4F^2 f_1^2 f_2^2 + \left(\begin{array}{c} -2Ff_1f_2 + l_s^2(-y_1 + F + f_2) + y_1^2(f_1 + f_2) \\ +Ff_1L + Ff_2L + f_1f_2L - y_1(f_1 + f_2)L \\ -l_s(y_1^2 + (F + f_2)L - y_1(2f_2 + L)) \end{array}\right)^2}}{2\left((y_1 - F)(l_s - f_1) + 2(-l_s - y_1 + F + f_1)f_2\right)}$$

(5.68)

The position of the beam waist x_{0b} is obtained as

$$x_{0b} = \frac{\begin{array}{c} -l_s^2 y_1 - l_s y_1^2 + l_s^2 F + 2l_s y_1 f_1 + y_1^2 f_1 - 2l_s F f_1 + l_s^2 f_2 + 2l_s y_1 f_2 \\ +y_1^2 f_2 - 2l_s f_1 f_2 - 2y_1 f_1 f_2 + l_s y_1 L \\ -l_s F L - y_1 f_1 L + F f_1 L - l_s f_2 L - y_1 f_2 L + F f_2 L + f_1 f_2 L \end{array}}{\left(2\left(l_s y_1 - l_s F - y_1 f_1 + F f_1 - l_s f_2 - y_1 f_2 + F f_2 + f_1 f_2\right)\right)}$$

(5.69)

The beam waist ω_{0b} can be obtained using

$$\omega_{0b} = \sqrt{\frac{\lambda z_{ob}}{\pi n_{ref}}}$$

(5.70)

The beam aperture $\omega_{1x_{0b}}$ on the mirror M_1 can be estimated using

$$\omega_1^2(x_{0b}) = \omega_{0b}^2 \left[1 + \left(\frac{x_{0b}}{z_{0b}}\right)^2\right]$$

(5.71)

The beam aperture $\omega_{2x_{0s}}$ on the lens L_1 can be estimated using

$$\omega_2^2(x_{0b}) = \omega_{0b}^2 \left[1 + \left(\frac{L - l_s - y_1 - x_{0b}}{z_{0b}}\right)^2\right]$$

(5.72)

The contribution of the Gouy phase from this section is given by

$$\phi_{G3}(RT) = \arctan\left(\frac{x_{0b}}{z_{0b}}\right) - \arctan\left(\frac{-L + l_s + y_1 + x_{0b}}{z_{0b}}\right)$$

(5.73)

Using the above calculations, we study the behaviour of beam waists, the positions of them, the spot sizes on the mirrors in each of the arms of 3CURC.

Therefore the accumulated round trip Gouy phase $\phi_G(RT)$ for the chosen cavity is the sum of $\phi_{G1}(RT)$, $\phi_{G2}(RT)$ and $\phi_{G3}(RT)$ which is given by

$$
\begin{aligned}
\phi_G(RT) \;=\; & \arctan\left(\frac{x_{0s}}{z_{0s}}\right) - \arctan\left(\frac{-l_s + x_{0s}}{z_{0s}}\right) \\
& + \arctan\left(\frac{x_{0y}}{z_{0y}}\right) - \arctan\left(\frac{-y_1 + x_{0y}}{z_{0y}}\right) \\
& + \arctan\left(\frac{x_{0b}}{z_{0b}}\right) - \arctan\left(\frac{-L + l_s + y_1 + x_{0b}}{z_{0b}}\right) \quad (5.74)
\end{aligned}
$$

We now proceed to study the Gouy phase in specific cases of 3CURC and discuss in the following section.

5.6 Variable Gouy phase in 3CURC

From the section 5.2.5, it is analyzed that there exist different stable contours for different combinations of l_s and y_1 for a fixed L. Even though we have identified different Gouy phase regions in each of the stability diagrams, in this section we consider three specific cases, in each of these cases we give attention to the system parameters for which at least the merging of two distinct stable regions takes place. We study the behaviour of half Rayleigh ranges, the positions of the beam waists, the spot sizes on the mirrors and the corresponding variable Gouy phase in each of the cases in the following.

5.6.1 Case(i): For a given $f_1 = f_2 = f$, F, l_s and L

Here in this case we consider the first combination of focal lengths of the mirrors M_1 and M_2 to be symmetric with the aim to remove the forbidden zone associated with them, as we have seen in the case of 2CURC. For the considered $f_1 = f_2 = 50$cm, $F = 100$cm, the merging of the stable regions is occurring for the value of cavity length $L = 400$cm and for $l_s = 120$cm, for which a long continuous stable region of y_1 from 7.33501cm to 272.665cm

is available. For this case the half Rayleigh ranges in each of the arms for

Figure 5.25: **Half Rayleigh ranges** z_{0s}, z_{0y}, **and** z_{0b} **as a function of** y_1 **for** $f_1 = f_2 = 50$**cm,** $F = 100$**cm,** $l_s = 120$**cm,** $L = 400$**cm**

varying y_1 are plotted in Fig. (5.25). It is observed that the half Rayleigh range z_{0s} in the arm of length l_s is varying very slowly, where as z_{0y} is raising suddenly at small values of y_1 on the other hand z_{0b} is raising at larger y_1. The positions x_{0s}, x_{0y}, and x_{0b} of the beam waists are plotted in the Fig. (5.26). The negative sign shows that beam spot size is positioned at the other side of beam waist. The spot sizes on the mirrors M_1, M_2 and the lens L_1 as a function of y_1 are plotted in the Fig. (5.27). It is noticed that initially for smaller stable y_1, the spot sizes are large and for the rest of the stable y_1, they are varying linearly. The Fig. (5.28) shows the Gouy phase variation in the arms l_s, y_1 and $(L - l_s - y_1)$ which are $\phi_{G1}(RT)$, $\phi_{G2}(RT)$, $\phi_{G3}(RT)$ and the accumulated Gouy phase $\phi_G(RT)$. It is found that there is a very small variation of Gouy phase around $\dfrac{2\pi}{3}$ is obtained for this case as shown. We move now to the case that is for a given f_1, $f_2 = F = f$, l_s and L and study the same parameters in the following.

Figure 5.26: **The positions x_{0s}, x_{0y}, and x_{0b} of the beam waists as a function of y_1 for $f_1 = f_2 = 50$cm, $F = 100$cm, $l_s = 120$cm, $L = 400$cm**

Figure 5.27: **The spot sizes on the mirrors M_1, M_2, and the lens L_1 as a function of y_1 for $f_1 = f_2 = 50$cm, $F = 100$cm, $l_s = 120$cm, $L = 400$cm**

5.6.2 Case(ii): For a given f_1, $f_2 = F = f$, l_s and L

Here in this case we consider the second combination of focal lengths of the mirrors M_2 and lens L_1 to be symmetric with the same aim to remove
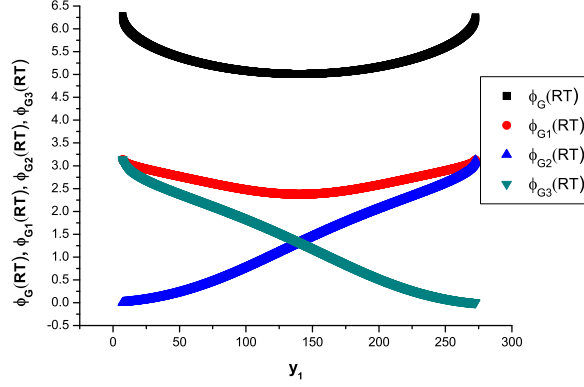
Figure 5.28: **Variable Gouy phases** $\phi_{G1}(RT)$, $\phi_{G2}(RT)$, $\phi_{G3}(RT)$ **and** $\phi_G(RT)$ **as a function of** y_1 **for** $f_1 = f_2 = 50\text{cm}$, $F = 100\text{cm}$, $l_s = 120\text{cm}$, $L = 400\text{cm}$

the forbidden zone associated with them. For the considered $f_1 = 50\text{cm}$, $f_2 = F = 100\text{cm}$, the merging of the stable regions is happening for the value of cavity length $L = 600\text{cm}$ and for $l_s = 200\text{cm}$, for which the stable region of y_1 from 200cm to 400cm is available. For this case the behaviour of half Rayleigh ranges for varying y_1 is plotted in Fig. (5.29). Here the half Rayleigh ranges z_{0y} and z_{0b} are behaving opposite to each other where as z_{0s} is very much confined within the arm of length l_s. The positions x_{0s}, x_{0y} and x_{0b} of the beam waists as a function of y_1 are shown in the Fig. (5.30). The spot sizes on the mirrors M_1, M_2 and the lens L_1 as a function of y_1 are plotted in Fig. (5.31). They are higher at the edges of the stable region and varying linearly in between these end points of the stable region. The Fig. (5.32) shows the Gouy phase variation in the arms l_s, y_1 and $(L - l_s - y_1)$ which are $\phi_{G1}(RT)$, $\phi_{G2}(RT)$, $\phi_{G3}(RT)$ and the accumulated Gouy phase $\phi_G(RT)$. Here also there is a very small variation of Gouy phase around $\dfrac{2\pi}{3}$ is achieved.
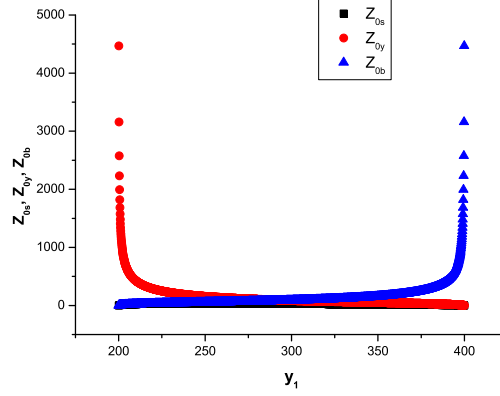
Figure 5.29: **Half Rayleigh ranges** z_{0s}, z_{0y} **and** z_{0b} **as a function of** y_1 **for** $f_1 = 50$**cm,** $f_2 = F = 100$**cm,** $l_s = 200$**cm,** $L = 600$**cm**
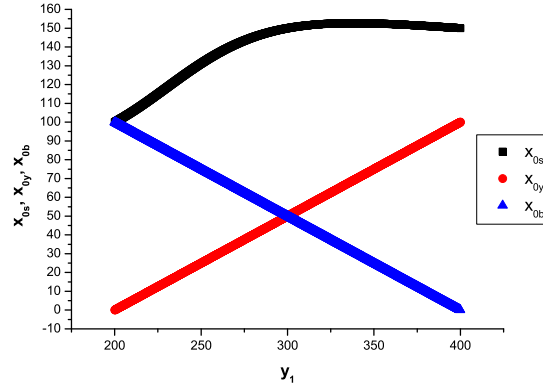
Figure 5.30: **The positions** x_{0s}, x_{0y} **and** x_{0b} **of the beam waists as a function of** y_1 **for** $f_1 = 50$**cm,** $f_2 = F = 100$**cm,** $l_s = 200$**cm,** $L = 600$**cm**

For the above two cases with two of the focal lengths to be symmetric, we have achieved a very small amount of Gouy phase, a variation of $\dfrac{2\pi}{3}$. Now what happens if all of the focal lengths of the 3CURC to be symmetric? Is it
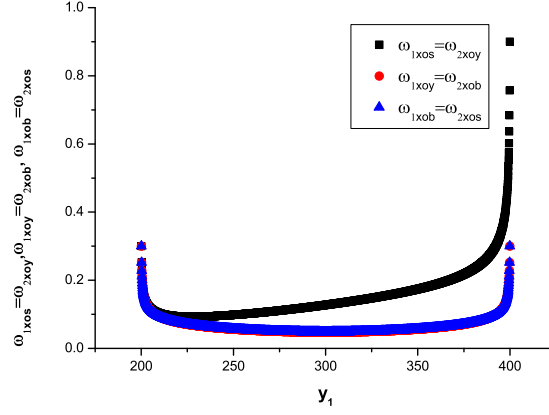
Figure 5.31: **The spot sizes on the mirrors M_1, M_2 and the lens L_1 as a function of y_1 for $f_1 = 50$cm, $f_2 = F = 100$cm, $l_s = 200$cm, $L = 600$cm**
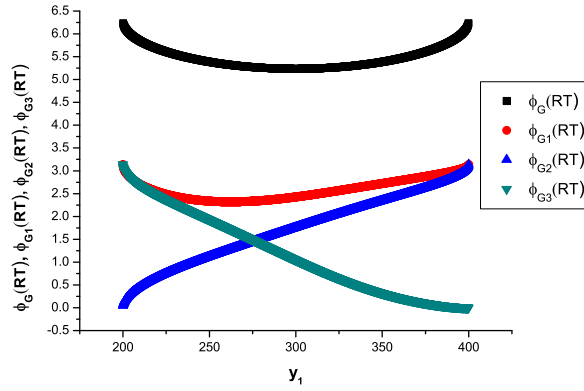
Figure 5.32: **Variable Gouy phases $\phi_{G1}\left(RT\right)$, $\phi_{G2}\left(RT\right)$, $\phi_{G3}\left(RT\right)$ and $\phi_G\left(RT\right)$ as a function of y_1 for $f_1 = 50$cm, $f_2 = F = 100$cm, $l_s = 200$cm, $L = 600$cm**

possible to achieve more variable Gouy phase? We take up this in the next

section.

5.6.3 Case(iii): For a given $f_1 = f_2 = F = f$, l_s and L

Consider the case when symmetric $f = 30$cm, $l_s = 120$cm, $L = 360$cm. For this set of parameters the marginal stable solutions of y_1 are $80, 120, 120, 160$cm. Therefore $y_1 = 80$cm to 120cm is a continuous stable region. For this range
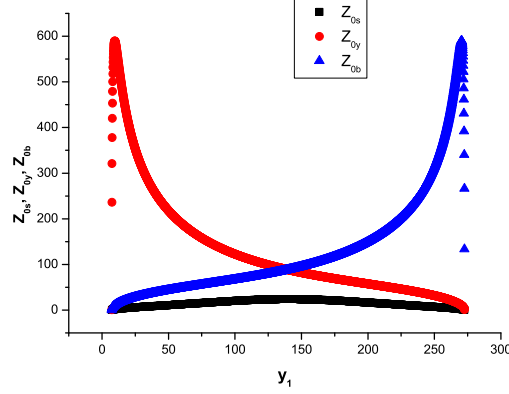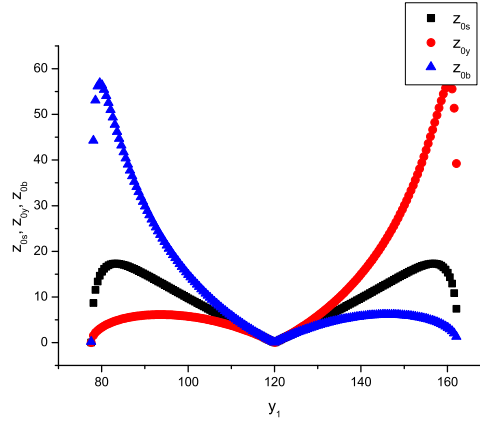

Figure 5.33: **Half Rayleigh ranges z_{0s}, z_{0y} and z_{0b} as a function of y_1 for $f_1 = f_2 = F = 30$cm, $l_s = 120$cm, $L = 360$cm**

of parameters, the Fig. (5.33) shows the half rayleigh ranges z_{0s}, z_{0y} and z_{0b} in the corresponding arms l_s, y_1 and $(L - l_s - y_1)$ of the cavity. All the half Rayleigh ranges are coinciding at $y_1 = 120$cm. z_{0s} increases varying y_1 then becomes 0 at $y_1 = 120$cm, as y_1 increases further z_{0s} increases again and it becomes zero at $y_1 = 160$cm. The other two half Rayleigh ranges in the arms y_1 and $(L - l_s - y_1)$ are behaving opposite to one another. z_{0y} is starting at lower values initially for small values of y_1 then it reaches 0 when $y_1 = 120$cm, as y_1 increases further, z_{0y} reaches the higher values, where as z_{0b} starts from higher values for small values of y_1 then decreases and as it

reaches $y_1 = 120$cm it becomes 0, after that it increases slightly and will be back to 0 as y_1 reaches to $y_1 = 160$cm. The corresponding positions of spot sizes are shown in the Fig. (5.34). All the positions of the spot sizes meet at a common point that is at 60cm at $y_1 = 120$cm, i.e., $l_s = 120$cm, $(L - l_s - y_1) = 120$cm for a given $L = 360$cm. Fig. (5.35) shows the variation
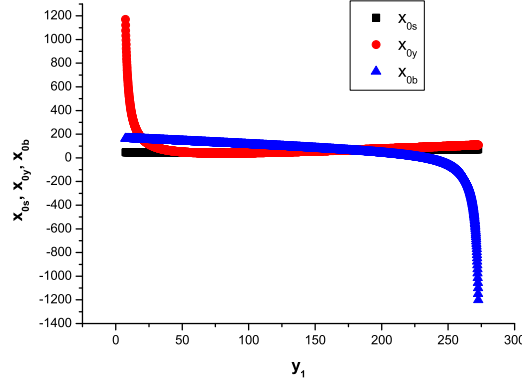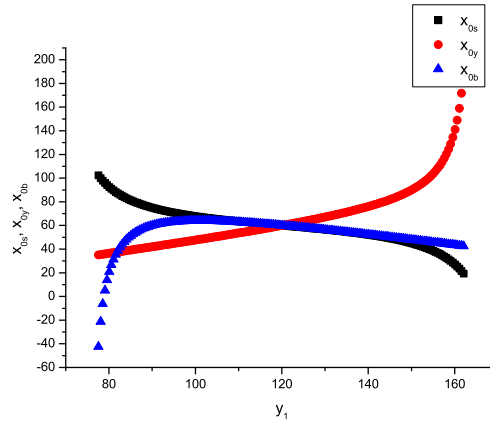

Figure 5.34: **The positions x_{0s}, x_{0y} and x_{0b} of the beam waists as a function of y_1 for $f_1 = f_2 = F = 30$cm, $l_s = 120$cm, $L = 360$cm**

of spot sizes on the lenses as the distance y_1 varies. From this figure it is seen that the spot sizes are higher at the starting point of the stable region that is around $y_1 = 80$cm and they are minimum at $y_1 = 160$cm. The Fig. (5.36) shows the variable Gouy phases $\phi_{G1}(RT)$, $\phi_{G2}(RT)$, $\phi_{G3}(RT)$ in the corresponding three arms l_s, y_1 and $(L - l_s - y_1)$ and the accumulated Gouy phase variation $\phi_G(RT)$. It is noticed that the variation of the accumulated Gouy phase as $2\pi - 3\pi - 2\pi$ with varying y_1. In the next section we understand the situations where mod hops[2] can occur before we demonstrate the tuning capability of the Gouy phase variation in the ring laser.
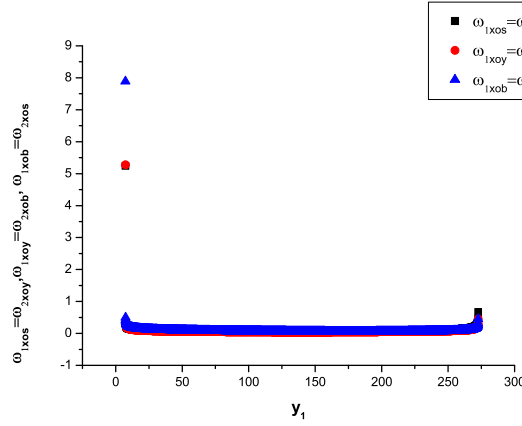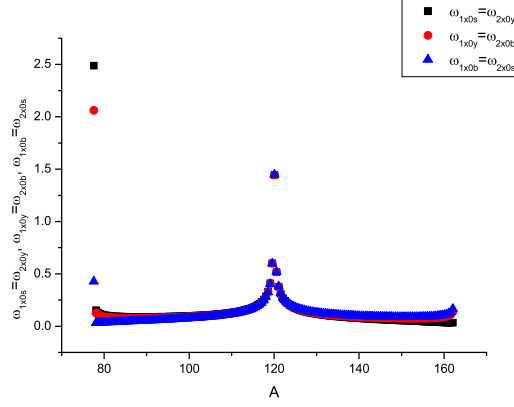
Figure 5.35: **The spot sizes on the mirrors M_1, M_2 and the lens L_1 as a function of y_1 for $f_1 = f_2 = F = 30$cm, $l_s = 120$cm, $L = 360$cm**
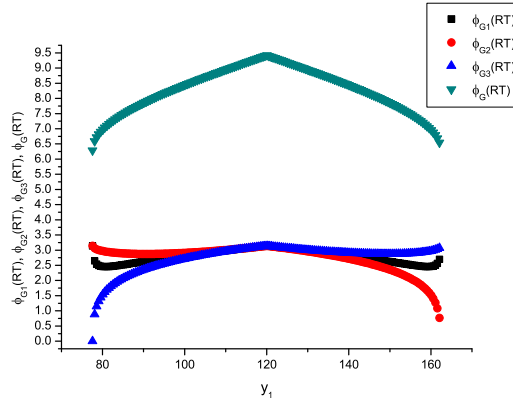
Figure 5.36: **Variable Gouy phases $\phi_{G1}\left(RT\right)$, $\phi_{G2}\left(RT\right)$, $\phi_{G3}\left(RT\right)$ and $\phi_G\left(RT\right)$ as a function of y_1 for $f_1 = f_2 = F = 30$cm, $l_s = 120$cm, $L = 360$cm**

5.7   Mode hop and stability regions

A mode hop is an indication of shift of stability from one region to another. To bring out the mode hop region the stability function is studied with y_1

for different l_s, shown in Fig. (5.37) for values of $f_1 = 100$cm, $f_2 = F = 50$cm, $L = 350$cm and l_s is varied from 5cm to 100cm. It is observed from the Fig. (5.37) that, for curves $(1), (2), (3)$ instability exists$((\frac{A+D}{2})^2 - 1 > 0)$ for three respective ranges of y_1. In an unstable region the beam spots on the mirror diverge off the mirror. This represents unstable mode and due to heavy losses for it, leads to small field amplitude in the cavity. Another region of vanishingly small field amplitude in the cavity occurs for the mode for which the total number of half wave lengths in the cavity length becomes odd, then the destructive interference occurs between the return beam and original beam propagating in the same direction. The unstable or mode hop demanding regions can be altered and thus can be controlled(see below).
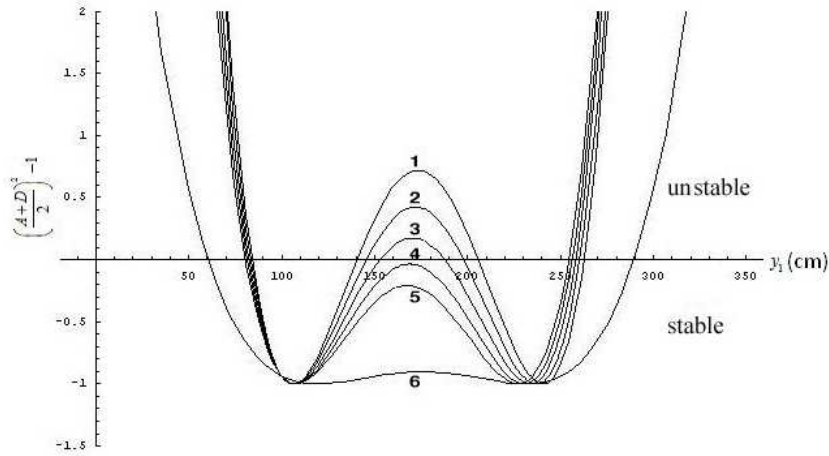
Figure 5.37: **Stability parameter variation as a function of y_1, for different l_s and $L = 350$cm. Here curves numbered 1, 2, 3, 4, 5, 6 are respectively for $l_s = 5, 10, 15, 20, 25, 100$cm**

5.7.1   Control of stability

The instability of the cavity can be eliminated as is seen from Fig. (5.37). One can have the middle unstable region converted to continuous stable region by a choice of l_s e.g. consider transition of curves like (1), (2), (3) to those like (4), (5), (6) in Fig. (5.37). There is one continuous region of stability for a wide range of y_1 in each of the (4), (5) and (6). In Fig. (5.38a),

(a) l_s **versus stable** y_1 (b) y_1 **versus** ϕ_G
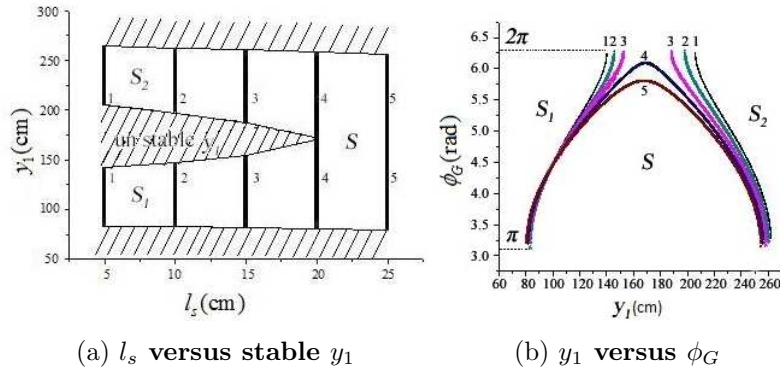
Figure 5.38: **All parameters and numberings are same as in Fig. 5.37**

we show the stable (unhatched) region of y_1, as a function of $l_s(5 < l_s < 25)$. Initially for small values of l_s, two stable regions marked S_1 and S_2 are seen bound by three unstable regions shown as hatched. No mode oscillates in the hatched regions. The vanishing/emergence of the middle hatched region is the source of mode hop discussed above. This region can be seen to vanish for $l_s \geq 20$ in Fig. (5.38a). The variation of Gouy phase for the cases discussed in Fig. (5.38a) is shown in Fig. (5.38b). It is observed that stable region S_1 contributes a variation in the Gouy phase from π to 2π and the stable region S_2 gives the variation in reverse that is from 2π to π. On elimination of unstable region for $l_s \geq 20$, i.e., in the region marked S, one may shift origin of the Gouy phase(on line 4&5) and see it as varying from $-\dfrac{\pi}{2}$ to $\dfrac{\pi}{2}$. The continuous variability of the Gouy phase dependent tuning without

encountering a mode hop in the region of interest is the important result of the 3CURC. In the following we use Gouy phase for path length control in a ring laser gyro.

5.8 Gouy Phase for Path Length Control in Ring Laser Gyroscopes

One possible application where this result can be useful is Ring laser gyroscopes (RLGs). Ring laser gyroscopes are used to determine angular displacement or angular rates of the platform on which they are fixed. Ring laser gyros have two laser beams counter propagating inside a ring cavity. These devices work on the principle of Sagnac effect. When RLG rotates a path length difference is created between the two beams. This difference is detected as the frequency difference between the two beams since the two beams pass through different cavity path lengths and hence have different frequencies. The beat frequency is given by the relation

$$\Delta\nu = \frac{4A}{\lambda L}.\Omega \tag{5.75}$$

where 'L' is optical path length of the cavity along which the laser beams traverse, 'A' is the area enclosed by the path 'L', 'λ' is the wavelength of the laser beams in the absence of rotation and 'Ω' is the rotation rate.

If for any reason, other than rotation, path length changes, then the beat frequency will be different for the same rotation rate. Therefore it is essential to maintain the path length and frequency of the laser beams to have a useful result from the RLG. The main reason for path length variation is temperature change. This is unavoidable and hence a control mechanism is required to keep the frequency constant. This control is in general done by moving one or two mirrors forming the ring cavity.

Consider the case of increasing path length. To keep the path length same and hence the frequency, at least one mirror has to be moved to compensate the increase. The mirror cannot be moved for large distances i.e., involving multiple λ change of length. Assume that mirror movement can control the length only for one λ variation in path length. Note that at the end of such a control the change in the cavity length has become such as to accommodate at the gain peak frequency $(n+1)^{th}$ longitudinal configuration if the mirror is reset to its unshifted position of nth longitudinal configuration at the gain peak. The laser could lase at the peak of the gain function. Thus, once the limit for control is reached, resetting the position of the mirrors is a good option. During a reset the beams may go through a zero intensity point if gain is not adjusted properly. This can lead to an unwarranted output.

An unexplored mechanism, to the authors' knowledge, to control frequency using Gouy phase during a reset is proposed.

By modifying the Gouy phase of the laser beam inside the ring resonator, the frequency of the laser can be changed, as has been learned in the last section. Change in frequency, when Gouy phase is varied by $\Delta\phi_G$, is given by

$$\Delta\nu = c.\frac{\Delta\phi_G}{2\pi L} \qquad (5.76)$$

Fig. 5.39 shows the frequency variation due to Gouy phase alone. Also, any change in length results not only in frequency change but Gouy phase change too. However the change in Gouy phase due to change in physical length by one wave length is negligible. Thus to keep the frequency constant on a small physical change of length an alternative is by changing Gouy phase. However Gouy phase can be varied by an amount of π for a ring resonator with one lens. This is equivalent to a length variation of $\frac{\lambda}{2}$. It only implies that Gouy phase can be used to control the frequency for a path length variation up to $\frac{\lambda}{2}$.

Before going into further discussion about frequency control using Gouy
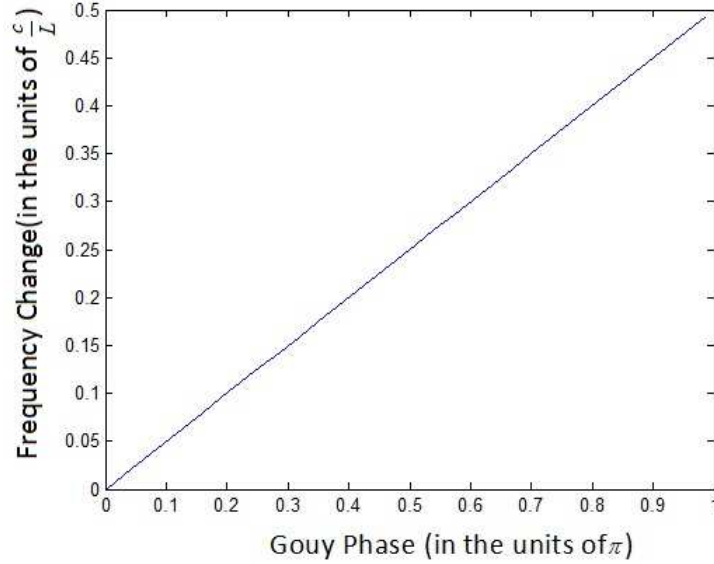
Figure 5.39: **Change in frequency versus Gouy phase**

phase, one should understand what happens during the resets. It is assumed that a reset is required for every λ change in path length. During reset option, the position of the mirror(s) is brought to its original position. As a result, the length of the cavity is increased by about one wavelength. During this, changes occur: first, the frequency of the mode under operation can drift away from the gain center and can get out of the gain width, and second, another mode can take birth on the other side of the gain peak which can reach the gain center when the path length has increased exactly by one wavelength. This brings the laser back to the same frequency as before the reset but for the next order mode. This result if put into Eq. (1.1) will give the following result. Before the reset

$$2n\pi = kL + \phi_G \qquad (5.77)$$

After reset

$$2(n+1)\pi = k(L + \lambda) + \phi_{G}\prime \tag{5.78}$$

$$\phi\prime_{G} - \phi_{G} = 2\pi - k\lambda = 2\pi - 2\pi = 0 \tag{5.79}$$

Therefore, Gouy phase before and after reset has to be same. Here, 'k' is same, before and after reset as the wavelength is same at the gain peak($\lambda = \lambda_c$). During mirror reset, the path length will vary by one wavelength (here it is
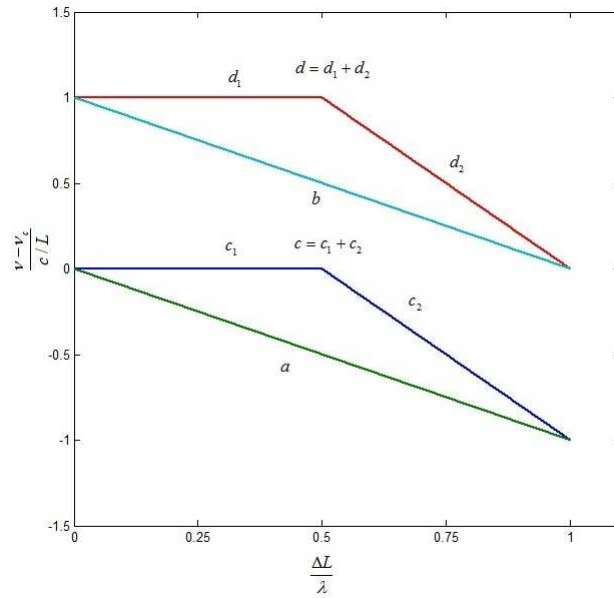
Figure 5.40: **Frequency variations during reset**

assumed that path length variation due to temperature during the reset period is negligible). Reset is considered to have two parts: first, till the path length varies by $\dfrac{\lambda_c}{2}$ and the second from $\dfrac{\lambda_c}{2}$ to λ_c.

Fig. 5.40 represents how Gouy phase can be used to modify the frequency of oscillating mode during mirror reset. On x-axis, path length variation normalized to one wavelength i.e., $\dfrac{\Delta L}{\lambda}$ is shown. While the y-axis

depicts the difference between the operating frequency(ν) and frequency at gain center(ν_c) normalized to the FSR ($\frac{c}{L}$) of the resonator, i.e., $\dfrac{\nu - \nu_c}{c/L}$.

Let curves 'a' and 'b' represent the change in frequency of two adjacent modes (0&1) during the mirror reset done at constant rate without exploiting Gouy phase effect. On the other hand c_1 and d_1 represent the constancy of the frequency of oscillating mode kept so by compensation of the change due to the mirror reset by using simultaneously and suitably the Gouy phase. This acts for half period of the reset. c_2 and d_2 represent, during the second half of the reset, the faster variation of the frequency of the oscillating modes due to the simultaneous reversal of the Gouy phase, and mirror position.

Thus, using Gouy phase has definite advantages. First, the frequency control could be extended in to half the mirror reset period. Second, the rate at which the reset takes place during the second part of the reset is faster.

To conclude major role of Gouy phase in the performance of RLGs, is anticipated.

5.9   Conclusion

The crucial role of Gouy phase in the selection of modes of the laser has been explained. This gives additional guidance for designing the tunable lasers with the inclusion of the Gouy phase effect. It is useful to have the option of variation of Gouy phase for tuning in situations where other tuning mechanisms have reached a restricted region of applicability. In the next chapter, to see the maximum variation of Gouy phase we consider the four converging unit ring cavity.

Bibliography

[1] M. Fatih Erden and Haldun M. Ozaktas, "Accumulated Gouy phase shift in Gaussian beam propagation through first-order optical systems," J. Opt. Soc. Am. A, vol. 14, No. 9, pp. 2190-2194, Sep 1997.

[2] K. Sudha Nirmala, M. Sree Ramana, S. P. Tewari, "Tuning of ring laser by varying Gouy phase", Optics Communicatons, vol. 284, Issues 10-11, pp. 2560-2564, May 2011.

6

Four Lens Ring Cavity

In the previous chapters 3, 4, and 5, it has been emphasized that one can create 'N' number of converging units, correspondingly 'N' Gaussian modes by inserting 'N' lenses in a cavity. The aim of achieving the accumulated Gouy phase variation of $N\pi$ is existing repeatedly.

Note again the overall conclusions of the analysis of SCURC, 2CURC and 3CURC in the following.

(a) SCURC for which $N = 1$, shows the Gouy phase variation of $0 - \pi$ or $\pi - 0$.

(b) The case of $N = 2$ corresponds to 2CURC, which can behave as SCURC($N = 1$) under the conditions of L, one can have the accu-

mulated Gouy phase variation either $0 - \pi$ or $\pi - 0$ in the limit of SCURC and $\pi - 2\pi$ or $2\pi - \pi$ or $\pi - 2\pi - \pi$ where two modes are present in 2CURC.

(c) The 3CURC for which $N = 3$, can be converted to SCURC and 2CURC, shows the accumulated Gouy phase variation discussed in the above two cases (a) and (b), in addition it also shows the accumulated Gouy phase variation of $2\pi - 3\pi$ or $3\pi - 2\pi$ or $2\pi - 3\pi - 2\pi$ when all the three modes are present in 3CURC.

From the analysis of 3CURC, it is noticed that there exist four disjointed stable regions, for $L > L_M = 4f_1 + 4f_2 + 4F$ and realized that each of them corresponds to a different phase variation. As a result, one can not be able to achieve an accumulation of the variable Gouy phase up to 3π, even though different phase regions are present. As length L varies from L_M to lower values of L, it is noticed that the merging of these distinct stable regions starts taking place. In such a case the amount of accumulated Gouy phase variation is turning out to be π and even less than π for some cases.

One of the reasons for the existence of disjointed regions could be the creation of an odd number of modes in between the three lenses in the cavity. Therefore as a final attempt here in this chapter we consider 4CURC, to create an even number of modes i.e., four converging gaussian modes and also symmetry between the optical elements of the cavity, to see whether it is possible to get an accumulation of Gouy phase up to $N\pi$ or not. We describe the configuration of 4CURC in the following.

6.1   4 Converging Unit Ring Cavity (4CURC)

A schematic of the 4CURC is shown in the Fig. (6.1). This ring configuration consists four lenses L_1, L_2, L_3 and L_4 of focal lengths f_1, f_2, f_3
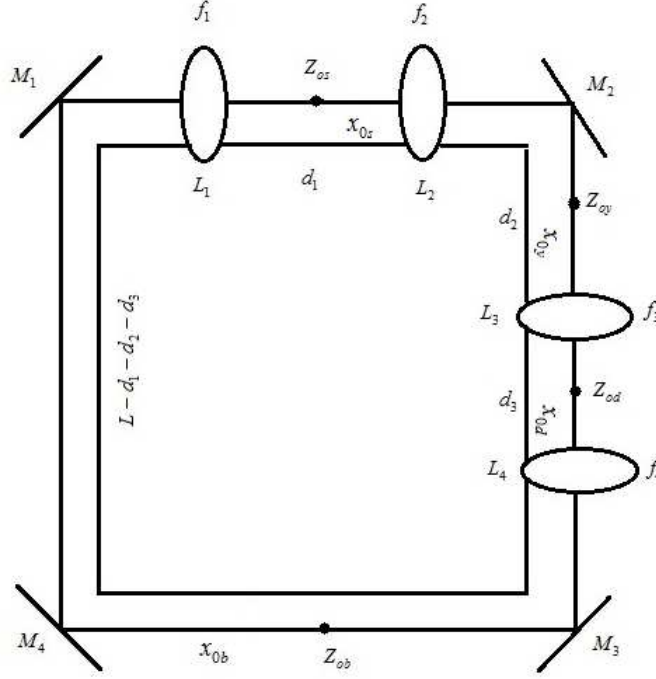
Figure 6.1: **The** 4 **Converging Unit Ring Cavity (4CURC)**

and f_4 which are separated from one another by a distances of d_1, d_2, d_3 and $L - d_1 - d_2 - d_3$ respectively, where L is the length of the cavity. In addition to these four lenses, it also contains four 100% plane mirrors M_1, M_2, M_3 and M_4.

For this configuration there exist four modes, one in the arm of d_1 in between the lenses L_1 and L_2, the second mode in the arm of length d_2, in between the lenses L_2 and L_3, the third mode in the arm of length d_3 in between the lenses L_3 and the lens L_4 and the fourth mode in the arm of length $(L - d_1 - d_2 - d_3)$ in between the lenses L_4 and L_1. The Gaussian beams in the respective sections constitute a part of stable configuration of radiation-travel in the ring, with half Rayleigh ranges z_{0s} in the d_1 arm, z_{0y} in the d_2 arm, z_{0d} in the d_3 arm and z_{0b} in the $L - d_1 - d_2 - d_3$ arm; with

waist locations x_{0s}, x_{0y}, x_{0d} and x_{0b} respectively.

Here also each Gaussian mode contributes its Gouy phase to the round trip Gouy phase in the ring. One can fix the gain medium in any one of the three separation distances d_1, d_2, d_3 and vary the remaining two distances, to vary the effective focal length of the combinations, to vary $\phi_G(RT)$ which is the sum of the Gouy phases of the four parts of the 4CURC.

We define here the coordinate x_p in the clockwise sense in the ring with L_1 at $x_p = 0$, L_2 at $x_p = d_1$, L_3 at $x_p = d_1 + d_2$ and L_4 at $x_p = d_1 + d_2 + d_3$. For the four Gaussian modes with half Rayleigh ranges z_{0s}, z_{0y}, z_{0d} and z_{0b}, the points $x_{0s}\,(x_p = d_1 - x_{0s})$, $x_{0y}\,(x_p = d_2 - x_{0y})$, $x_{0d}\,(x_p = d_3 - x_{0d})$, and $x_{0b}\,(x_p = L - d_1 - d_2 - d_3 - x_{0b})$ determine the positions of the beam waists ω_{0s}, ω_{0y}, ω_{0d} and ω_{0b} respectively. Next we study and analyze the stability of the 4CURC in detail in the following section.

6.2   Stability Analysis:

For consideration of the stability let the radiation just enter before the lens L_1 of focal length f_1 and refracts off it, in the clockwise direction travel through a distance d_1 from the lens L_1, as it hits another lens L_2 of focal length f_2, travel through a distance d_2 from the lens L_2, strikes the lens L_3 of focal length f_3, travel through a distance d_3 from the lens L_3, hits the lens L_4 of focal length f_4, it refracts off it, reflecting off the mirrors M_2, M_3, M_4 and M_1 in the order, travel through the distance $(L - d_1 - d_2 - d_3)$, complete the round trip just before the lens L_1 where it starts its journey. The round trip $ABCD$-matrix at the lens L_1 in the ring is

$$\begin{pmatrix} A & B \\ C & D \end{pmatrix} = \begin{pmatrix} 1 & L - d_1 - d_2 - d_3 \\ 0 & 1 \end{pmatrix} \begin{pmatrix} 1 & 0 \\ -\frac{1}{f_4} & 1 \end{pmatrix} \begin{pmatrix} 1 & d_3 \\ 0 & 1 \end{pmatrix}$$

$$\begin{pmatrix} 1 & 0 \\ -\frac{1}{f_3} & 1 \end{pmatrix} \begin{pmatrix} 1 & d_2 \\ 0 & 1 \end{pmatrix} \begin{pmatrix} 1 & 0 \\ -\frac{1}{f_2} & 1 \end{pmatrix} \begin{pmatrix} 1 & d_1 \\ 0 & 1 \end{pmatrix} \begin{pmatrix} 1 & 0 \\ -\frac{1}{f_1} & 1 \end{pmatrix} \quad (6.1)$$

The complete round trip matrix elements can be calculated using matrix multiplication. The self consistency requires that

$$(A + D)^2 - 4 \leq 0 \qquad (6.2)$$

The two alternatives for the marginal stability case of (6.2)

$$
\begin{aligned}
A + D + 2 \;=\; & \frac{1}{f_1 f_2 f_3 f_4} [-d_3^2 \left(f_1 f_2 - f_1 f_3 - f_2 f_3\right) + d_2^2 (f_1 + f_2)(d_3 - f_3 - f_4) + 4 f_1 f_2 f_3 f_4 \\
& + d_1^2 \left(-f_2 f_3 + d_3(f_2 + f_3) - (f_2 + f_3) f_4 + d_2(-d_3 + f3 + f_4)\right) \\
& d_3 f_1 f_2 L + d_3 f_1 f_3 L + d_3 f_2 f_3 L - f_1 f_2 f_3 L - f_1 f_2 f_4 L - f_1 f_3 f_4 L - f_2 f_3 f_4 L \\
& + d_2(f_1 + f_2) \left(d_3^2 + (f_3 + f_4)L - d_3(2 f_3 + L)\right) + d_1 d_3^2 (f_2 + f_3) \\
& + d_1 d_2^2 (-d_3 + f_3 + f_4) + d_1(f_2 f_3 + (f_2 + f_3) f_4)L - d_1 d_3 (2 f_2 f_3 + (f_2 + f_3)L) \\
& - d_1 d_2 \left(d_3^2 + (f_3 + f_4)(2 f_2 + L) - d_3(2(f_2 + f_3) + L)\right)] \qquad (6.3)
\end{aligned}
$$

$$
\begin{aligned}
A + D - 2 \;=\; & \frac{1}{f_1 f_2 f_3 f_4} [-d_3^2 \left(f_2 f_3 + f_1(f_2 + f_3)\right) + d_2^2 (f_1 + f_2)(d_3 - f_3 - f_4) \\
& + d_1^2 \left(-f_2 f_3 + d_3(f_2 + f_3) - (f_2 + f_3) f_4 + d_2(-d_3 + f_3 + f_4)\right) \\
& + \left(d_3 f_1 f_2 + d_3 f_1 f_3 + d_3 f_2 f_3 - f_1 f_2 f_3 - (f_2 f_3 + f_1(f_2 + f_3)) f_4\right) L \\
& + d_2(f_1 + f_2) \left(d_3^2 + (f_3 + f_4)L - d_3(2 f_3 + L)\right) + d_1 d_3^2 (f_2 + f_3) \\
& + d_1 \left(+ d_2^2(-d_3 + f_3 + f_4) + (f_2 f_3 + (f_2 + f_3) f_4) L\right) - 2 d_1 d_3 f_2 f_3 \\
& + d_1 d_3 (f_2 + f_3) L - d_1 d_2 \left(d_3^2 + (f_3 + f_4)(2 f_2 + L) - d_3(2(f_2 + f_3) + L)\right)]
\end{aligned}
$$

$$(6.4)$$

For this case the marginal stability of the condition (6.2) becomes

$$
\begin{aligned}
(A + D)^2 - 4 \;=\; & -4 + \frac{1}{f_1^2 f_2^2 f_3^2 f_4^2} [d_3^2(f_1 f_2 + f_1 f_3 + f_2 f_3) - d_2^2(f_1 + f_2)(d_3 - f_3 - f_4) \\
& - 2 f_1 f_2 f_3 f_4 + d_1^2 \left(f_2 f_3 - d_3(f_2 + f_3) + d_2(d_3 - f_3 - f_4) + (f_2 + f_3) f_4\right) \\
& - d_3 f_1 f_2 L - d_3 f_1 f_3 L - d_3 f_2 f_3 L + f_1 f_2 f_3 L + f_1 f_2 f_4 L + f_1 f_3 f_4 L \\
& + f_2 f_3 f_4 L - d_2(f_1 + f_2) \left(d_3^2 + (f_3 + f_4)L - d_3(2 f_3 + L)\right) \\
& + d_1 d_3(f_2 + f_3) L - d_1 \left(f_2 f_3 + (f_2 + f_3) f_4\right) L \\
& + d_1 d_2 \left(d_3^2 + (f_3 + f_4)(2 f_2 + L) - d_3(2(f_2 + f_3) + L)\right)]^2 \qquad (6.5)
\end{aligned}
$$

The configuration of 4CURC in the Fig. (6.1) can behave equivalent to 3CURC, 2CURC and as well as SCURC, by making the separation distances go to zero as required. Before going to the analysis of the 4CURC, let us look at various possibilities, where these conversions are being taking place. First, we start with the conversion from 4CURC to 3CURC in the following section.

6.2.1   Conversion from 4CURC to 3CURC

There are four different possibilities where the configuration of the 4CURC can be converted to 3CURC as shown in the Fig. (6.2).

1(a). Consider the case when $d_1 = 0$, then (6.5) becomes (5.10), with the effective focal length $\left(\dfrac{f_1 f_2}{f_1 + f_2}\right)_{4CURC}$ of the combination of lenses L_1 and L_2 now behaves as a lens L_1 of 3CURC as shown in the first configuration of the Fig. (6.2).

For this case of 3CURC, we denote the value of L_M of 3CURC by $L_{M_{(1,2),3,4}}$, and is given by

$$L_{M_{(1,2),3,4}} = 4\left(\frac{f_1 f_2}{f_1 + f_2}\right) + 4f_3 + 4f_4 \qquad (6.6)$$

1(b). Consider the case when $d_2 = 0$, then (6.5) becomes (5.10), with the effective focal length $\left(\dfrac{f_2 f_3}{f_2 + f_3}\right)_{4CURC}$ of the combination of lenses L_2 and L_3 now behaves as a lens L_2 of 3CURC as shown in the second configuration of the Fig. (6.2).

The value of $L_{M_{1,(2,3),4}}$ is given by

$$L_{M_{1,(2,3),4}} = 4f_1 + 4\left(\frac{f_2 f_3}{f_2 + f_3}\right) + 4f_4 \qquad (6.7)$$
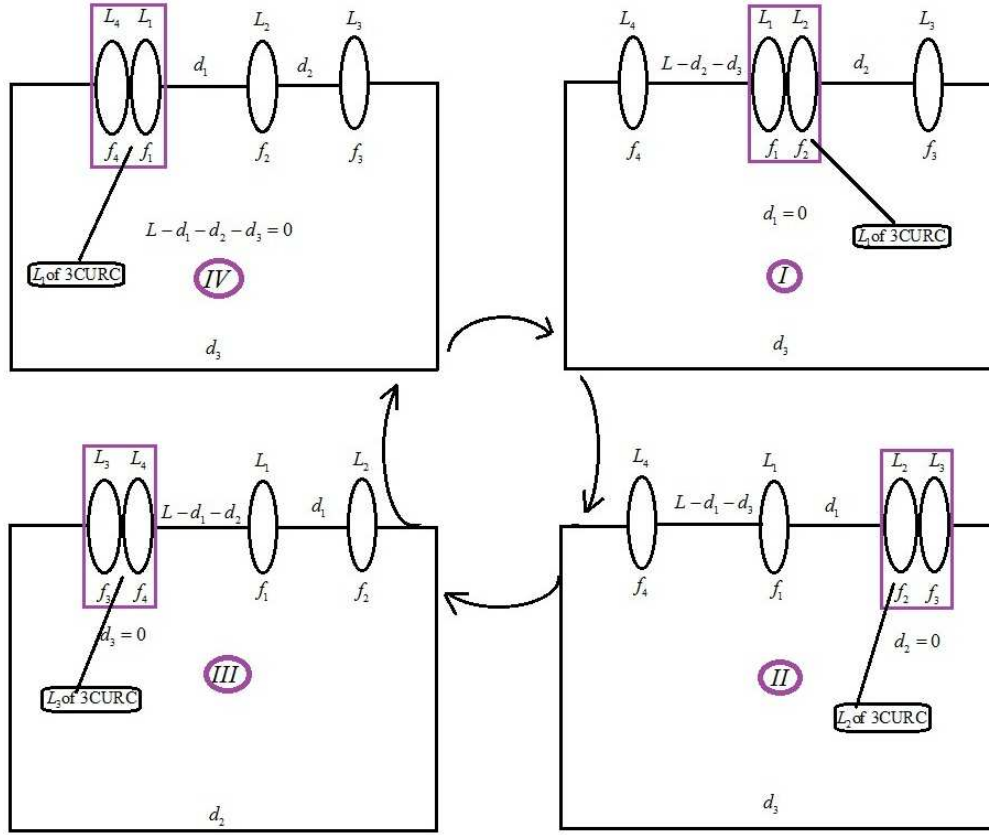
Figure 6.2: **Conversion from 4CURC to 3CURC**

1(c). Consider the case when $d_3 = 0$, then (6.5) becomes (5.10), with the effective focal length $\left(\dfrac{f_3 f_4}{f_3 + f_4} \right)_{4CURC}$ of the combination of lenses L_3 and L_4 now behaves as a lens L_3 of 3CURC as shown in the third configuration of the Fig. (6.2). For this case

$$L_{M_{1,2,(3,4)}} = 4f_1 + 4f_2 + 4\left(\frac{f_3 f_4}{f_3 + f_4} \right) \tag{6.8}$$

1(d). Consider the case when $L - d_1 - d_2 - d_3 = 0$, then (6.5) becomes (5.10), with the effective focal length $\left(\dfrac{f_4 f_1}{f_4 + f_1} \right)_{4CURC}$ of the combination of

lenses L_4 and L_1 now behaves as a lens L_1 of 3CURC as shown in the fourth configuration of the Fig. (6.2).

The value of $L_{M_{1,2,(3,4)}}$ is given by

$$L_{M_{(4,1),2,3}} = 4\left(\frac{f_4 f_1}{f_4 + f_1}\right) + 4f_2 + 4f_3 \qquad (6.9)$$

For the case of $f_1 < f_2 < f_3 < f_4$, the value of $L_{M_{(1,2),3,4}}(6.6)$ is the largest length among the four values. In the following we look for the possibilities of converting 4CURC to 2CURC.

6.2.2 Conversion from 4CURC to 2CURC

There are two possible configurations for which the 4CURC can be converted to 2CURC as shown in the Fig. (6.3). To do this, we make any two of the separation distances go to zero.
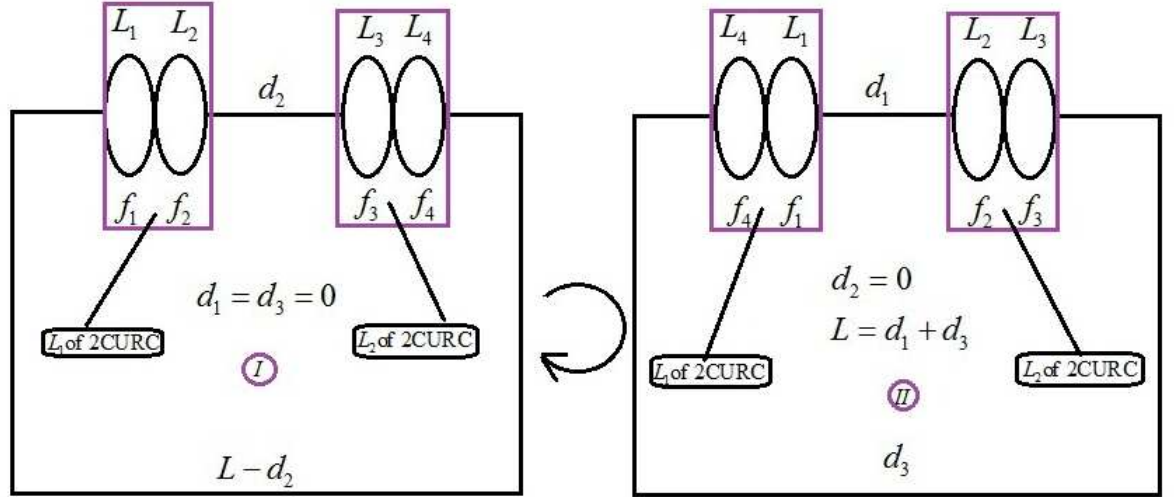
Figure 6.3: **Conversion from 4CURC to 2CURC**

1(a). Consider the case $d_1 = 0$ and $d_3 = 0$, for which the lenses L_1, L_2 and L_3, L_4 are combined to create only two modes in the cavity. Then the condition (6.5) becomes (4.12), the effective focal lengths $\left(\dfrac{f_1 f_2}{f_1 + f_2}\right)_{4CURC}$ of the combination of lenses L_1 and L_2 of 4CURC now behaves as a lens L_1 of 2CURC and $\left(\dfrac{f_3 f_4}{f_3 + f_4}\right)_{4CURC}$ of the combination of lenses L_3 and L_4 behaves as a lens L_2 of 2CURC as shown in the first configuration of the Fig. (6.3).

For this case of 2CURC, we denote L_M of 2CURC by $L_{M_{(1,2),(3,4)}}$, which is given by

$$L_{M_{(1,2),(3,4)}} = 4\left(\frac{f_1 f_2}{f_1 + f_2}\right) + 4\left(\frac{f_3 f_4}{f_3 + f_4}\right) \qquad (6.10)$$

1(b). Similarly consider the case $d_2 = 0$ and $L = d_1 + d_3$, for which the lenses L_4, L_1 and L_2, L_3 are combined to create only two modes in the cavity. Then the condition (6.5) becomes (4.12), with the effective focal lengths $\left(\dfrac{f_4 f_1}{f_4 + f_1}\right)_{4CURC}$ of the combination of lenses L_4 and L_1 of 4CURC behaves as a lens L_1 of 2CURC and $\left(\dfrac{f_2 f_3}{f_2 + f_3}\right)_{4CURC}$ of the combination of lenses L_2 and L_3 of 4CURC behaves as a lens L_2 of 2CURC as shown in the second configuration of the Fig. (6.3). Here $L_{M_{(4,1),(2,3)}}$ is given by

$$L_{M_{(4,1),(2,3)}} = 4\left(\frac{f_4 f_1}{f_4 + f_1}\right) + 4\left(\frac{f_2 f_3}{f_2 + f_3}\right) \qquad (6.11)$$

Finally, we discuss the possibility where the 4CURC can become SCURC in the following.

6.2.3   Conversion from 4CURC to SCURC

The one and only possibility where the 4CURC can behave as a SCURC is shown in the Fig. (6.4), that is when all the lenses L_1, L_2, L_3 and L_4 are
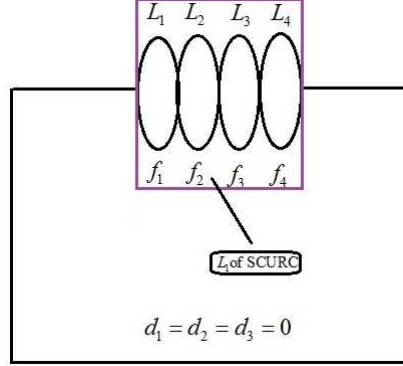
Figure 6.4: **Conversion from 4CURC to SCURC**

joined together with $d_1 = d_2 = d_3 = 0$. In this case $L_{eff_{1234}}$ is given by

$$L_{eff_{1234}} = 4\frac{f_1 f_2 f_3 f_4}{f_1 f_2 f_3 + f_1 f_2 f_4 + f_2 f_3 f_4 + f_3 f_4 f_1} \qquad (6.12)$$

So far we have understood that the 4CURC contains all the features of 3CURC, 2CURC and SCURC. As a result, the expectations on 4CURC are high, as it is possible for the 4CURC to contain the different phase regions of 3CURC, 2CURC and SCURC and one may get rid off the forbidden zones just as it done for the 2CURC. Therefore, it is motivating further and giving assurance that one can achieve the accumulated Gouy phase variation more than π using 4CURC. Before going to the analysis of the Gouy phase, we study the stability analysis of 4CURC.

6.2.4   Stability of 4CURC

It is noticed that the stability function (6.5) of the considered 4CURC is quartic in d_1, d_2 and d_3. For a given L, the parameters of the system which can be varied to create a variable Gouy phase are d_1, d_2 and d_3. Varying any of the distances d_1, d_2 and d_3 is equivalent to varying the effective focal length of the combined systems comprising the focal lengths (f_1, f_2), (f_2, f_3)

and (f_3, f_4). First, we study (6.5) with respect to d_1, keeping the rest of the system parameters fixed in the following.

6.2.5 Stable solutions of d_1 for a given L, f_1, f_2, f_3, f_4, d_2 and d_3

We look for the stable solutions of d_1 in terms of the system parameters L, f_1, f_2, f_3, f_4, d_2 and d_3. The marginal stability of $(A + D + 2)$(6.3) gives the stable solutions of d_1 as

$$d_{1_+}^{(1,2)} = \frac{[D_0 \pm \sqrt{D_1 D_2}\,]}{(2(f_2 f_3 - d_3(f_2 + f_3) + d_2(d_3 - f_3 - f_4) + (f_2 + f_3)f_4))} \tag{6.13}$$

where D_0, D_1 and D_2 are given by

$$D_0 = d_3^2(f_2 + f_3) + d_2^2(-d_3 + f_3 + f_4) + (f3f4 + f_2(f_3 + f_4))L$$
$$- d_3(2f_2 f_3 + (f_2 + f_3)L) - d_2\left(d_3^2 + (f_3 + f_4)(2f2 + L) - d_3(2(f_2 + f_3) + L)\right) \tag{6.14}$$

$$D_1 = -d_3^2(f_2 + f_3) + d_2^2(d_3 - f_3 - f_4) - d_3(f_2 + f_3)(4f_1 - L) + f_2 f_3(4f_1 - L)$$
$$+ ((f_2 + f_3)f_4)(4f_1 - L) + d_2\left(d_3^2 + d_3(4f_1 - 2f_3 - L) + (f_3 + f_4)(-4f_1 + L)\right) \tag{6.15}$$

$$D_2 = -d_3^2(f_2 + f_3) + d_2^2(d_3 - f_3 - f_4) + 4f_2 f_3 f_4 + d_3(f_2 + f_3)L$$
$$- (f_2 f_3 + (f_2 + f_3)f_4)L + d_2\left(d_3^2 + (f_3 + f_4)L - d_3(2f_3 + L)\right) \tag{6.16}$$

The parameters D_0, D_1 and D_2 are again quadratic in d_2 and as well as in d_3. Solving D_1 for marginal stability of d_2

$$d_{2_+}^{(1,2)} = \frac{1}{2(d_3 - f_3 - f_4)}[(-d_3^2 - d_3(4f_1 - 2f_3 - L) - (f_3 + f_4)(-4f_1 + L))$$
$$\pm \sqrt{d_3^2 + 4d_3 f_1 - 4f_1 f_3 - 4f_1 f_4 - d_3 L + f_3 L + f_4 L}$$
$$\sqrt{d_3^2 + 4d_3 f_1 - 4f_1 f_3 - 4f_1 f_4 - d_3 L + f_3 L + f_4 L}\,] \tag{6.17}$$

(6.17) is again quartic in d_3, first quadratic of the discriminant gives

$$d_{3_+}^{(1,2)} = \frac{1}{2} \left(L - 4f_1 \pm \sqrt{4f_1 - L} \sqrt{4f_1 + 4f_3 + 4f_4 - L} \right) \tag{6.18}$$

The second quadratic in d_3 of the discriminant gives

$$d_{3_+}^{(3,4)} = \frac{1}{2} \left(L - 4f_1 - 4f_2 \pm \sqrt{4f_1 + 4f_2 + 4f_3 - L} \sqrt{4f_1 + 4f_2 + 4f_4 - L} \right) \tag{6.19}$$

Similarly solving D_2 for marginal stability

$$\begin{aligned} d_{2_+}^{(3,4)} &= \frac{1}{2(d_3 - f_3 - f_4)} [\left(-d_3^2 - (f_3 + f_4)L + d_3(2f_3 + L) \right) \\ &\pm \sqrt{d_3^2 + 4d_3 f_2 - 4f_2 f_3 - 4f_2 f_4 - d_3 L + f_3 L + f_4 L} \\ &\quad \sqrt{d_3^2 - 4f_3 f_4 - d_3 L + f_3 L + f_4 L} \,] \end{aligned} \tag{6.20}$$

The above condition (6.20) is quartic in d_3, first quadratic of the discriminant gives

$$d_{3_+}^{(1,2)} = \frac{1}{2} \left(L - 4f_2 \pm \sqrt{4f_2 - L} \sqrt{4f_2 + 4f_3 + 4f_4 - L} \right) \tag{6.21}$$

The second quadratic in d_3 of the discriminant gives

$$d_{3_+}^{(3,4)} = \frac{1}{2} \left(L \pm \sqrt{-4f_3 + L} \sqrt{-4f_4 + L} \right) \tag{6.22}$$

Finally, for d_1 to be real, there are four pairs of conditions in d_3 which are given by the conditions (6.18), (6.19), (6.21) and (6.22) and can be written as

$$d_{3_+}^{(1,2)} = \frac{L - 4f_1}{2} \pm \frac{r_{11}}{2} \tag{6.23}$$

$$d_{3_+}^{(3,4)} = \frac{L - 4f_1 - 4f_2}{2} \pm \frac{k_{11}}{2} \tag{6.24}$$

$$d_{3_+}^{(1,2)} = \frac{L - 4f_2}{2} \pm \frac{t_{11}}{2} \tag{6.25}$$

$$d_{3_+}^{(3,4)} = \frac{L}{2} \pm \frac{p_{11}}{2} \tag{6.26}$$

where

$$r_{11}^2 = (4f_1 - L)(4f_1 + 4f_3 + 4f_4 - L) \tag{6.27}$$

$$k_{11}^2 = (4f_1 + 4f_2 + 4f_3 - L)(4f_1 + 4f_2 + 4f_4 - L) \tag{6.28}$$

$$t_{11}^2 = (4f_2 - L)(4f_2 + 4f_3 + 4f_4 - L) \tag{6.29}$$

$$p_{11}^2 = (L - 4f_3)(L - 4f_4) \tag{6.30}$$

The second alternative of the marginal stability (6.4) gives

$$d_{1_-}^{(1,2)} = \frac{[D_1 \pm \sqrt{D_{11}D_{21}}\,]}{(2(f_2f_3 - d_3(f_2 + f_3) + d_2(d_3 - f_3 - f_4) + (f_2 + f_3)f_4))} \tag{6.31}$$

where

$$D_0 = d_3^2(f_2 + f_3) + d_2^2(-d_3 + f_3 + f_4) + (f3f4 + f_2(f_3 + f_4))L - 2d_3f_2f_3$$
$$- (d_3(f_2 + f_3)L) - d_2\left(d_3^2 + (f_3 + f_4)(2f_2 + L) - d_3(2(f_2 + f_3) + L)\right) \tag{6.32}$$

$$D_{11} = -d_3^2(f_2 + f_3) + d_2^2(d_3 - f_3 - f_4) + 4(f_1f_2f_3 + f_2f_3f_4 + f_1(f_2 + f_3)f_4)$$
$$- d_3(f_2 + f_3)(4f_1 - L) - (f_3f_4 + f_2(f_3 + f_4))L$$
$$+ d_2\left(d_3^2 + d_3(4f_1 - 2f_3 - L) + (f_3 + f_4)(-4f_1 + L)\right) \tag{6.33}$$

$$D_{21} = -d_3^2(f_2 + f_3) + d_2^2(d_3 - f_3 - f_4) + d_3(f_2 + f_3)L$$
$$- (f_2f_3 + (f_2 + f_3)f_4)L + d_2\left(d_3^2 + (f_3 + f_4)L - d_3(2f_3 + L)\right) \tag{6.34}$$

D_{11} and D_{21} are quadratic in d_2 and as well as in d_3. Solving D_{11} for marginal stability of d_2

$$d_{2_-}^{(1,2)} = \frac{1}{2(d_3 - f_3 - f_4)}[\left(-d_3^2 - d_3(4f_1 - 2f_3 - L) - (f_3 + f_4)(-4f_1 + L)\right)$$
$$\pm \sqrt{d_3^2 + 4d_3f_1 + 4d_3f_2 - 4f_1f_3 - 4f_2f_3 - 4f_1f_4 - 4f_2f_4 - d_3L + f_3L + f_4L}$$
$$\sqrt{d_3^2 + 4d_3f_1 - 4f_1f_3 - 4f_1f_4 - 4f_3f_4 - d_3L + f_3L + f_4L}\,] \tag{6.35}$$

From the first quadratic of the discriminant, the marginal stability for d_3 gives

$$d_{3-}^{(1,2)} = \frac{1}{2} \left(L - 4f_1 - 4f_2 \pm \sqrt{4f_1 + 4f_2 - L} \sqrt{4f_1 + 4f_2 + 4f_3 + 4f_4 - L} \right)$$

(6.36)

The second quadratic in d_3 of the discriminant gives

$$d_{3-}^{(3,4)} = \frac{1}{2} \left(L - 4f_1 \pm \sqrt{4f_1 + 4f_3 - L} \sqrt{4f_1 + 4f_4 - L} \right)$$ (6.37)

Similarly solving D_{21} for marginal stability of d_2

$$\begin{aligned} d_{2-}^{(3,4)} &= \frac{1}{2(d_3 - f_3 - f_4)} [\left(-d_3^2 + 2d_3 f_3 + d_3 L - f_3 L - f_4 L \right) \\ &\pm \sqrt{d_3^2 - d_3 L + f_3 L + f_4 L} \\ &\sqrt{d_3^2 + 4d_3 f_2 - 4f_2 f_3 - 4f_2 f_4 - 4f_3 f_4 - d_3 L + f_3 L + f_4 L} \,] \end{aligned}$$

(6.38)

Again the above equation is quartic in d_3, first quadratic of the discriminant gives

$$d_{3-}^{(1,2)} = \frac{1}{2} \left(L \pm \sqrt{-4f_3 L - 4f_4 L + L^2} \right)$$ (6.39)

The second quadratic in d_3 of the discriminant gives

$$d_{3-}^{(3,4)} = \frac{1}{2} \left(L - 4f_2 - \sqrt{4f_2 + 4f_3 - L} \sqrt{4f_2 + 4f_4 - L} \right)$$ (6.40)

Finally, for d_1 to be real, there are four pairs of conditions in d_3 which are given by the conditions (6.36), (6.37), (6.39) and (6.40) can be written as

$$d_{3-}^{(1,2)} = \frac{L - 4f_1 - 4f_2}{2} \pm \frac{s_{11}}{2}$$ (6.41)

$$d_{3-}^{(3,4)} = \frac{L - 4f_1}{2} \pm \frac{q_{11}}{2}$$ (6.42)

$$d_{3-}^{(1,2)} = \frac{L}{2} \pm \frac{m_{11}}{2}$$ (6.43)

$$d_{3_-}^{(3,4)} = \frac{L - 4f_2}{2} \pm \frac{i_{11}}{2} \tag{6.44}$$

where

$$s_{11}^2 = (4f_1 + 4f_2 - L)(4f_1 + 4f_2 + 4f_3 + 4f_4 - L) \tag{6.45}$$

$$q_{11}^2 = (4f_1 + 4f_3 - L)(4f_1 + 4f_4 - L) \tag{6.46}$$

$$m_{11}^2 = (-4f_3L - 4f_4L + L^2) \tag{6.47}$$

$$i_{11}^2 = (4f_2 + 4f_3 - L)(4f_2 + 4f_4 - L) \tag{6.48}$$

For $f_1 = f_2 = 50$cm, $f_3 = f_4 = 100$cm, $L = 700$cm, $d_1 = 120$cm, $d_3 = 201$cm,
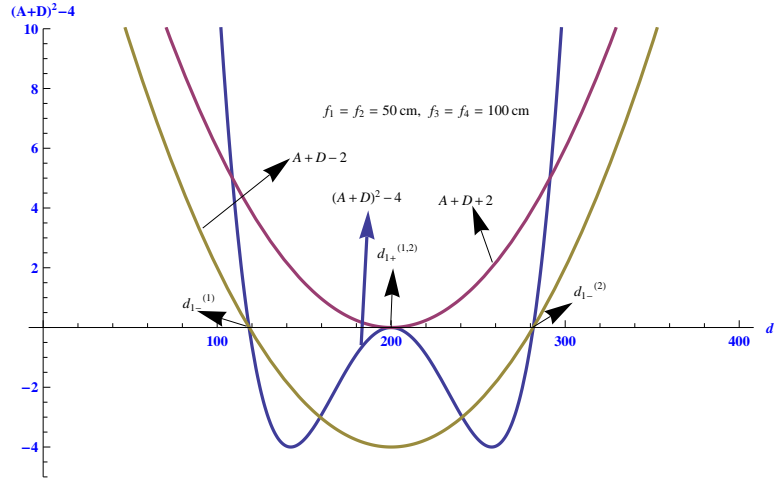
Figure 6.5: **For $f_1 = f_2 = 50$cm, $f_3 = f_4 = 100$cm, $L = 700$cm, $d_2 = 200$cm, $d_3 = 100$cm, the stability functions $(A + D)^2 - 4$(6.5), $A + D + 2$(6.3), $A + D - 2$(6.4) with respect to $d_1 = \dfrac{L - d_2 - d_3}{2}$**

the stability function (6.5) and the two parabolas (6.3), (6.4) with respect to d_1 are plotted in the Fig. (6.5). The stability function i.e., the product of $(A + D + 2)$ and $(A + D - 2)$ is a parabola, but not inverted as in the earlier cases. For this case it is in the direction of the individual parabolas of $A + D \pm 2$ only, for a given d_2 and d_3. The above four solutions $d_{1+}^{(1,2)}$, $d_{1-}^{(3,4)}$

are identified in the Fig. (6.5). To know the behaviour of the function (6.5) further, we determine its extremum points by taking the partial derivative with respect to d_1 and equating it to zero, i.e.,

$$
\begin{aligned}
\frac{\partial}{\partial d_1} \left[(A+D)^2 - 4 \right] = {} & \frac{2}{f_1^2 f_2^2 f_3^2 f_4^2} \left[2d_3 f_2 f_3 - d_3^2 (f_2 + f_3) + d_2^2 (d_3 - f_3 - f_4) \right. \\
& + 2d_1 (f_2 f_3 - d_3 (f_2 + f_3) + d_2 (d_3 - f_3 - f_4) + (f_2 + f_3) f_4) + d_3 (f_2 + f_3) L \\
& - (f_2 f_3 + (f_2 + f_3) f_4) L + d_2 \left(d_3^2 + (f_3 + f_4)(2f_2 + L) - d_3 (2(f_2 + f_3) + L) \right) \right] \\
& \left[d_3^2 f_1 f_2 + d_3^2 f_1 f_3 + d_3^2 f_2 f_3 - d_2^2 (f_1 + f_2)(d_3 - f_3 - f_4) - 2f_1 f_2 f_3 f_4 \right. \\
& + d_1^2 \left(f_2 f_3 - d_3 (f_2 + f_3) + d_2 (d_3 - f_3 - f_4) + (f_2 + f_3) f_4 \right) \\
& - d_3 f_1 f_2 L - d_3 f_1 f_3 L - d_3 f_2 f_3 L + f_1 f_2 f_3 L + f_1 f_2 f_4 L + f_1 f_3 f_4 L + f_2 f_3 f_4 L \\
& - d_2 (f_1 + f_2) \left(d_3^2 + (f_3 + f_4) L \left(-d_3 (2f_3 + L) \right) \right) \\
& + d_1 \left(2d_3 f_2 f_3 - d_3^2 (f_2 + f_3) + d_2^2 (d_3 - f_3 - f_4) + d_3 (f_2 + f_3) L \right. \\
& \left. \left. - (f_2 f_3 + (f_2 + f_3) f_4) L + d_2 \left(d_3^2 + (f_3 + f_4)(2f_2 + L) - d_3 (2(f_2 + f_3) + L) \right) \right) \right] = 0
\end{aligned}
$$

$$(6.49)$$

One can get three solutions of d_1, which are obtained as

$$
d_{1C} = \frac{\left[\begin{array}{c} -2d_3 f_2 f_3 + d_3^2 (f_2 + f_3) - d_2^2 (d_3 - f_3 - f_4) \\ -d_3 (f_2 + f_3) L + (f_2 f_3 + (f_2 + f_3) f_4) L \\ -d_2 \left(d_3^2 + (f_3 + f_4)(2f_2 + L) - d_3 (2f_2 + f_3) + L \right) \end{array} \right]}{2 (f_2 f_3 - d_3 (f_2 + f_3) + d_2 (d_3 - f_3 - f_4) + (f_2 + f_3) f_4)}
$$

$$(6.50)$$

$$d_1^{(1,2)} = d_{1C} \pm \frac{1}{2(f_2 f_3 - d_3(f_2 + f_3) + d_2(d_3 - f_3 - f_4) + (f_2 + f_3)f_4)}$$

$$\sqrt{(-4(f_2 f_3 - d_3(f_2 + f_3) + d_2(d_3 - f_3 - f_4) + (f_2 + f_3)f_4)}$$

$$\left(d_3^2 f_1 f_2 + d_3^2 f_1 f_3 + d_3^2 f_2 f_3 - d_2^2(f_1 + f_2)(d_3 - f_3 - f_4) - 2f_1 f_2 f_3 f_4 - d_3 f_1 f_2 L\right.$$

$$- d_3 f_1 f_3 L - d_3 f_2 f_3 L + f_1 f_2 f_3 L + f_1 f_2 f_4 L + f_1 f_3 f_4 L + f_2 f_3 f_4 L$$

$$- d_2(f_1 + f_2)\left(d_3^2 + (f_3 + f_4)L - d_3(2f_3 + L)\right)$$

$$+ \left(2d_3 f_2 f_3 - d_3^2(f_2 + f_3) + d_2^2(d_3 - f_3 - f_4) + d_3(f_2 + f_3)L\right.$$

$$\left.\left. - (f_2 f_3 + (f_2 + f_3)f_4)L + d_2\left(d_3^2 + (f_3 + f_4)(2f_2 + L) - d_3(2(f_2 + f_3) + L))\right)\right)^2\right)$$

$$(6.51)$$

The determination of height H_1 from axis d_1 of the central extremum can be done by the substitution of d_1 given by (6.50) in the condition (6.5). We have

$$H_1 = \frac{\left(d_2 - d_{2+}^{(1,2)}\right)\left(d_2 - d_{2+}^{(3,4)}\right)\left(d_2 - d_{2-}^{(1,2)}\right)\left(d_2 - d_{2-}^{(3,4)}\right)}{\left(16 f_1^2 f_2^2 f_3^2 f_4^2 \left(f_2 f_3 - d_3(f_2 + f_3) + d_2(d_3 - f_3 - f_4) + (f_2 + f_3)f_4\right)^2\right)}$$

$$(6.52)$$

where $d_{2+}^{(1,2)}$, $d_{2+}^{(3,4)}$, $d_{2-}^{(1,2)}$ and $d_{2-}^{(3,4)}$ are related to the coefficients r_{11}, k_{11}, t_{11}, p_{11}, s_{11}, q_{11}, m_{11} and i_{11} which are given by the conditions (6.23-6.26), and (6.45-6.48). $H_1 \gtrless 0$ depending on the values of d_2 for a given L, d_3, f_1, f_2, f_3 and f_4 which also decide the stable zones of d_1. One can also look for the values of L numerically, where H_1 becomes -4. In the next section we construct the length chart of 4CURC, in which all the possible cases of L will be consolidated, for the case of $f_1 < f_2 < f_3 < f_4$.

6.3 The Length Chart of 4CURC

The parameters r_{11}, k_{11}, t_{11}, p_{11}, s_{11}, q_{11}, m_{11} and i_{11} which are given in the Fig. (6.6) show that the maximum length L_M for the 4CURC is now extended up to $4f_1 + 4f_2 + 4f_3 + 4f_4$ and also additional new marginal

lengths are generated in between, compare to the case of 3CURC. It can

$$f_1 < f_2 < f_3 < f_4$$

$$L_{\text{eff}1234} = 4\frac{f_1 f_2 f_3 f_4}{f_1 f_2 f_3 + f_1 f_2 f_4 + f_2 f_3 f_4 + f_3 f_4 f_1}$$

$$L_{(1,2),(3,4)} = 4\left(\frac{f_1 f_2}{f_1 + f_2}\right) + 4\left(\frac{f_3 f_4}{f_3 + f_4}\right)$$

$$L_{(4,1),(2,3)} = 4\left(\frac{f_4 f_1}{f_4 + f_1}\right) + 4\left(\frac{f_2 f_3}{f_2 + f_3}\right)$$

$$L_{(1,2),3,4} = 4\left(\frac{f_1 f_2}{f_1 + f_2}\right) + 4\left(\frac{f_3 f_4}{f_3 + f_4}\right)$$

$$L_{M_{1,(23)4}} = 4f_1 + 4\left(\frac{f_2 f_3}{f_2 + f_3}\right) + 4f_4$$

$$L_{M_{12,(3,4)}} = 4f_1 + 4f_2 + 4\left(\frac{f_3 f_4}{f_3 + f_4}\right)$$

$$L_{M_{(4,1)2,3}} = 4\left(\frac{f_4 f_1}{f_2 + f_3}\right) + 4f_2 + 4f_3$$

$$L_{M1} = 4f_1; L_{M2} = 4f_2$$

$$L_{M3} = 4f_3; L_{M4} = 4f_4$$

$$L_M = L_{M1} + L_{M2} + L_{M3} + L_{M4}$$

$$r_{11}^2 = (4f_1 - L)(4f_1 + 4f_3 + 4f_4 - L)$$

$$k_{11}^2 = (4f_1 + 4f_2 + 4f_3 - L)(4f_1 + 4f_2 + 4f_4 - L)$$

$$t_{11}^2 = (4f_2 - L)(4f_2 + 4f_3 + 4f_4 - L)$$

$$p_{11}^2 = (L - 4f_3)(L - 4f_4)$$

$$s_{11}^2 = (4f_1 + 4f_2 - L)(4f_1 + 4f_2 + 4f_3 + 4f_4 - L)$$

$$q_{11}^2 = (4f_1 + 4f_3 - L)(4f_1 + 4f_4 - L)$$

$$m_{11}^2 = L(L - 4f_3 - 4f_4)$$

$$\hat{t}_{11}^2 = (4f_2 + 4f_3 - L)(4f_2 + 4f_4 - L)$$

Figure 6.6: **Description of length parameters in terms of focal lengths of 4CURC**

be generalized that adding an additional lens in the cavity is allowing one to extend the stable length of the corresponding cavity and also generating new additional lengths as it has been realized earlier for the cases 2CURC, 3CURC and now for 4CURC. If we consider the focal lengths f_1, f_2, f_3 and f_4 to be prime numbers then twenty three distinct and finite values of length L are possible for 4CURC as shown in the Fig. (6.7). But for the case of non primed focal lengths, the coincidence of marginal stable lengths L takes place.

Therefore for a fixed d_1, at the marginal stable L we study the behaviour of the stability between the separation distances d_2 and d_3.

To analyze the stability condition(6.5), we construct 3D plots for different cases of L of 4CURC, when all the four modes present, where (6.5)i.e., $(A + D)^2 - 4$ is along z axis, while d_2 and d_3 are respectively along x and y axes. We also construct plots for the cases of L, where 4CURC can get converted to 3CURC, 2CURC and SCURC, to show the behaviour of stability

$f_1 = 47cm, f_2 = 73cm, f_3 = 91cm, f_4 = 127cm$;

L	Conditions
$L = 0$;	$r_{11}^2 > 0, k_{11}^2 > 0, t_{11}^2 > 0, p_{11}^2 > 0, s_{11}^2 > 0, q_{11}^2 > 0, m_{11}^2 = 0, i_{11}^2 > 0$
$L = L_{eff1234}$;	$r_{11}^2 > 0, k_{11}^2 > 0, t_{11}^2 > 0, p_{11}^2 > 0, s_{11}^2 > 0, q_{11}^2 > 0, m_{11}^2 < 0, i_{11}^2 > 0$
$L = L_{M1}$;	$r_{11}^2 = 0, k_{11}^2 > 0, t_{11}^2 > 0, p_{11}^2 > 0, s_{11}^2 > 0, q_{11}^2 > 0, m_{11}^2 < 0, i_{11}^2 > 0$
$L = L_{M2}$;	$r_{11}^2 < 0, k_{11}^2 > 0, t_{11}^2 = 0, p_{11}^2 > 0, s_{11}^2 > 0, q_{11}^2 > 0, m_{11}^2 < 0, i_{11}^2 > 0$
$L = L_{M(4,1)(2,3)}$;	$r_{11}^2 < 0, k_{11}^2 > 0, t_{11}^2 < 0, p_{11}^2 > 0, s_{11}^2 > 0, q_{11}^2 > 0, m_{11}^2 < 0, i_{11}^2 > 0$
$L = L_{M(1,2)(3,4)}$;	$r_{11}^2 < 0, k_{11}^2 > 0, t_{11}^2 < 0, p_{11}^2 > 0, s_{11}^2 > 0, q_{11}^2 > 0, m_{11}^2 < 0, i_{11}^2 > 0$
$L = L_{M3}$;	$r_{11}^2 < 0, k_{11}^2 > 0, t_{11}^2 < 0, p_{11}^2 = 0, s_{11}^2 > 0, q_{11}^2 > 0, m_{11}^2 < 0, i_{11}^2 > 0$
$L = L_{M1} + L_{M2}$;	$r_{11}^2 < 0, k_{11}^2 > 0, t_{11}^2 < 0, p_{11}^2 < 0, s_{11}^2 = 0, q_{11}^2 > 0, m_{11}^2 < 0, i_{11}^2 > 0$
$L = L_{M4}$;	$r_{11}^2 < 0, k_{11}^2 > 0, t_{11}^2 < 0, p_{11}^2 = 0, s_{11}^2 < 0, q_{11}^2 > 0, m_{11}^2 < 0, i_{11}^2 > 0$
$L = L_{M1} + L_{M3}$;	$r_{11}^2 < 0, k_{11}^2 > 0, t_{11}^2 < 0, p_{11}^2 > 0, s_{11}^2 < 0, q_{11}^2 = 0, m_{11}^2 < 0, i_{11}^2 > 0$
$L = L_{M2} + L_{M3}$;	$r_{11}^2 < 0, k_{11}^2 > 0, t_{11}^2 < 0, p_{11}^2 > 0, s_{11}^2 < 0, q_{11}^2 < 0, m_{11}^2 < 0, i_{11}^2 = 0$
$L = L_{M1,2,(3,4)}$;	$r_{11}^2 < 0, k_{11}^2 > 0, t_{11}^2 < 0, p_{11}^2 > 0, s_{11}^2 < 0, q_{11}^2 < 0, m_{11}^2 < 0, i_{11}^2 < 0$
$L = L_{M1} + L_{M4}$;	$r_{11}^2 < 0, k_{11}^2 > 0, t_{11}^2 < 0, p_{11}^2 > 0, s_{11}^2 < 0, q_{11}^2 = 0, m_{11}^2 < 0, i_{11}^2 < 0$
$L = L_{M(4,1)2,3}$;	$r_{11}^2 < 0, k_{11}^2 > 0, t_{11}^2 < 0, p_{11}^2 > 0, s_{11}^2 < 0, q_{11}^2 > 0, m_{11}^2 < 0, i_{11}^2 < 0$
$L = L_{M2} + L_{M4}$;	$r_{11}^2 < 0, k_{11}^2 > 0, t_{11}^2 < 0, p_{11}^2 > 0, s_{11}^2 < 0, q_{11}^2 > 0, m_{11}^2 < 0, i_{11}^2 = 0$
$L = L_{M1} + L_{M2} + L_{M3}$;	$r_{11}^2 < 0, k_{11}^2 = 0, t_{11}^2 < 0, p_{11}^2 > 0, s_{11}^2 < 0, q_{11}^2 > 0, m_{11}^2 < 0, i_{11}^2 > 0$
$L = L_{M1,(2,3)4}$;	$r_{11}^2 < 0, k_{11}^2 < 0, t_{11}^2 < 0, p_{11}^2 > 0, s_{11}^2 < 0, q_{11}^2 > 0, m_{11}^2 < 0, i_{11}^2 > 0$
$L = L_{M3} + L_{M4}$;	$r_{11}^2 < 0, k_{11}^2 < 0, t_{11}^2 < 0, p_{11}^2 > 0, s_{11}^2 < 0, q_{11}^2 > 0, m_{11}^2 = 0, i_{11}^2 > 0$
$L = L_{M(1,2)3,4}$;	$r_{11}^2 < 0, k_{11}^2 < 0, t_{11}^2 < 0, p_{11}^2 > 0, s_{11}^2 < 0, q_{11}^2 > 0, m_{11}^2 > 0, i_{11}^2 > 0$
$L = L_{M1} + L_{M2} + L_{M4}$;	$r_{11}^2 < 0, k_{11}^2 = 0, t_{11}^2 < 0, p_{11}^2 > 0, s_{11}^2 < 0, q_{11}^2 > 0, m_{11}^2 > 0, i_{11}^2 > 0$
$L = L_{M1} + L_{M3} + L_{M4}$;	$r_{11}^2 = 0, k_{11}^2 > 0, t_{11}^2 < 0, p_{11}^2 > 0, s_{11}^2 < 0, q_{11}^2 > 0, m_{11}^2 > 0, i_{11}^2 > 0$
$L = L_{M2} + L_{M3} + L_{M4}$;	$r_{11}^2 > 0, k_{11}^2 > 0, t_{11}^2 = 0, p_{11}^2 > 0, s_{11}^2 < 0, q_{11}^2 > 0, m_{11}^2 > 0, i_{11}^2 > 0$
$L = L_M$;	$r_{11}^2 > 0, k_{11}^2 > 0, t_{11}^2 > 0, p_{11}^2 > 0, s_{11}^2 = 0, q_{11}^2 > 0, m_{11}^2 > 0, i_{11}^2 > 0$
$L > L_M$;	$r_{11}^2 > 0, k_{11}^2 > 0, t_{11}^2 > 0, p_{11}^2 > 0, s_{11}^2 > 0, q_{11}^2 > 0, m_{11}^2 > 0, i_{11}^2 > 0$

Figure 6.7: **Length chart for 4CURC for the case of** $f_1 < f_2 < f_3 < f_4$

function with the corresponding variation of the length of the arms which also noted in Fig. (6.7).

For the considered case of $f_1 < f_2 < f_3 < f_4$, we choose $f_1 = 50$cm, $f_2 = 75$cm, $f_3 = 100$cm, $f_4 = 125$cm and $d_1 = 160$cm.

(a). $L > L_M$. For a fixed $L > L_M = 1500$cm the stable contours of d_2

Figure 6.8: **Stability diagram as a function of d_2 and d_3 for fixed $f_1 = 50$cm, $f_2 = 75$cm, $f_3 = 100$cm, $f_4 = 125$cm, $d_1 = 160$cm and $L > L_M = 1500$cm**

and d_3 are plotted in the Fig. (6.8). There exist four stable zones of different Gouy phase variations of $2\pi - 3\pi$, $3\pi - 2\pi$ and $3\pi - 4\pi$. Out of these four the central contour is completely stable inside and surrounded outside by an unstable region, where as the other three contours are surrounded inside and outside by an unstable region.

(b). $L = L_M$. For $L = L_M = 1400$cm, one can see that the central contour with the Gouy phase variation $3\pi - 4\pi$ starts decreasing as shown in the Fig. (6.9). But the remaining three stable contours are still existing in the same manner as in the previous case $L > L_M$.

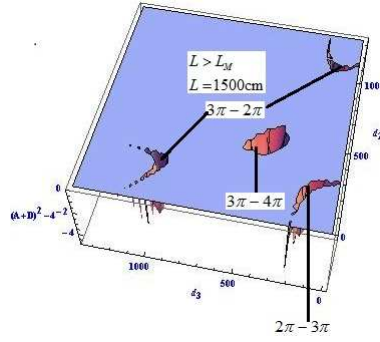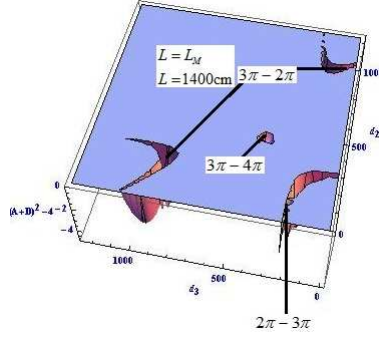(c). $L = L_{M2} + L_{M3} + L_{M4}$. For the case of $L = L_{M2} + L_{M3} + L_{M4} = 1200$cm,

Figure 6.9: **Stability diagram as a function of d_2 and d_3 for fixed** $f_1 = 50\text{cm}$, $f_2 = 75\text{cm}$, $f_3 = 100\text{cm}$, $f_4 = 125\text{cm}$, $d_1 = 160\text{cm}$ **and** $L = L_M = 1400\text{cm}$
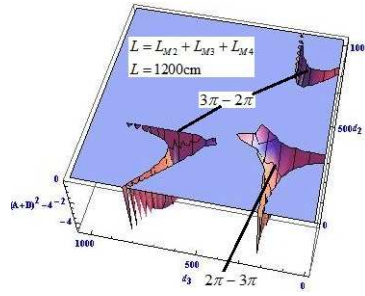

Figure 6.10: **Stability diagram as a function of d_2 and d_3 for fixed** $f_1 = 50\text{cm}$, $f_2 = 75\text{cm}$, $f_3 = 100\text{cm}$, $f_4 = 125\text{cm}$, $d_1 = 160\text{cm}$ **and** $L = L_{M2} + L_{M3} + L_{M4} = 1200\text{cm}$

the central contour is completely vanished and the other three stable contours are giving an impression that, they are coming closely to merge which is shown in the Fig. (6.10).

(d). $L = L_{M1} + L_{M3} + L_{M4}$. Interestingly, one can see here in this Fig. (6.11) that for $L = L_{M1} + L_{M3} + L_{M4} = 1100\text{cm}$, all the three stable contours are merged.
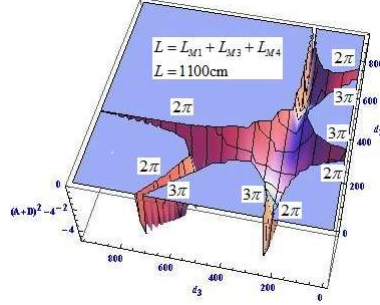
Figure 6.11: **Stability diagram as a function of d_2 and d_3 for fixed $f_1 = 50$cm, $f_2 = 75$cm, $f_3 = 100$cm, $f_4 = 125$cm, $d_1 = 160$cm and $L = L_{M1} + L_{M3} + L_{M4} = 1100$cm**

The length region of 4CURC where the 4CURC can act as a 3CURC will come into the length chart from here onwards.

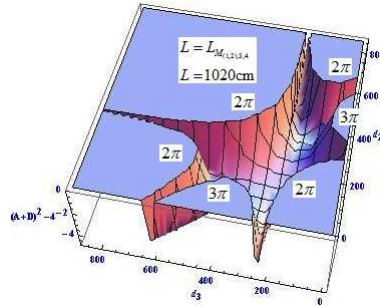(e). $L = L_{M_{(1,2),3,4}}$. For $L = L_{M_{(1,2),3,4}} = 1020$cm, the merging is taking

Figure 6.12: **Stability diagram as a function of d_2 and d_3 for fixed $f_1 = 50$cm, $f_2 = 75$cm, $f_3 = 100$cm, $f_4 = 125$cm, $d_1 = 160$cm and $L = L_{M_{(1,2),3,4}} = 1020$cm**

place and it is wider compare to the previous case even though the instabilities are existing as shown in the Fig. (6.12).

146

(f). $L = L_{M1} + L_{M2} + L_{M4}$. As this $L = L_{M1} + L_{M2} + L_{M4} = 1000$cm
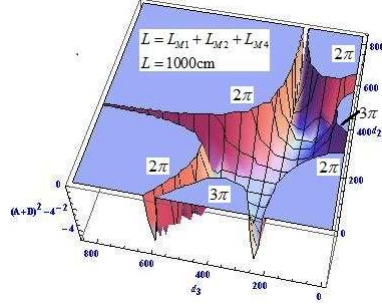

Figure 6.13: **Stability diagram as a function of d_2 and d_3 for fixed $f_1 = 50$cm, $f_2 = 75$cm, $f_3 = 100$cm, $f_4 = 125$cm, $d_1 = 160$cm and $L = L_{M1} + L_{M2} + L_{M4} = 1000$cm**

is close to the previous L, there is no much difference in the stability compare to Fig. (6.12) which is shown in the Fig. (6.13).

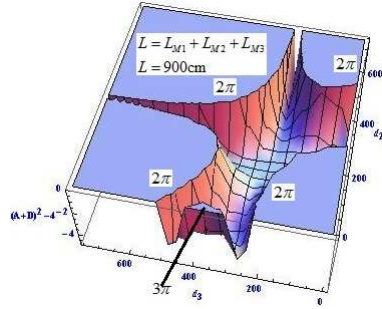(g). $L = L_{M1} + L_{M2} + L_{M3}$. The stability for this case of $L = L_{M1} + L_{M2} +$

Figure 6.14: **Stability diagram as a function of d_2 and d_3 for fixed $f_1 = 50$cm, $f_2 = 75$cm, $f_3 = 100$cm, $f_4 = 125$cm, $d_1 = 160$cm and $L = L_{M1} + L_{M2} + L_{M3} = L_{M3} + L_{M4} = 900$cm**

$L_{M3} = 900$cm is plotted in the Fig. (6.14). It is observed that the un

stable region of d_2 around 400cm to 600cm for smaller d_3 is eliminated and the un stable region of d_3 around 300cm to 500cm for smaller d_2 is reduced for smaller d_2.

(h). $L = L_{M_{1,(2,3),4}}$. As we change L further to $L = L_{M_{1,(2,3),4}} = 871.4285$cm,

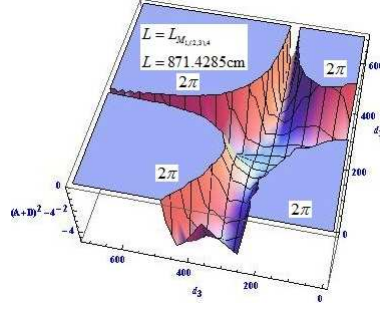Figure 6.15: **Stability diagram as a function of d_2 and d_3 for fixed $f_1 = 50$cm, $f_2 = 75$cm, $f_3 = 100$cm, $f_4 = 125$cm, $d_1 = 160$cm and $L = L_{M_{1,(2,3),4}} = 871.4285$cm**

the un stable region of d_3 for smaller d_2 is completely removed as shown in the Fig. (6.15).

Here onwards the length region of 4CURC where it cam behave as 2CURC will start.

(i). $L = L_{M_{(4,1),2,3}}$. For the case of $L = L_{M_{(4,1),2,3}} = 842.8571$cm, the stable contour is started becoming narrower with respect to d_3 as shown in the Fig. (6.16).

(j). $L = L_{M2} + L_{M4}$. For this case of $L = L_{M2} + L_{M4} = 800$cm, the stable contours of d_2 and d_3 are plotted in the Fig. (6.17). It is noted that just as in the case of 2CURC, there exist two disconnected stable contours.

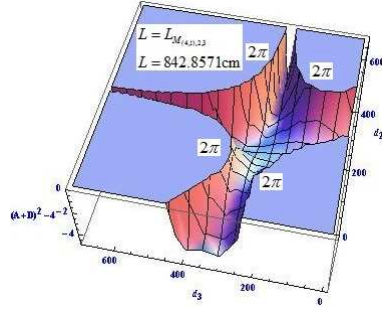(k). $L = L_{M_{1,2,(3,4)}}$. For this very $L = L_{M_{1,2,(3,4)}} = 722.22$cm, it is shown in

Figure 6.16: **Stability diagram as a function of d_2 and d_3 for fixed** $f_1 = 50$**cm,** $f_2 = 75$**cm,** $f_3 = 100$**cm,** $f_4 = 125$**cm,** $d_1 = 160$**cm and** $L = L_{M_{1,(2,3),4}} = 842.8571$**cm**

Figure 6.17: **Stability diagram as a function of d_2 and d_3 for fixed** $f_1 = 50$**cm,** $f_2 = 75$**cm,** $f_3 = 100$**cm,** $f_4 = 125$**cm,** $d_1 = 160$**cm and** $L = L_{M2} + L_{M4} = 800$**cm**

the Fig. (6.18) that the stable zone is reduced further even though it is merged again.

(l). $L = L_{M1} + L_{M4} = L_{M2} + L_{M3}$. For this $L = L_{M1} + L_{M4} = L_{M2} + L_{M3} = 700$cm, again there exist two un connected stable contours as shown in the Fig. (6.19).

(m). $L = L_{M1} + L_{M3}$.

Figure 6.18: **Stability diagram as a function of d_2 and d_3 for fixed $f_1 = 50$cm, $f_2 = 75$cm, $f_3 = 100$cm, $f_4 = 125$cm, $d_1 = 160$cm and $L = L_{M_{1,2,(3,4)}} = 722.22$cm**
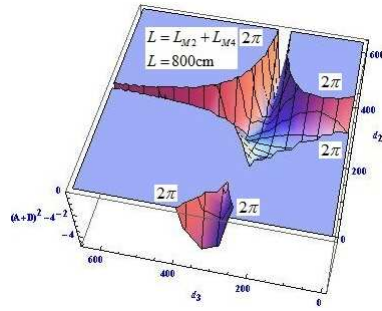

Figure 6.19: **Stability diagram as a function of d_2 and d_3 for fixed $f_1 = 50$cm, $f_2 = 75$cm, $f_3 = 100$cm, $f_4 = 125$cm, $d_1 = 160$cm and $L = L_{M1} + L_{M4} = L_{M2} + L_{M3} = 700$cm**

(n). $L = L_{M4}$. For the cases (m) and (n) there is very small stable contours as shown in the Fig. (6.20) and Fig. (6.21).

(o). $L = L_{M3}$.

(p). $L = L_{M_{(1,2),(3,4)}}$.

(q). $L = L_{M_{(4,1),(2,3)}}$.

Figure 6.20: **Stability diagram as a function of d_2 and d_3 for fixed $f_1 = 50$cm, $f_2 = 75$cm, $f_3 = 100$cm, $f_4 = 125$cm, $d_1 = 160$cm and $L = L_{M1} + L_{M3} = 600$cm**
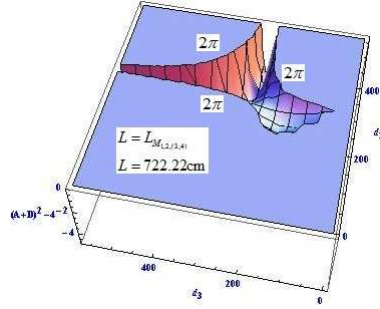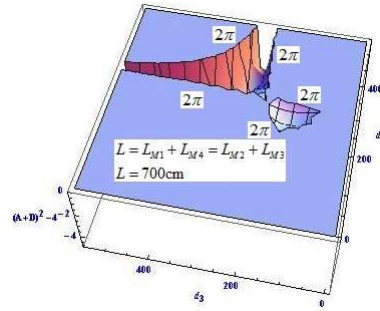

Figure 6.21: **Stability diagram as a function of d_2 and d_3 for fixed $f_1 = 50$cm, $f_2 = 75$cm, $f_3 = 100$cm, $f_4 = 125$cm, $d_1 = 160$cm and $L = L_{M4} = 500$cm**

(r). $L = L_{M2}$. For the cases (o), (p), (q) and (r) there are stability contours but they are linear with the Gouy phase variation less than π. See Fig. (6.22)-Fig. (6.25).

(s). $L = L_{M1}$. For the considered $d_1 = 160$cm, the minimum length of L which can be used is up to $L = L_{M1}$, even for this there is no stable region of d_2 and d_3 exist as shown in the Fig. (6.26).

Figure 6.22: **Stability diagram as a function of d_2 and d_3 for fixed $f_1 = 50$cm, $f_2 = 75$cm, $f_3 = 100$cm, $f_4 = 125$cm, $d_1 = 160$cm and $L = L_{M3} = 400$cm**
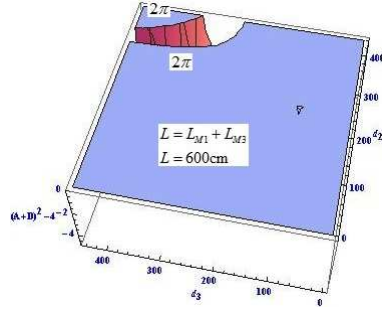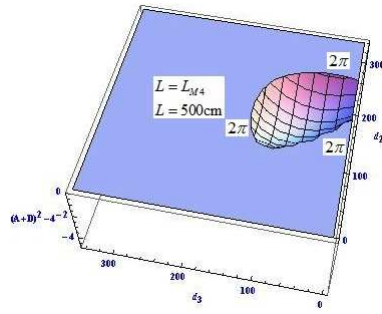

Figure 6.23: **Stability diagram as a function of d_2 and d_3 for fixed $f_1 = 50$cm, $f_2 = 75$cm, $f_3 = 100$cm, $f_4 = 125$cm, $d_1 = 160$cm and $L = L_{M_{(1,2),(3,4)}} = 342.222$cm**

(t). $L = L_{eff1234}$. For the considered f_1, f_2, f_3 and f_4, the range of L, from 0 to $L_{eff1234}$ as shown in the Fig. (6.27) is available for which the 4CURC behaves as a SCURC for which the Gouy phase variation is from 0 to π.

From the stability of 4CURC it is analyzed that for distinct $f_1 < f_2 < f_3 < f_4$, the unstable regions are still present. In fact, it is continuing to have
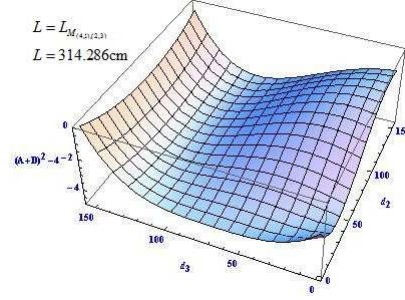
Figure 6.24: **Stability diagram as a function of d_2 and d_3 for fixed $f_1 = 50$cm, $f_2 = 75$cm, $f_3 = 100$cm, $f_4 = 125$cm, $d_1 = 160$cm and $L = L_{M_{(4,1),(2,3)}} = 314.286$cm**
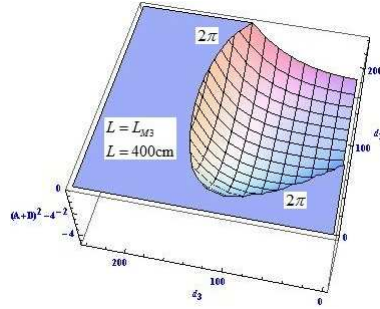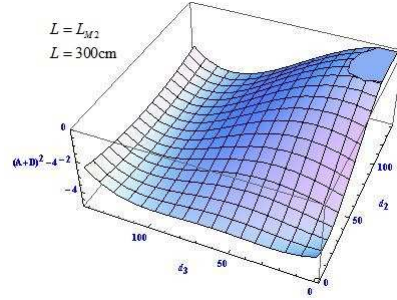

Figure 6.25: **Stability diagram as a function of d_2 and d_3 for fixed $f_1 = 50$cm, $f_2 = 75$cm, $f_3 = 100$cm, $f_4 = 125$cm, $d_1 = 160$cm and $L = L_{M2} = 300$cm**

the accumulated Gouy phase equivalent to π, but not more than π. As a final attempt, we check the stability of 4CURC for symmetric f. We will not present the analytical solutions but we discuss some of the numerical results in the following section.
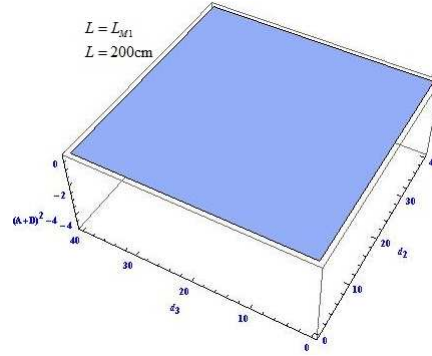
Figure 6.26: **Stability diagram as a function of d_2 and d_3 for fixed $f_1 = 50$cm, $f_2 = 75$cm, $f_3 = 100$cm, $f_4 = 125$cm, $d_1 = 160$cm and $L = L_{M2} = 200$cm**
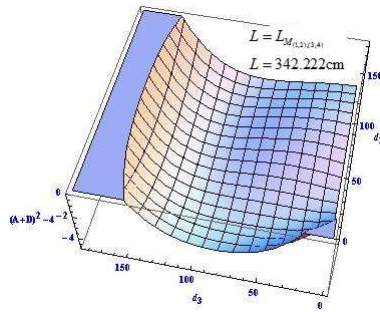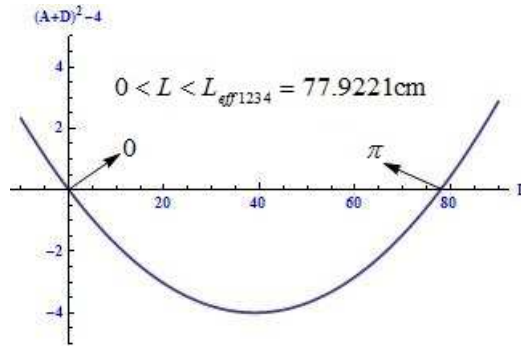

Figure 6.27: **Stability diagram as a function of d_2 and d_3 for fixed $f_1 = 50$cm, $f_2 = 75$cm, $f_3 = 100$cm, $f_4 = 125$cm, $d_1 = d_2 = d_3 = 0$cm and $L = L_{eff1234} = 77.9221$cm**

6.3.1 Stable solutions of d_1 for a given L, d_2, d_3 and for symmetric f

For a given $f = 100$cm, $d_1 = 100$cm, at $L = 6f$cm onwards the merging of the stable contours starts taking place. For $L = 600$, the stability is

plotted between d_2 and d_3 is shown in the Fig. (6.28). It is realized that even with the symmetric f, the unstable zones are occurring in between the stable zones. The corresponding Gouy phase regions are identified for this and for the following cases too. For the cases of $L = 5f$cm and $L = 4f$cm
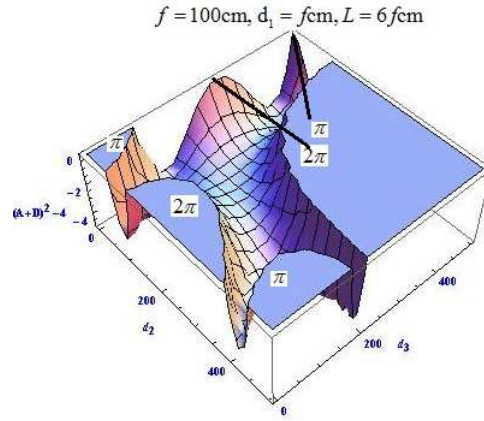
Figure 6.28: **Stability diagram as a function of d_2 and d_3 for fixed $f = 100$cm, $d_1 = 100$cm and $L = 6f$cm**

the stability is plotted in Fig. (6.29) and Fig. (6.30). It is again made it clear that it is not possible to achieve the accumulated Gouy phase variation beyond 4π. We calculate the half rayleigh ranges and the positions of the beam waists in each of the arms of the 4CURC by using

$$z_{0i} = \pm \frac{1}{C} \sqrt{1 - \left(\frac{A + D}{2}\right)^2} \tag{6.53}$$

$$x_{0i} = \frac{A - D}{2C} \tag{6.54}$$

Here the index $i = s$ corresponds to the arm d_1, $i = y$ corresponds to the arm d_2, $i = d$ corresponds to the arm d_3 and $i = b$ corresponds to the arm $L - d_1 - d_2 - d_3$ of the cavity. Having calculated the half Rayleigh ranges and

Figure 6.29: **Stability diagram as a function of d_2 and d_3 for fixed** $f = 100$**cm,** $d_1 = 100$**cm and** $L = 5f$**cm**
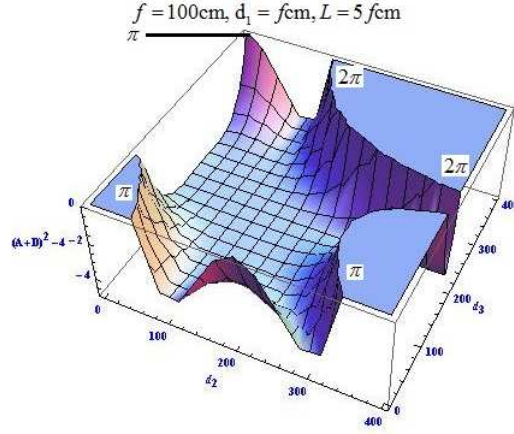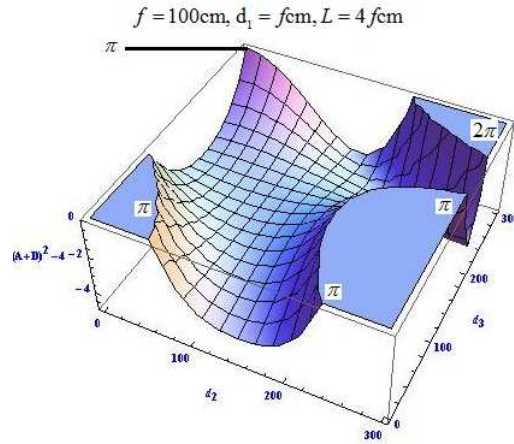

Figure 6.30: **Stability diagram as a function of d_2 and d_3 for fixed** $f = 100$**cm,** $d_1 = 100$**cm and** $L = 4f$**cm**

their positions, one can proceed to calculate the accumulated Gouy phase

$\phi_G(RT)$ for the chosen cavity and is given by

$$
\begin{aligned}
\phi_G(RT) \;=\; & \arctan\left(\frac{x_{0s}}{z_{0s}}\right) - \arctan\left(\frac{-d_1 + x_{0s}}{z_{0s}}\right) \\
& + \arctan\left(\frac{x_{0y}}{z_{0y}}\right) - \arctan\left(\frac{-d_2 + x_{0y}}{z_{0y}}\right) \\
& + \arctan\left(\frac{x_{0d}}{z_{0d}}\right) - \arctan\left(\frac{-d_3 + x_{0d}}{z_{0d}}\right) \\
& + \arctan\left(\frac{x_{0b}}{z_{0b}}\right) - \arctan\left(\frac{-L + d_1 + d_2 + d_3 + x_{0b}}{z_{0b}}\right)
\end{aligned}
$$

$$(6.55)$$

We discuss the Gouy phase variation for some peculiar cases and other mode properties as well in the following section.

6.4   Variable Gouy phase of 4CURC

In this section we analyze different cases of 4CURC to study the Gouy phase variation.

6.4.1   Case(i): For a given $f_1 = f_2 = f$, f_3, f_4, d_1 and L

First we start with the case, when the focal lengths f_1 and f_2 of the lenses L_1 and L_2 are symmetric. For a given d_1, d_3 and L, we vary the distance d_2. For a given $f_1 = f_2 = 50$cm, $f_3 = 75$cm, $f_4 = 100$cm, and for fixed $d_1 = 200$cm, $d_3 = 150$cm, $L = 650$cm, the stable range of d_2, which can be varied to create variable Gouy phase is from 105.104cm-344.896cm. For this range of d_2, we plot all the mode properties in the following Fig. (6.31)-(6.34).

The half Rayleigh ranges z_{0s}, z_{0y}, z_{0d} and z_{0b} are plotted in the Fig. (6.31). It is observed that z_{0y} and z_{0b} are linear through out the stable range of d_2 where as z_{0s} is showing a rapid increase at the edges of stable d_2. The Half
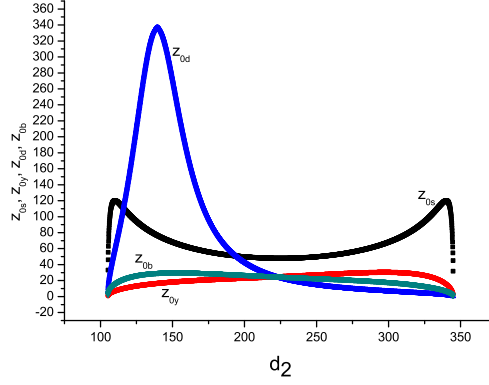
Figure 6.31: **Half Rayleigh ranges** z_{0s}, z_{0y}, z_{0d} **and** z_{0b} **as a function of** d_2 **for** $f_1 = f_2 = 50$**cm,** $f_3 = 75$**cm,** $f_4 = 100$**cm,** $d_1 = 200$**cm,** $d_3 = 150$**cm,** $L = 650$**cm**

Rayleigh range between the lenses L_3 and L_4, i.e., z_{0d} reached a maximum value of 340cm around $d_2 = 130$cm. The corresponding positions of the beam waists x_{0s}, x_{0y}, x_{0d} and x_{0b} are plotted with d_2 in the Fig. (6.32). The spot sizes before and after the lenses L_1, L_2, L_3 and L_4 are equal and given by ω_{1x1}, ω_{2x1}, ω_{3x1} and ω_{4x1} are plotted with d_2 in the Fig. (6.33). At the edges they are increasing rapidly but varying linearly through out the stable range of d_2. The variable Gouy phases for full round trip in each of the arms of lengths d_1, d_2, d_3 and $L - d_1 - d_2 - d_3$ are correspondingly $\phi_{G1}(RT)$, $\phi_{G2}(RT)$, $\phi_{G3}(RT)$, $\phi_{G4}(RT)$ and the accumulated Gouy phase $\phi_G(RT)$ as a function of d_2 is plotted in the Fig. (6.34). The Gouy phase variation for this case amounts to be $\frac{2\pi}{3}$ which is less than π. In the next section we consider the second and third lenses to be symmetric and analyze the mode properties in the same manner.

Figure 6.32: **The positions of the beam spot sizes** x_{0s}, x_{0y}, x_{0d} **and** x_{0b} **as a function of** d_2 **for** $f_1 = f_2 = f = 50$**cm,** $f_3 = 75$**cm,** $f_4 = 100$**cm,** $d_1 = 200$**cm,** $d_3 = 150$**cm,** $L = 650$**cm**
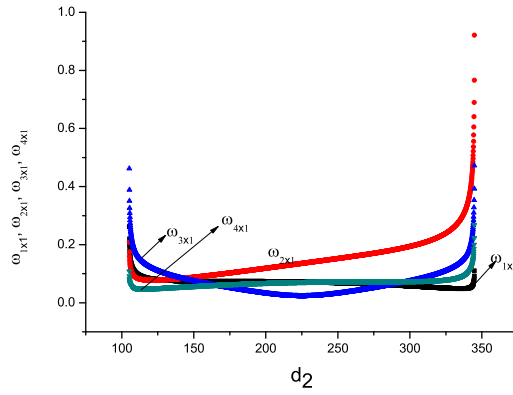
Figure 6.33: **The spot sizes on the lenses** L_1, L_2, L_3 **and** L_4 **as a function of** d_2 **for** $f_1 = f_2 = 50$**cm,** $f_3 = 75$**cm,** $f_4 = 100$**cm,** $d_1 = 200$**cm,** $d_3 = 150$**cm,** $L = 650$**cm**

159

Figure 6.34: **Variable Gouy phases** $\phi_{G1}(RT)$, $\phi_{G2}(RT)$, $\phi_{G3}(RT)$, $\phi_{G4}(RT)$ **and** $\phi_G(RT)$ **as a function of** d_2 **for** $f_1 = f_2 = 50$**cm,** $f_3 = 75$**cm,** $f_4 = 100$**cm,** $d_1 = 200$**cm,** $d_3 = 150$**cm,** $L = 650$**cm**

6.4.2 Case(ii): For a given f_1, $f_2 = f_3 = f$, f_4, d_1 and L

Consider the focal lengths f_2, f_3 of the lenses L_2 and L_3 to be symmetric. For $f_1 = 50$cm, $f_2 = f_3 = 75$cm, $f_4 = 100$cm and $d_1 = 200$cm, $d_3 = 100$cm, $L = 700$cm, the stable range of d_2 which is available is from 163.397cm-336.603cm. For this range of d_2, the half Rayleigh ranges z_{0s}, z_{0y}, z_{0d} and z_{0b} are plotted in the Fig. (6.35). The corresponding positions of the beam waists x_{0s}, x_{0y}, x_{0d} and x_{0b} are plotted with d_2 in the Fig. (6.32). The spot sizes before and after the lenses L_1, L_2, L_3 and L_4 are equal and given by ω_{1x1}, ω_{2x1}, ω_{3x1} and ω_{4x1} are plotted with d_2 in the Fig. (6.37). The variable Gouy phases for full round trip in each of the arms of lengths d_1, d_2, d_3 and $L - d_1 - d_2 - d_3$ are correspondingly $\phi_{G1}(RT)$, $\phi_{G2}(RT)$, $\phi_{G3}(RT)$, $\phi_{G4}(RT)$ and the accumulated Gouy phase $\phi_G(RT)$ as a function of d_2 is plotted in the Fig. (6.38). The Gouy phase variation observed for this case is $\dfrac{2\pi}{3}$.

Figure 6.35: **Half Rayleigh ranges** z_{0s}, z_{0y}, z_{0d} **and** z_{0b} **as a function of** d_2 **for** $f_1 = 50$**cm,** $f_2 = f_3 = 75$**cm,** $f_4 = 100$**cm,** $d_1 = 200$**cm,** $d_3 = 100$**cm,** $L = 700$**cm**
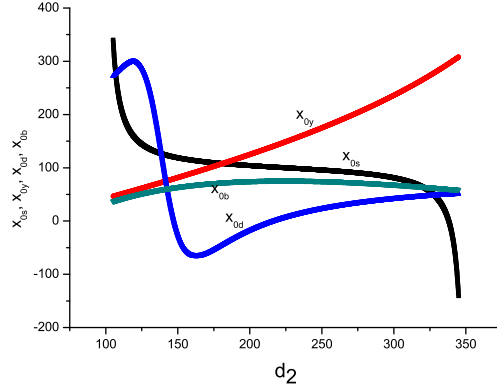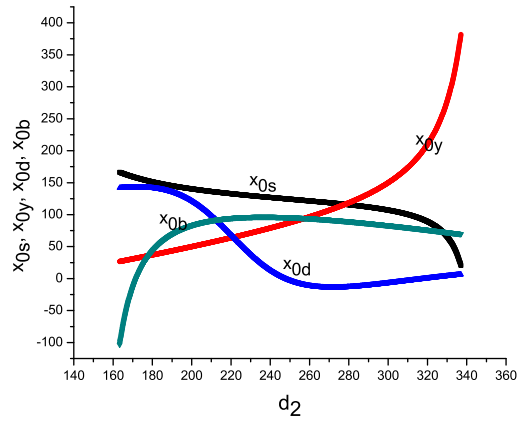

Figure 6.36: **The positions of the beam spot sizes** x_{0s}, x_{0y}, x_{0d} **and** x_{0b} **as a function of** d_2 **for** $f_1 = 50$**cm,** $f_2 = f_3 = 75$**cm,** $f_4 = 100$**cm,** $d_1 = 200$**cm,** $d_3 = 100$**cm,** $L = 700$**cm**
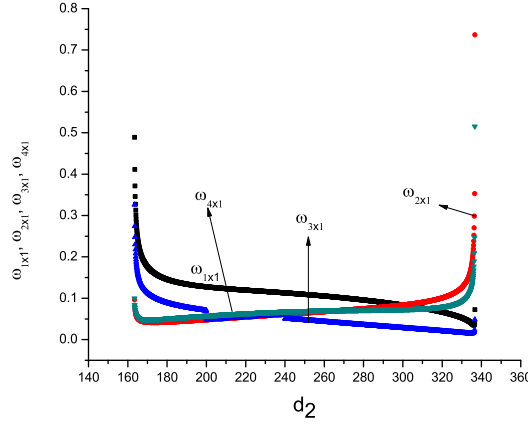
Figure 6.37: **The spot sizes on the lenses** L_1, L_2, L_3 **and** L_4 **as a function of** d_2 **for** $f_1 = 50$**cm,** $f_2 = f_3 = 75$**cm,** $f_4 = 100$**cm,** $d_1 = 200$**cm,** $d_3 = 100$**cm,** $L = 700$**cm**

6.4.3 Case(iii): For a given f_1, f_2, $f_3 = f_4 = f$, d_1 and L

Consider the focal lengths f_3, f_4 of the lenses L_3 and L_4 to be symmetric. For $f_1 = 50$cm, $f_2 = 75$cm, $f_3 = f_4 = 100$cm and $d_1 = 200$cm, $d_3 = 180$cm, $L = 800$cm, the stable range of d_2 which is available is from 41.1508cm-445.516cm. For this long range of d_2, the half Rayleigh ranges z_{0s}, z_{0y}, z_{0d} and z_{0b} are plotted in the Fig. (6.39). The corresponding positions of the beam waists x_{0s}, x_{0y}, x_{0d} and x_{0b} are plotted with d_2 in the Fig. (6.40). The variable Gouy phases for full round trip in each of the arms of lengths d_1, d_2, d_3 and $L - d_1 - d_2 - d_3$ are correspondingly $\phi_{G1}(RT)$, $\phi_{G2}(RT)$, $\phi_{G3}(RT)$, $\phi_{G4}(RT)$ and the accumulated Gouy phase $\phi_G(RT)$ as a function of d_2 is plotted in the Fig. (6.42). For this case the Gouy phase variation is turning out to be $\dfrac{2\pi}{3}$. It is realized that even if we make any two of the lenses of the 4CURC to be symmetric the accumulated Gouy phase variation
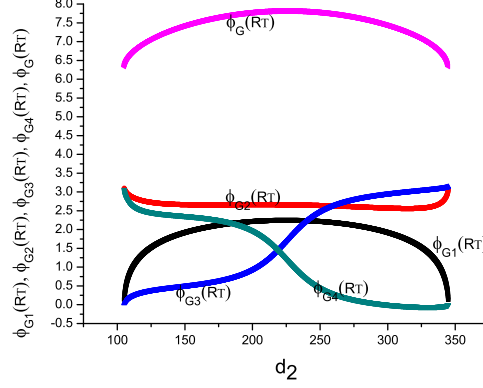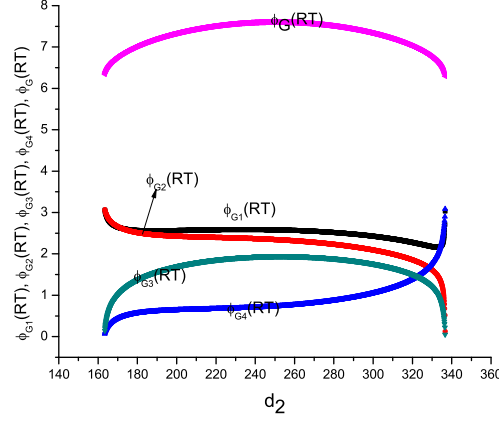
Figure 6.38: **Variable Gouy phases** $\phi_{G1}(RT)$, $\phi_{G2}(RT)$, $\phi_{G3}(RT)$, $\phi_{G4}(RT)$ **and** $\phi_G(RT)$ **as a function of** d_2 **for** $f_1 = 50$**cm,** $f_2 = f_3 = 75$**cm,** $f_4 = 100$**cm,** $d_1 = 200$**cm,** $d_3 = 100$**cm,** $L = 700$**cm**

which one can get is of the order of $\dfrac{2\pi}{3}$. Therefore, what happens to the Gouy phase variation when all of the lenses are symmetric? In the following section we study different cases leading to different Gouy phase variations with the symmetric focal lengths.

6.5 For a symmetric $f_1 = f_2 = f_3 = f_4 = f$

Consider all the focal lengths of the 4CURC to be symmetric i.e., $f_1 = f_2 = f_3 = f_4 = f$. At different values of L, d_1, d_2 and d_3 we check the Gouy phase variation as in the following.
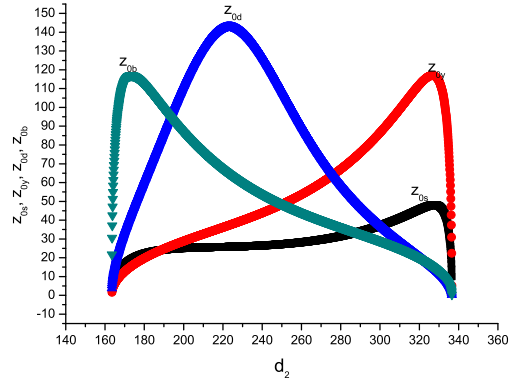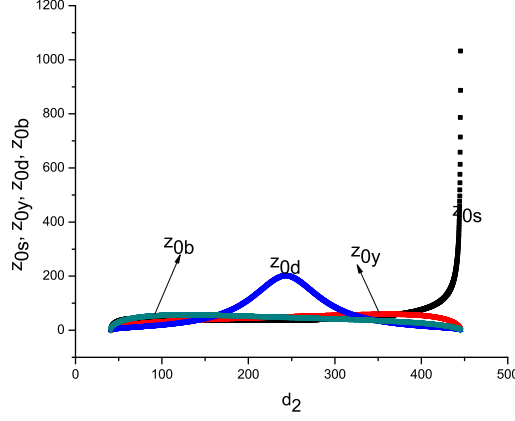
Figure 6.39: **Half Rayleigh ranges z_{0s}, z_{0y}, z_{0d} and z_{0b} as a function of d_2 for $f_1 = 50$cm, $f_2 = 75$cm, $f_3 = f_4 = 100$cm, $d_1 = 200$cm, $d_3 = 180$cm, $L = 800$cm**

6.5.1   Case(i): $3\pi - 4\pi - 3\pi$

For the given values of $f = 30$cm, $L = 480$cm, $d_2 = 120$cm, $d_3 = 120$cm, the stable range of d_1 which satisfies the stability function is from 85.359cm to 154.641cm. Therefore for this range of d_1, we plot all the beam properties which are shown in the Figs. (6.43)-(6.46). The Fig. (6.43) shows the behaviour of half Rayleigh ranges z_{0s}, z_{0y}, z_{0d} and z_{0b} in between the lens combinations (L_1, L_2), (L_2, L_3), (L_3, L_4) and (L_4, L_1) respectively. It is noticed that all of them are becoming zero at $d_1 = 120$cm. The corresponding positions of the beam waists are plotted in the Fig. (6.44). The spot sizes on the lenses ω_{1x1}, ω_{2x1}, ω_{3x1} and ω_{4x1} are plotted in the Fig. (6.45). The Gouy phase variation in all the four sections $\phi_{G1}(RT)$, $\phi_{G2}(RT)$, $\phi_{G3}(RT)$, $\phi_{G4}(RT)$ and the accumulated Gouy phase $\phi_G(RT)$ is plotted in the Fig. (6.46). It is noticed that the accumulated Gouy phase shows the variation
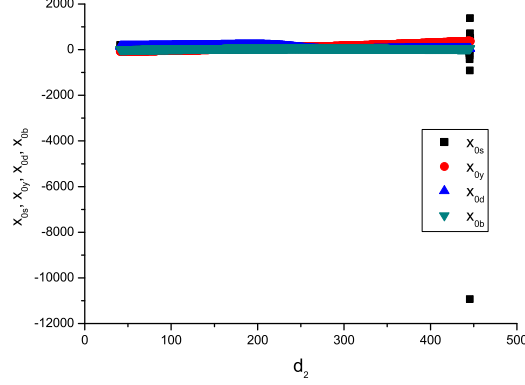
Figure 6.40: **The positions of the beam spot sizes x_{0s}, x_{0y}, x_{0d} and x_{0b} as a function of d_2 for $f_1 = 50$cm, $f_2 = 75$cm, $f_3 = f_4 = 100$cm, $d_1 = 200$cm, $d_3 = 180$cm, $L = 800$cm**

The spot sizes before and after the lenses L_1, L_2, L_3 and L_4 are equal and given by ω_{1x1}, ω_{2x1}, ω_{3x1} and ω_{4x1} are plotted with d_2 in the Fig. (6.41).

$3\pi - 4\pi - 3\pi$.

6.5.2 Case(ii): $3\pi - 2\pi$, $2\pi - 3\pi$

For the chosen $f = 30$cm, $L = 470$cm, $d_2 = 120$cm and $d_3 = 274$cm, there are two stable regions of d_1 available, in between 24cm to 75cm. First region of d_1 is from 27cm to 41cm and the second region of d_1 is from 46cm to 75cm which are separated by an unstable region. For this case the half Rayleigh ranges z_{os}, z_{0y}, z_{0d} and z_{ob} are plotted in the Fig. (6.47). The corresponding positions of the beam waists are plotted in the Fig. (6.48). The corresponding spot sizes on the lenses ω_{1x1}, ω_{2x1}, ω_{3x1} and ω_{4x1} are plotted in the Fig. (6.49). The Gouy phase variation in all the four sections $\phi_{G1}(RT)$, $\phi_{G2}(RT)$, $\phi_{G3}(RT)$, $\phi_{G4}(RT)$ and the accumulated Gouy phase
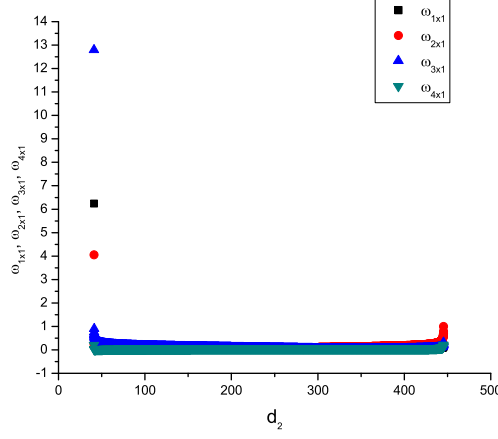
Figure 6.41: **The spot sizes on the lenses** L_1, L_2, L_3 **and** L_4 **as a function of** d_2 **for** $f_1 = 50$**cm,** $f_2 = 75$**cm,** $f_3 = f_4 = 100$**cm,** $d_1 = 200$**cm,** $d_3 = 180$**cm,** $L = 800$**cm**

$\phi_G(RT)$ is plotted for two regions and is shown in Fig. (6.50). In the first region of d_1 the accumulated Gouy phase is varying from $3\pi - 2\pi$ where as in the second region of d_1 it is varying from $2\pi - 3\pi$.

6.5.3   Case(iii): $\pi - 2\pi$, $2\pi - \pi$

As it is discussed, the Gouy phase variations $\pi - 2\pi$ and $2\pi - \pi$ correspond to the length region of 2CURC. For this case we make $d_2 = d_3 = 0$cm. For the chosen $f = 30$cm, $L = 470$cm there exist two small stable regions of d_1. First stable region of d_1 is from 41.0284cm to 44.1284cm and the second stable region is from 425.8535cm to 428.9535cm. For this set of parameters the half Rayleigh ranges are plotted for the two stable regions separately which are shown in the Figs. (6.51a) and (6.51b).

In the first region of d_1, the half Rayleigh ranges z_{0s}, z_{0y} and z_{0d} are
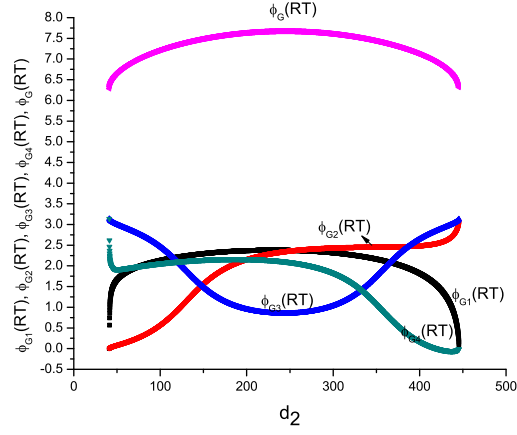
Figure 6.42: **Variable Gouy phases** $\phi_{G1}(RT)$, $\phi_{G2}(RT)$, $\phi_{G3}(RT)$, $\phi_{G4}(RT)$ **and** $\phi_G(RT)$ **as a function of** d_2 **for** $f_1 = 50$**cm,** $f_2 = 75$**cm,** $f_3 = f_4 = 100$**cm,** $d_1 = 200$**cm,** $d_3 = 180$**cm,** $L = 800$**cm**
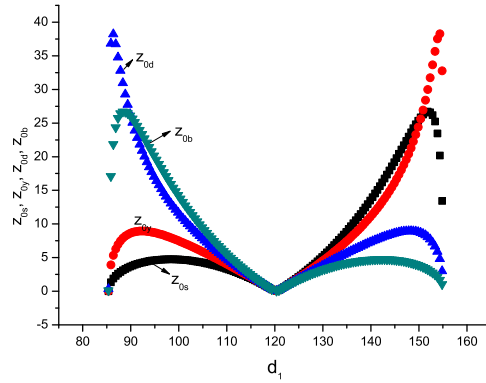
Figure 6.43: **Half Rayleigh ranges** z_{0s}, z_{0y}, z_{0d} **and** z_{0b} **as a function of** d_1 **for** $f = 30$**cm,** $d_2 = 120$**cm,** $d_3 = 120$**cm,** $L = 480$**cm**

Figure 6.44: **The positions of the beam spot sizes x_{0s}, x_{0y}, x_{0d} and x_{0b} as a function of d_1 for $f = 30$cm, $d_2 = 120$cm, $d_3 = 120$cm, $L = 480$cm**
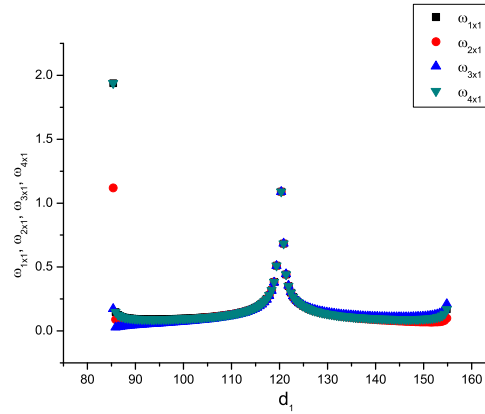
Figure 6.45: **The spot sizes on the lenses L_1, L_2, L_3 and L_4 as a function of d_1 for $f = 30$cm, $d_2 = 120$cm, $d_3 = 120$cm, $L = 480$cm**

very small compare to z_{0b}. For the second region, z_{0s} reaches higher values, where as the other three half Rayleigh ranges z_{oy}, z_{0d} and z_{ob} are very much confined and they are small in the size.

Figure 6.46: **Variable Gouy phases** $\phi_{G1}(RT)$, $\phi_{G2}(RT)$, $\phi_{G3}(RT)$, $\phi_{G4}(RT)$ **and** $\phi_{G}(RT)$ **as a function of** d_1 **for** $f = 30$**cm,** $d_2 = 120$**cm,** $d_3 = 120$**cm,** $L = 480$**cm**
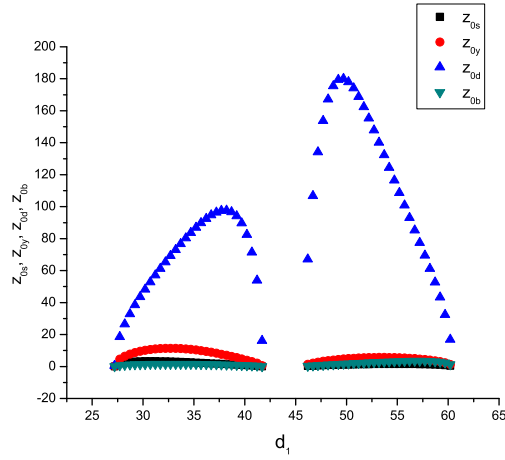
Figure 6.47: **Half Rayleigh ranges** z_{0s}, z_{0y}, z_{0d}, z_{0b} **as a function of** d_1 **for fixed** $f = 30$**cm,** $d_2 = 120$**cm,** $d_3 = 120$**cm,** $L = 470$**cm**
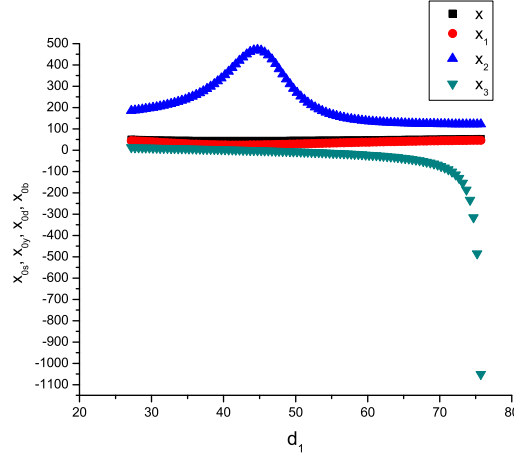
Figure 6.48: **The positions of the beam spot sizes x_{0s}, x_{0y}, x_{0d} and x_{0b} as a function of d_1 for fixed $f = 30$cm, $d_2 = 120$cm, $d_3 = 120$cm, $L = 470$cm**
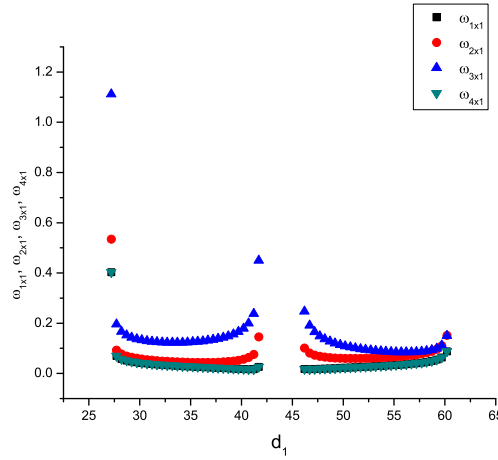
Figure 6.49: **The spot sizes on the lenses L_1, L_2, L_3 and L_4 as a function of d_1 for fixed $f = 30$cm, $d_2 = 120$cm, $d_3 = 120$cm, $L = 470$cm**
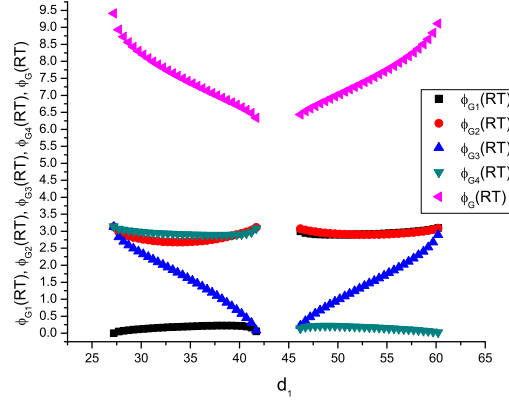
Figure 6.50: **Variable Gouy phases** ϕ_{G1}, ϕ_{G2} , ϕ_{G3}, ϕ_{G4} **and** $\phi_G(RT)$ **as a function of** d_1 **for fixed** $f = 30\text{cm}$, $d_2 = 120\text{cm}$, $d_3 = 120\text{cm}$ **and** $L = 470\text{cm}$
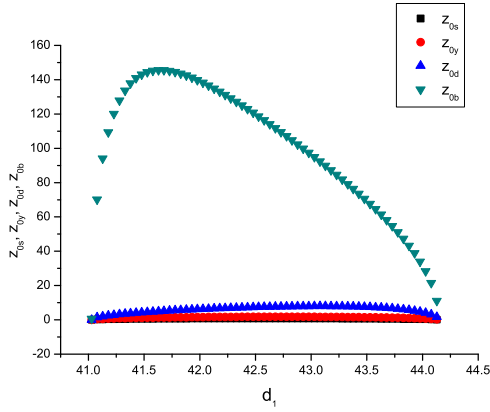
(a) **for the first stable region**
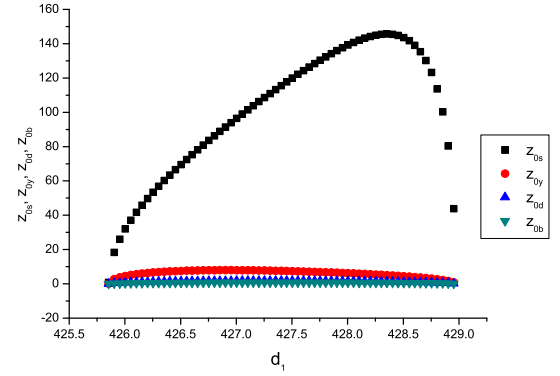
(b) **for the second stable region**

Figure 6.51: **Half Rayleigh ranges** z_{0s}, z_{0y}, z_{0d}, z_{0b} **as a function of** d_1 **for fixed** $f = 30\text{cm}$, $d_2 = d_3 = 0\text{cm}$, $L = 470\text{cm}$

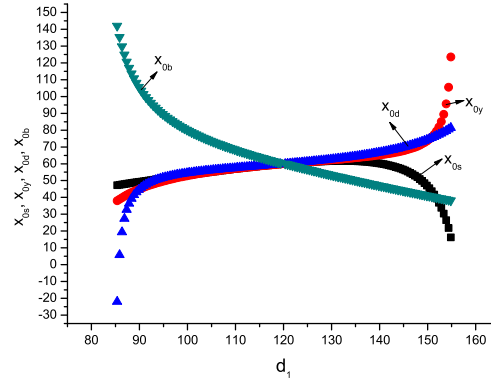(a) **for the first stable region**

(b) **for the second stable region**
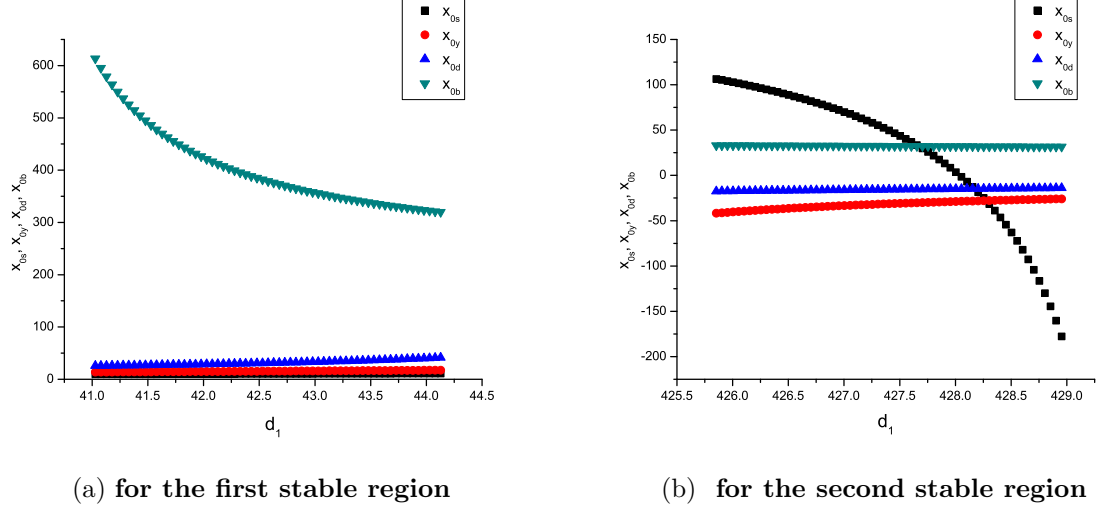
Figure 6.52: **The positions of the beam spot sizes x_{0s}, x_{0y}, x_{0d} and x_{0b} as a function of d_1 for fixed $f = 30$cm, $d_2 = d_3 = 0$cm, $L = 470$cm**

The corresponding positions x_{0s}, x_{0y}, x_{0d} and x_{0b} of the beam waists are plotted in the Fig. (6.52a) for the first stable region of d_1 and in Fig. (6.52b) for the second stable region of d_1.

The corresponding spot sizes on the lenses ω_{1x1}, ω_{2x1}, ω_{3x1} and ω_{4x1} are plotted in the Figs. (6.53a) and (6.53b). The Gouy phase variation in all the four sections $\phi_{G1}(RT)$, $\phi_{G2}(RT)$, $\phi_{G3}(RT)$, $\phi_{G4}(RT)$ and the accumulated Gouy phase $\phi_G(RT)$ is plotted for two regions in Figs. (6.54b). In the first stable region of d_1 the accumulated Gouy phase is varying from $\pi - 2\pi$ where as in the second stable region of d_1 it is varying from $2\pi - \pi$.

To summarize, we have analyzed the Gouy phase variation for different cases of 4CURC. By the insertion of 'N' lenses into the cavity, one can generate N regions showing different phases, but with the accumulated Gouy phase variation to be π.

(a) **for the first stable region**

(b) **for the second stable region**
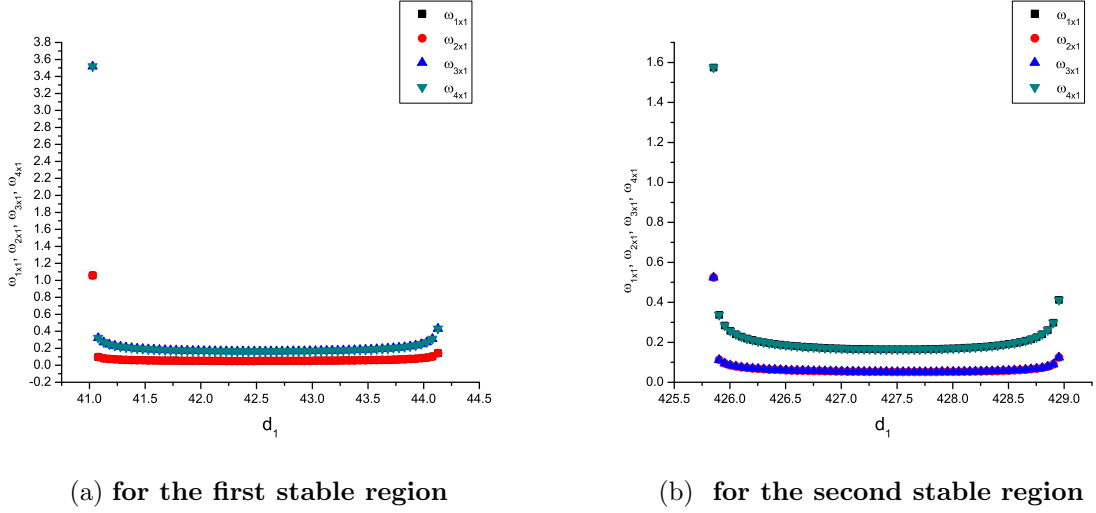
Figure 6.53: **The spot sizes on the lenses** L_1, L_2, L_3 **and** L_4 **as a function of** d_1 **for fixed** $f = 30$**cm**, $d_2 = d_3 = 0$**cm**, $L = 470$**cm**

(a) **for the first stable region**

(b) **for the second stable region**
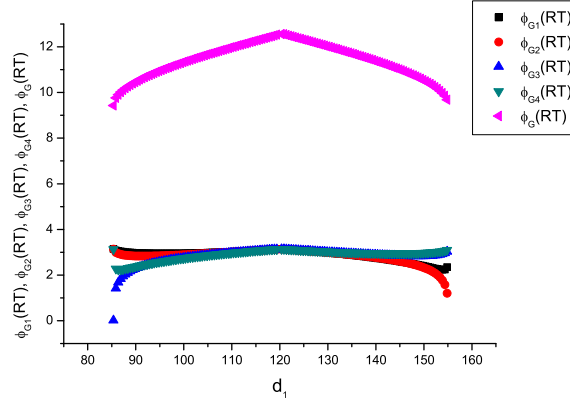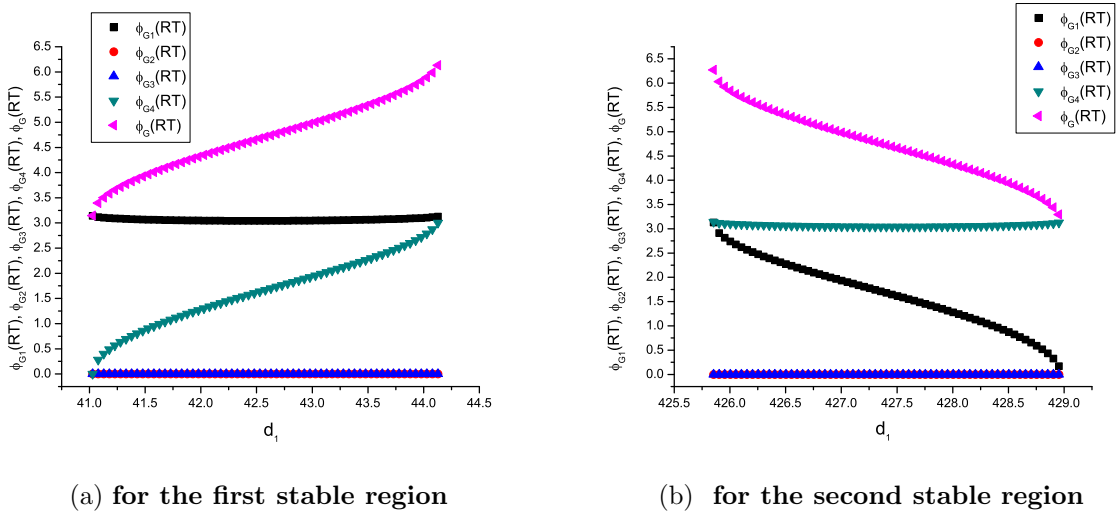
Figure 6.54: $\phi_{G1}(RT)$, $\phi_{G2}(RT)$, $\phi_{G3}(RT)$, $\phi_{G4}(RT)$ **and** $\phi_G(RT)$ **as a function of** d_1 **for fixed** $f = 30$**cm**, $d_2 = d_3 = 0$**cm**, $L = 470$**cm**

6.6   Conclusion

The stability analysis of SCURC, 2CURC, 3CURC and 4CURC is presented in the chapters 3, 4, 5 and 6 in detail. This study suggests that it is not possible to get the accumulated Gouy phase variation more than π. But the advantage of this very amount of π in the Ring laser gyros has been explained in the chapter 5. Chapter-7 deals with the question (b) raised at the end of Chapter-3.

7

The structured point and its equivalence to Huygen's point source for secondary wavelets

We pick the thread left at the end of the Chapter-3. Recall that the structured point source proposed there is the Rayleigh zone - the focal region lying between $-z_0$ to $+z_0$ with the beam waist ω_0 at $z = 0$ in the fundamental Gaussian mode. It was observed in Chapter-3 that by varying the perimeter L of the ring cavity, in Fig. 3.3 one could examine the image focal spot $\omega_0\prime$ and the image point $O\prime$ after the lens L_2, for the object beam waist(ω_0) and a superimposed object point O - kept inside the ring-cavity. The location of $\omega_0\prime$

i.e., the image of the beam waist remains fixed, in the same plane as that of the object beam waist ω_0; on the other hand the position of the point-image $O\prime$ shows variation expected from the geometrical optics (u, v, F) formalism. Besides the locations, it is interesting to compare the variation in the size of the Rayleigh zone, with the size of the point image $O\prime$ as a function of the perimeter L, for a given F. The Rayleigh zone size outside and inside the cavity for a given L, F are exactly same($z_0 = z_0\prime$); the image-point $\omega_0\prime$ however obeys the geometrical magnification $m = \dfrac{v}{u}$ - in transverse direction and $\dfrac{dv}{du} = -m^2$ in longitudinal direction. At $L = 4F$, note that Rayleigh zone shrinks also to the size of the point image($z_0 = z_0\prime \to 0$).

The feature, dramatized in this experiment is related to the two images of the two distinct objects viz. (1) that of Rayleigh zone($-z_0, +z_0$) and (2) that of the point object O. This feature has not been discussed and compared in this way. However it is well known. For example the variation is implied in the parameter w, discussed in connection with metaplectic group analysis of the Gouy phase in the corresponding hyperbolic geometry[1]. This variation also emerges physically as a result of varying the focal length or combination of focal lengths - as discussed in Chapters 4-6. The experiment of Chapter-3, under discussion here is distinct as it varies L for a given F. This in principle permits one to achieve $\omega_0 = 0$ limit which cannot be achieved by varying alone the focal length F of lens for a fixed L. Thus the experiments of Chapter-3 help compare the Cavity-mode-Rayleigh-zone with the point focus of geometrical optics. The point focus gets achieved naturally for $L \geq 4F$, in a graphic way. The cavity mode of finite size z_0 helps one to see the inside region of the geometrical point image($z_0\prime \to 0$).

We will conclude below that the Rayleigh region is the expanded/enlarged point of geometrical optics. That is the point of geometrical optics, which is the point to which the focused geometrical rays advancing from infinitely distant spherical wave front congregate(converge to), has an internal structure

like that of the Rayleigh zone of a Gaussian mode - this internal structure lies inside the surfaces of minimum radii of curvature on the boundaries at $z = -z_0, +z_0$.

The location of the point of congregation for an infinitely distant ($|z| \rightarrow \infty$) wavefront can be located at $z \simeq 0$. For wave fronts at distance $|z| > z_0$, the points of congregation are seen to lie in the volume with boundaries at $-z_0$ and $+z_0$ along the z axis. All rays outside the Rayleigh zone are well known to have normal congruence and intensity given by the number of rays per unit area normal to the ray direction of propagation, and that they have their congregation points (meaning their centers of curvature) inside the Rayleigh zone.

The above picture of the Rayleigh zone is as characterized by the rays outside the Rayleigh zone. The entire inside of the Rayleigh zone is being referred to as the structured point of geometrical optics - i.e., the entire voluminous-point is simply called a structured point. The internal structure of the structured point is dependent on the Gaussian mode and can be elaborated as follows.

The volume occupied inside the surface of minimum radius of curvature is the volume of interest now. The principles of geometric optics (i.e, normal congruence, and intensity equal to the number of rays per unit area normal to axis of propagation) are obeyed inside the Rayleigh zone as well. We may call the inside volume as the congregation volume of the outside region. The rays of the inside region do the reversal.

The tangents to every location on rays inside the Rayleigh zone congregate to/de-congregate from (i.e., have convergence/divergence at) points lying in the region outside the Rayleigh zone: that is they do not congregate inside but outside the Rayleigh zone. This is the reversal mentioned above.

As the location on the rays inside moves in the positive direction from the first surface of congregation (i.e, the wave front surface with minimum

radius of curvature existing at $z = -z_0$ on the left of $z = 0$ and reaches the middle ($z = 0$) the associated wave fronts grow in radius of curvature with the centre of curvature out side the Rayleigh zone (at $z > +z_0$) - and acquire the infinite radius of curvature, when at $z = 0$, with centre of curvature at positive infinity. This is a sign of no congregation(convergence at positive infinity). Further down the inside region i.e., for $0 < z < z_0$ they congregate away (have centre of divergence at negative infinity) outside the Rayleigh zone. At the exiting surface of Rayleigh zone at $z = z_0$ the congregation point lies at $-z_0$ at the left boundary of Rayleigh zone, and vice versa.

These properties of the rays in the Rayleigh zone define the structure of the point of geometrical optics in the premise of the structured point.

The concept of such a structured point invites one to re-examine the phase anomaly near $z = 0$, the focus of the Gaussian mode[2, 3]. While arbitrary phase value may be assigned to any one of the location in a volume filled with electromagnetic field, the relative value of phases of all other locations are determined by the Maxwell's equations and corresponding solution for a coherent field. For example the phase value assigned to focus has been $+\frac{\pi}{2}$ or $-\frac{\pi}{2}$ in different contexts by different authors([3] see page 445 foot note). In that respect the internal structure of the structured point suggests to take the phase at focus at $z = 0$ to be with zero value. The relative values of the phase of the infinitely distant($z = -\infty$) spherical wave front converging towards the focal point at $z = 0$, and that of infinitely distant(at ($z = +\infty$)) spherical wave front diverging away from the focal point at $z = 0$ are $-\frac{\pi}{2}$ and $+\frac{\pi}{2}$(given by the Gouy phase) respectively for a Gaussian mode propagating in positive z-direction.

Question that is raised now is: Is this consistent with the Huygens point source for secondary wavelets?

Note that Huygen's point source of secondary wavelets needs to send disturbance only in the forward direction like a specific Gaussian mode. On

attaching a Gaussian mode of infinitely small z_0 with it this condition gets satisfied automatically. Consequently the phase at any other location from such a Huygens point source is also automatically given by the corresponding Gouy phase as a function of the distance z along direction of propagation, along with its transverse spread in direction r normal to the direction of propagation.

Two more points are required to be paid attention to: 1. distinction has to be made due to the curvature of the wave front as to what phase would one assign to the point source of Huygens being assumed on it; 2. The mode function $\frac{e^{ikr}}{r}$ usually assigned to an atomic spontaneous emitter according to the quantum mechanical probability distribution is not to be confused with the forward propagating mode like the Gaussian mode; while the quantum mechanical probability to emit radiation in any direction is an integral over uniformly distributed modes in all directions, once a photon is emitted it must conform to a forward propagating mode in the direction of emission. The question is: will that mode be with a plane wave front or a Gaussian mode of a chosen z_0 with a plane wave front at its point of location?

Is this, then, consistent with the requirement of Huygens construction of the secondary wavelets? Wherein the point source-on the infinitely distant spherical wave front is taken customarily to be with phase $-\frac{\pi}{2}$ and the point to which it advances is obtained with the phase 0(after an integral over the intermediate wave front); then the field at the final point of arrival turns out to be with the right phase; assumed to be the one obtained by the ultimate wave front at the point of arrival should the wave propagate directly from the point source from which it physically originated in the first instance.

Alternatively assigning to the Huygens point source the initial phase value to be the value of the (Gouy) phase of the spherical wave from its previous history will obviate this difficulty. Indeed one may place at a location on the intermediate wave front a fundamental Gaussian mode of beam waist of size

$\pi\omega_0^2$ tangential to the wave front, with direction of propagation given by the normal to the wave front.

Thus one gets a consistent mathematical expression for the Huygens source of secondary wavelets - satisfying the properties assigned to it in the original suggestion. It also determines the right relative phase of any wave front created at distance z front the location of the point source. This way of sequencing the wave fronts including that of different foci connected through lens transformations and accumulating the relative phases is consistent with the phase accumulations considered in Chapters 4-6 in this thesis.

The Huygens point source is then identifiable literally, with the Rayleigh zone of the fundamental Gaussian mode with the infinite radius of curvature plane at the beam waist coincident with the point given the phase of the wave front history.

It is interesting also to ask, what is the origin of the Gouy phase? The Gouy phase in this thesis is taken to coincide with the phase of any wave front in a sequence of transformations involving lenses and propagations, given on the basis of the fundamental Gaussian mode.

Finally for the demonstration of above analysis, note the expression for the fundamental Gaussian mode incorporating the amplitude determined by the energy density it carries is represented as

$$e_x = \sqrt{\frac{16\pi <w_e>}{\epsilon}} \left(\frac{z_0}{z_0 - iz}\right) e^{-ikz-ik\frac{r^2}{2q(z)}} \tag{7.1}$$

$$h_y = \sqrt{\frac{\epsilon}{\mu}}.e_x \tag{7.2}$$

$$\omega^2(z) = \omega_0^2 \left[1 + \left(\frac{z}{z_0}\right)^2\right] \tag{7.3}$$

$$z_0 = \frac{\pi\omega_0^2}{\lambda} \tag{7.4}$$

$$q(z) = z + iz_0 \tag{7.5}$$

Examining the expressions(7.1-7.5) reveals an interesting result that the geometric optics limit of the expression(7.1) obtained by the normal procedure of taking limit $k \to \infty$[1] is achieved from the expression (7.1) by going to limit $z_0 \to \infty$. This implies ω_0 goes to infinity is independent of λ. This is the domain with $z < z_0$ i.e., inside of the Rayleigh zone. Eq. (7.1) inside Rayleigh zone is replaced by

$$e_x = \sqrt{\frac{16\pi < w_e >}{\epsilon}} e^{-k\frac{r^2}{2z_0} - \frac{ikr^2}{2z_0^2}} e^{-ikz - itan^{-1}\frac{z}{z_0}} \qquad (7.6)$$

Note that a control on z_0 is available without resorting to the conditions of ω_0 finite with $\lambda \to 0$. When z_0 is large then the amplitude is nearly unity unless r is sufficiently large, usually not considered in that range; similarly the phase term that appears in addition to the eikonal of geometrical optics, is nearly zero for all $z \ll z_0$. This observation is not only surprising but also revealing. Note that all what is said about geometric optics viz.1. Constant amplitude; 2. No phase other than eikonal; 3. Hydrodynamics like tubular flow systems of optical rays with variable cross sections; 4. Local orthogonal nature of wave front with respect to the geometric rays, all are applicable in $z \ll z_0$ region.

The other region where $z_0 \ll z$, has the Eq. (7.1) replaced by

$$e_x = \sqrt{\frac{16\pi < w_e >}{\epsilon}} \left(\frac{z_0}{z} e^{itan^{-1}\left(\frac{z}{z_0}\right)} e^{-\frac{\pi r^2}{z_0\lambda}} \right) e^{-ikz - ik\frac{zr^2}{2z_0^2}} \qquad (7.7)$$

Here depending on the sign of z, to the left or to the right of $z = 0$, the phase term is $\mp\frac{\pi}{2}$ respectively; for large z the inverse square law of intensity is evident; the wave front at every z is spherical with respective sign for different positions; note the k dependence of amplitude. This function shows that the field produced at point on the axis at the focal point is similar to the contribution from the first Fresnel zones as required by the discussion

[1]See Born and Wolf solution $e_x = \sqrt{\frac{16\pi <w_e>}{\epsilon}} e^{+ikz} e^{-i\omega t}$ where $< w_e > = \frac{\epsilon}{16\pi} e.e^\star$.

in [3], and also the value it must have according to the Kirchoff's integral equation, provided we take the phase at the focal point to be zero.

Since the mode functions are realizable (which was not so before they were discovered during the considerations on optical cavity) in practice by putting in the constraints of a lens in ring cavity, or by a pair of mirrors, they have come to stay and reveal a domain of mathematical analysis for the solution of Maxwell's equations. That is the amplitude function of the Maxwell's equations can be a function in terms of positive powers of k, in addition to the negative powers of k which emerge as corrections to the Geometrical optics results, which are obtained from L, M components as discussed in reference [3].

Thus the domain $z < z_0$(Eq. (7.6)), i.e., inside the structured point belongs to the geometrical optics, where as the domain $z > z_0$(Eq. (7.7)) behaves according to Kirchoff's integral equation, provided we take the phase at focal point to be zero.

Bibliography

[1] R. Simon and N. Mukunda, "Bargmann invariant and the geometry of the Gouy effect," Phys. Rev. Lett, vol. 70, Issue 7, pp. 880-883, Feb 1993.

[2] L. Mandel and Emil. Wolf, **Optical coherence and Quantum Optics,** Cambridge University Press, 1995(See Page 137(4.4-23) and page 271(5.6-38)).

[3] Max Born and Emil Wolf, **Principles of Optics,** Pergamon Press, 1980(See 8.2-14, 8.3.2-20).

Conclusion

In this thesis, we have investigated the possibility of using the Gouy phase to bring out the tuning capability. This is suggested here for the first time. The case of a single lens in a ring cavity has been used to compare the Gaussian mode optics with geometric optics - as is shown in chapter-3. A systematic way of increasing the Gouy phase accumulation is presented. The variability of Gouy phase for a stable branch is turning out to be $0 - \pi$. Accumulated Gouy phase is the phase a wavefront acquires in a sequence of transformations involving lenses and propagations and it is given on the basis of the Gaussian mode. The numerical results which are presented in the thesis are verified with the analytical solutions. Finally, the concept of structured point at various limits of z_0 is discussed and it is concluded that the Rayleigh range can be considered as the expanded picture of a point focus of geometrical optics.

Appendix A

It is investigated that only the for the cases of $H_1 < 0$ of Fig. (4.16), one can have the continuous variation of the Gouy phase. The Gouy phases $\phi_{G1}(RT)$, $\phi_{G2}(RT)$ in the arms d_1, $L - d_1$ respectively and the accumulated Gouy phase $\phi_G(RT)$ varying d_1 is shown for the respective cases as the following.
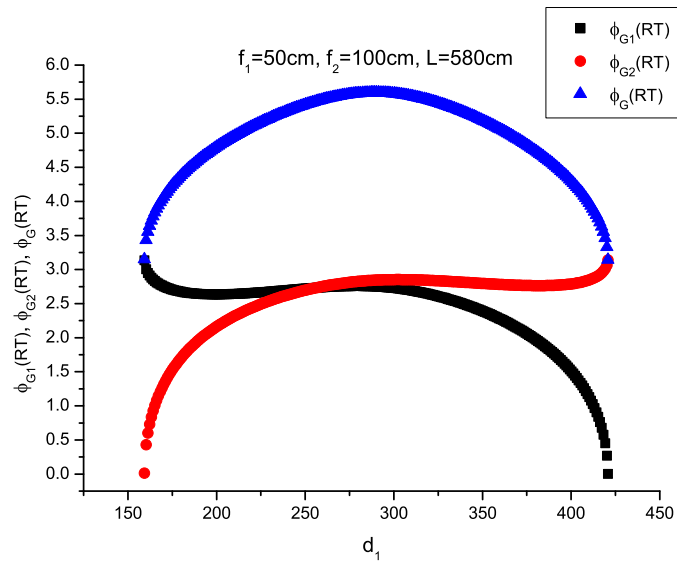
Figure 1: **The Gouy phases** $\phi_{G1}(RT)$**,** $\phi_{G2}(RT)$ **in the arms** d_1**,** $(L-d_1)$ **and** $\phi_G(RT) = \phi_{G1}(RT) + \phi_{G2}(RT)$ **varying** d_1 **corresponding to Fig. (4.10)**
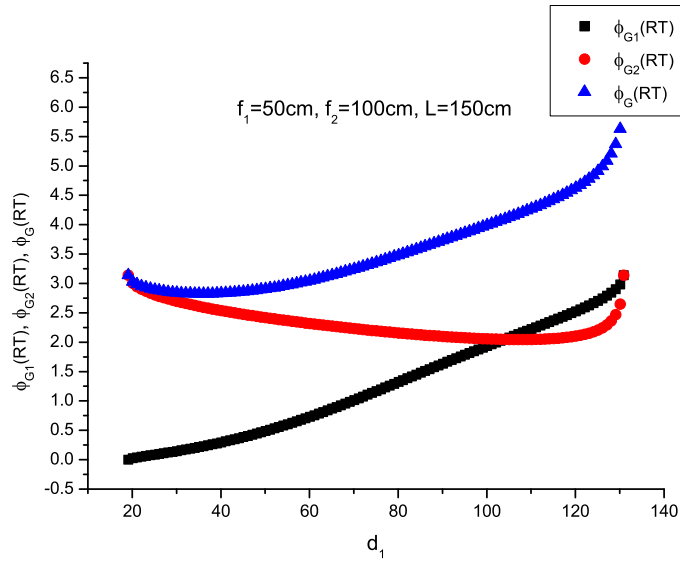
Figure 2: **The Gouy phases** $\phi_{G1}(RT)$**,** $\phi_{G2}(RT)$ **in the arms** d_1**,** $(L-d_1)$ **and** $\phi_G(RT) = \phi_{G1}(RT) + \phi_{G2}(RT)$ **varying** d_1 **corresponding to Fig. (4.11)**
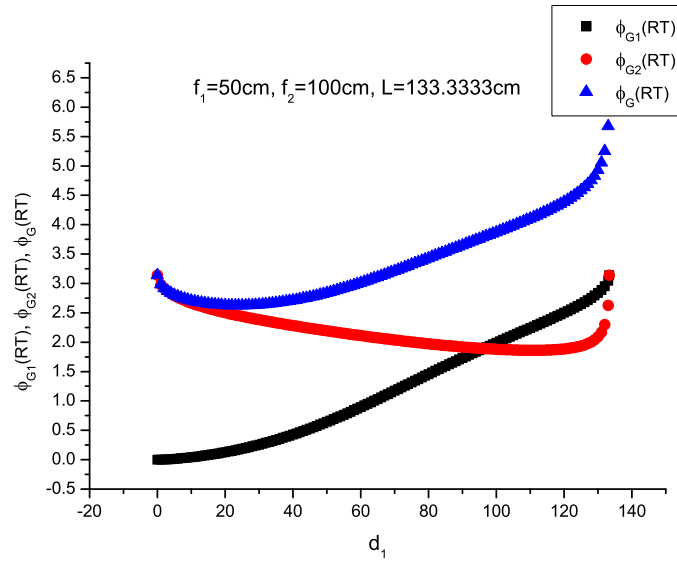
Figure 3: **The Gouy phases** $\phi_{G1}(RT)$**,** $\phi_{G2}(RT)$ **in the arms** d_1**,** $(L-d_1)$ **and** $\phi_G(RT) = \phi_{G1}(RT) + \phi_{G2}(RT)$ **varying** d_1 **corresponding to Fig. (4.12)**
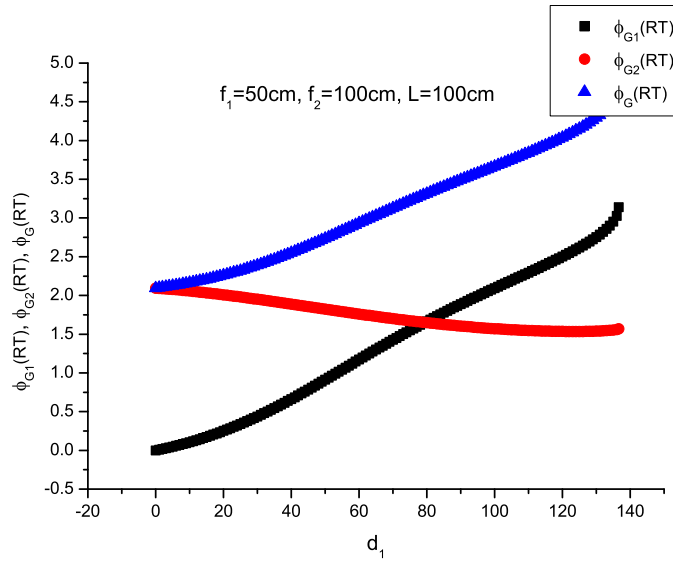
Figure 4: **The Gouy phases** $\phi_{G1}\left(RT\right)$**,** $\phi_{G2}\left(RT\right)$ **in the arms** d_1**,** $\left(L-d_1\right)$ **and** $\phi_G\left(RT\right) = \phi_{G1}\left(RT\right) + \phi_{G2}\left(RT\right)$ **varying** d_1 **corresponding to Fig. (4.13)**

Appendix B

The circle diagram representation of Gaussian mode was proposed for the first time by Collins[1]. A dual form of this Gaussian beam chart was given by Li[2]. Later, the logarithmic version of this chart which covers a much wider region has been discussed[3]. These diagrams can help one to analyze the propagation of Gaussian beam in free space and through lenses, to meet a common requirement in laser optical systems i.e., Gaussian beam mode matching. The purpose of this appendix is to display the equivalent circle diagrams or Gaussian beam charts for the considered systems of the thesis.

In the Collins chart representation, a Gaussian beam is recognized as a circle in two dimensional complex (x, y) plane, with the variables $\left(\dfrac{\lambda}{\pi \omega^2(z)}, \dfrac{1}{R(z)} \right)$, where λ is the wave length, $\omega(z)$ is the spot size and $R(z)$ is the radius of curvature of the phase front at location z. So, the trajectory of a freely propagating Gaussian mode is represented by the circle, and is given by

$$\left(x - \frac{1}{2z_0} \right)^2 + y^2 = \frac{1}{4z_0^2} \tag{8}$$

Here the radius of the circle is $(2z_0)^{-1}$ and the center is at $\left(\dfrac{1}{2z_0}, 0 \right)$, where z_0 is the half Rayleigh range of the Gaussian mode[2]. The entire $x > 0$ side is fully covered by the family of circles with $0 < z_0 < \infty$. Thus the entire

---

[2]In terms of z and z_0, x and y are $x = \dfrac{z_0}{z^2 + z_0^2}$; $y = \dfrac{z}{z^2 + z_0^2}$.

x, y plane is spanned by all possible freely propagating modes. A point on a circle relates the angle ϕ_z to the distance z from the beam waist of Gaussian mode by

$$tan\phi_z = \frac{y}{x} = \frac{z}{z_0} \qquad (9)$$

ϕ_z being the angle the vector-$(x + iy)$ makes with the x-axis (Refer chapter-2 for other properties of the Gaussian beam).

Before going to the cases discussed in the thesis, consider first the linear resonator shown in figure (6.63), formed by two mirrors of radii R_1 and R_2 which are separated by a distance L. The corresponding graphical representation of this cavity is shown for the two cases:(i)$R_1 = R_2$ and (ii) $R_1 \neq R_2$. Since there exists only one Gaussian mode in such a linear cavity, only one
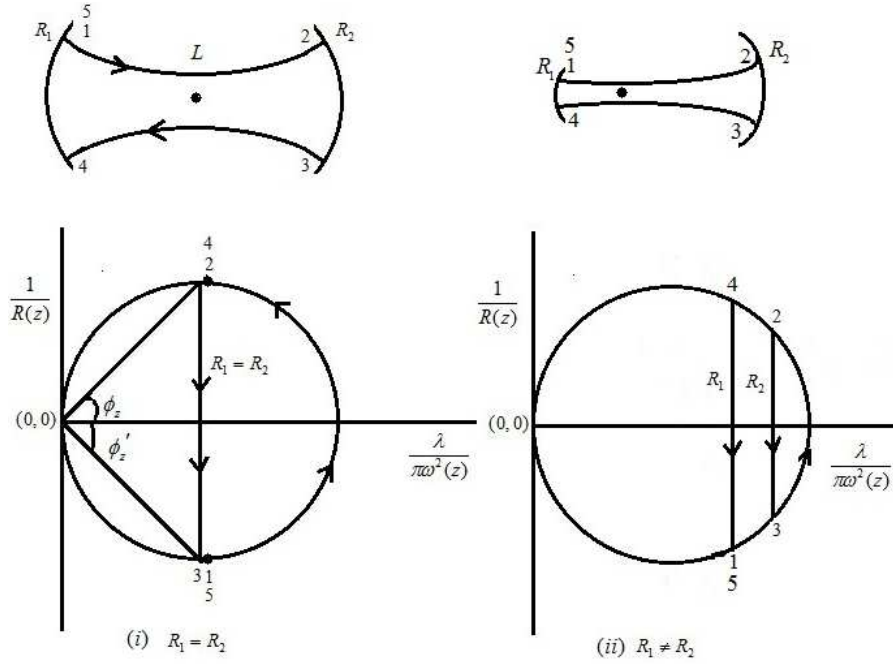

Figure 5: **Linear Cavity**

circle is present, corresponding to a unique half Rayleigh range z_0.

To know the center of the circle through an arbitrary point (x, y) in the complex plane obtain the point of intersection of the perpendicular bisector of the line segment formed by the points $(0, 0)$, (x, y) with the positive x-axis, which determines the center $(x_c, 0)$ of the circle. Note that larger the radius of the circle, smaller is the value of the z_0 and vice versa. The positions of the mirrors along the propagation direction z is related to the points on the x-axis, which get fixed by the beam spot sizes on the mirrors.

The z_0 in terms of the parameters of the Gaussian mode for the case of symmetrical mirror resonatori.e, when $R_2 = -R_1 = R^3$ is given by[4]

$$z_0^2 = \frac{(2R - L)L}{4} \tag{10}$$

and for $R_1 \neq R_2$

$$z_0^2 = \frac{L(-R_1 - L)(R_2 - L)(R_2 - R_1 - L)}{(R_2 - R_1 - 2L)^2} \tag{11}$$

Let us look at the circle diagrams for the cases (i)&(ii) in detail. In both the cases the transformation of a Gaussian beam in a free-space section from point 1 to 2, corresponds to a transformation around a circular arc in the complex $\frac{i}{q}$ plane as shown in figure (6.63) by the arc segment $1 \to 2$ implying that the Gaussian beam propagation $1 \to 2$ corresponds to the propagation from $-z$ to $+z$ through $z = 0$. The beam traverses twice through the vertical line of length $\frac{2}{R}$ for the case(i), once for $2 \to 3$ and second for $4 \to 5$. Thus, the Gaussian beam covers the propagation of the beam in the order from $1(z_0, z < 0) \to 2(z_0, z > 0) \to 3(z_0, z < 0) \to 4(z_0, z > 0) \to 5(z_0, z < 0)$, reaches the starting point.

For the case(ii) when $R_1 \neq R_2$ the effect of a mirror R_2 is a vertical line of distance $\dfrac{2}{R_2}$, shown by a line segment $2 \to 3$, which converts $+z$ to $-z$

---

[3]Convention used here is $R < 0$ for $z < 0$, $R > 0$ for $z > 0$. Propagation of Gaussian mode is always in $-ve \to 0 \to +ve$.

on reflection. Now it travels further from 3 to 4, which is from $-z$ to $+z$ and is represented by the arc segment $3 \to 4$, finally on reflection from the mirror R_1, it is shown by another vertical line corresponding to the distance $\frac{2}{R_1}$, it converts $+z$ to $-z$ and finishes one complete round trip propagation. The effect of a mirror can be a vertical line dropping down($\downarrow$) or a vertical line going up($\uparrow$), depending on the direction of propagation of the Gaussian beam.

The above described graphical representation is different from the representation in fig(8) and fig(9) of Collins[1] because one has to give attention to the full round trip propagation and also the reflection from the curved mirrors which has not been shown there in the way it is represented above.

The accumulated Gouy phase for the round trip is given by

$$\phi_G(RT) = 2\left(\arctan(\phi_z) - \arctan(\phi\prime_z)\right) \tag{12}$$

With this knowledge, we consider now Collins charts for the cases of ring resonator. Consider a single-converging-unit ring cavity which is discussed in the Chapter-3. It consists of a lens L_1 of focal length F placed as shown in the Fig. (6.64) in a ring cavity of length L. The mirrors M_1, M_2, M_3 and M_4 are 100% plane mirrors. Let the fundamental Gaussian mode with half Rayleigh range z_{01} exist in it. Assume a point at 2 be (x_1, y_1). Then one can write the corresponding radius of the circle associated with this point as

$$\frac{1}{z_{01}} = \frac{x_1^2 + y_1^2}{x_1} \tag{13}$$

The corresponding z_1 is given by

$$z_1 = z_{01} tan\phi_1 \tag{14}$$

The transformation through lens L_1 changes (x_1, y_1) to $(x_1, y_1\prime)$ where $y_1\prime = y_1 - \frac{1}{F}$. This transformation shifts it to another z_{02} defined in terms of the
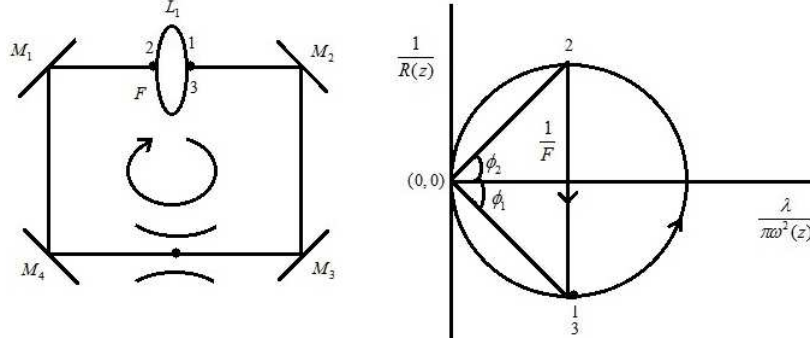
Figure 6: **Single lens Converging unit ring cavity(SCURC)**

parameters z_1, z_{01} and F by

$$\frac{1}{z_{02}} = \frac{1}{z_{01}} + \frac{z_1^2 + z_{01}^2}{F^2 z_{01}} - \frac{2z_1}{F z_{01}} \qquad (15)$$

To get the stable solution of the cavity, the condition to be imposed along with the round trip propagation is that $z_{01} = z_{02}$(since there exists only one mode). By applying these conditions, one can determine the position of the beam waist and spot size which are the same as shown in the Chapter-3.

In the Collins representation of figure(6.64), the beam propagation from the point 1 to 2 corresponds to the propagation from $-z$ to $+z$, and is shown by the arc segment $1 \rightarrow 2$. The lens L_1 transforms this beam from $+z$ to $-z$ shifting to the new radius of curvature by a vertical line, with out changing the spot size. Finally the Gaussian mode reaches point 3 which is equivalent to that at point 1.

The accumulated Gouy phase for the round trip is given by

$$\phi_G(RT) = \arctan(\phi_2) - \arctan(\phi_1) \qquad (16)$$

We discuss the case of 2CURC next. A schematic of 2CURC of the length L, consisting of two lenses L_1 and L_2 of focal lengths f_1 and f_2, which are separated by a distance is shown in Fig. (6.65). Here the mirrors M_1, M_2, M_3

and M_4 are 100% plane mirrors. The corresponding Collins chart is drawn by the side. We get the similar conditions for 2CURC as in SCURC; but there
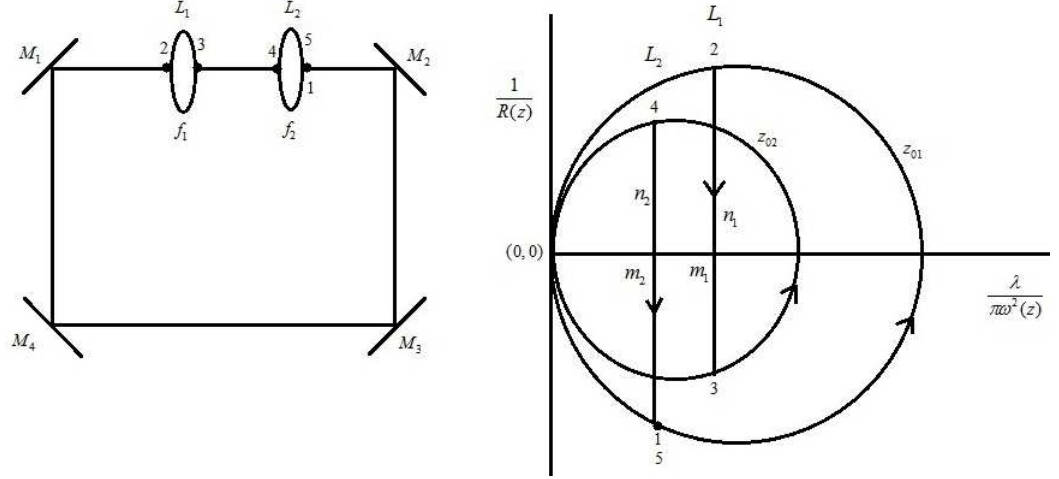

Figure 7: **Two lens Converging unit ring cavity(2CURC)**

exist two modes in this cavity. So the number of conditions are doubled as given below.

We approach the problem by taking two vertical lines i.e., two lenses n_1, and n_2 on the chart and trying to look for the circular arcs formed by the gaussian modes.

For a given lens n_1 one must have two coordinates (x_2, y_2), (x_3, y_3) which are the end points of the vertical line with the value inverse of focal length and maintaining the same beam spot size given by

$$y_2 - y_3 = \frac{1}{f_1} \tag{17}$$

$$x_2 = x_3 = m_1 \tag{18}$$

Similarly for the second lens n_2, the points connecting the vertical line are assumed to be (x_4, y_4), (x_5, y_5) relating the inverse of focal length of lens 2,

and maintaining the same spot size across the lens, as

$$y_4 - y_5 = \frac{1}{f_2} \tag{19}$$

$$x_4 = x_5 = m_2 \tag{20}$$

There are four points associated with these two lenses, correspondingly there have to be four circles. For the resonator to be stable, it is required to satisfy the following mode matching conditions:

(1) The points (x_4, y_4), (x_3, y_3) and $(0, 0)$ should lie on the same circle i.e., $R_4 = R_3$ and

(ii) The points (x_2, y_2), (x_5, y_5) and $(0, 0)$ should lie on the same circle i.e., $R_2 = R_5$.

Using the above conditions we can calculate the half Rayleigh ranges z_{01} and z_{02}. The corresponding positions of the beam waist and the accumulated round trip Gouy phase for the considered system are reported in the numerical results of the Chapter-4.

Bibliography

[1] S. A. Collins, Jr., "Analysis of Optical Elements involving focusing elements," Applied Optics 3, pp. 1263-1275, Nov 1964.

[2] T. Li, "Dual forms of the Gaussian beam Chart," Applied Optics 3, pp. 1315-1317, Nov 1964.

[3] G. Seifert, "A Logarithmic Gaussian Beam Chart," Applied Optics 7, pp. 337-340, Feb 1968.

[4] A. Yariv, **Quantum Electronics,** 3rd edition, Braun-Brumfield, Inc., 1989.

List of Publications

1. K. Sudha Nirmala, M. Sree Ramana, S. P. Tewari,"Tuning of ring laser by varying Gouy phase," Optics Communications, vol. 284, Issues 10-11, pp. 2560-2564, May 2011.

2. K. Sudha Nirmala, S. P. Tewari, "Characterization of the Longitudinal Gouy phase branches in Cascaded Optical Systems", to be published in **SPIE** Proceedings.